Chapter 6
Polarization in cascade decays

It often happens that vector particles are not produced directly from the partonic collision but are, together with an accompanying "recoil" system, the fruit of the decay or transformation of another particle or object. In inclusive production studies the two-step process usually remains unobserved and the dilepton decay distribution is studied as if the vector particle were produced directly.

The basic, intuitive expectation is that the isotropic decay from a $J = 0$ (mother) state should lead to the observation of a rotationally smeared angular distribution of the (daughter) vector particle decay, while, for $J > 0$, the observed polarization of the vector particle should somehow reflect the one of the mother particle.

We will address the following specific questions.

- In what kind of measurement and kinematic conditions can we indeed expect that a vector particle indirectly produced from the decay of a $J = 0$ particle ($\chi_{c0} \to \mathrm{J}/\psi\,\gamma$, $\mathrm{B} \to \mathrm{J}/\psi\,\mathrm{K}$, $\mathrm{H} \to \mathrm{Z}\,\gamma$, etc.) tends to look as unpolarized?
- How can the observation, made at the LHC, of almost unpolarized "directly" produced J/ψ mesons be justified in terms of fundamental production mechanisms? Is it not true that those coming from the decays of ($J = 0$) B mesons are the ones most reasonably expected to be unpolarized?
- How do the polarizations of $J = 1$ or $J = 2$ mother particles transform into the observed polarization of the vector particle ($\chi_{c1,2} \to \mathrm{J}/\psi\,\gamma$, $\mathrm{Z} \to \mathrm{J}/\psi\,\gamma$, etc.)?
- What polarization frame definitions can be adopted to describe the two-step process and what are their respective advantages?

P. Faccioli and C. Lourenço, *Particle Polarization in High Energy Physics*,
Lecture Notes in Physics 1002,
https://doi.org/10.1007/978-3-031-08876-6_6

6.1 Observing unpolarized vector-particle production

In this chapter we describe how the polarization is transferred from the mother particle to the daughter particle in a cascade (two-step) decay, where the daughter is a vector particle further decaying into a lepton-antilepton pair. Most of the chapter is devoted to the detailed discussion of the simplest case, the one where the mother particle is a $J = 0$ state. This is not only the easiest possible template of a general description, but it also corresponds to several interesting physics cases. Moreover, it represents a bridge to the subject of the previous chapter, where we proposed examples of "smearing" effects reducing the "amount" of the observed polarization. In fact, we can see the cascade production from a $J = 0$ particle as the potential source of the most extreme of the smearing effects, leading, in certain limits and conditions, to an effectively unpolarized production, thereby seemingly violating the unavoidable mathematical constraint that vector particles are necessarily intrinsically polarized (Theorem 1.1, Section 1.10).

We will consider examples of the cascade process $O \to V + X$, $V \to \ell^+\ell^-$, where O is (in the first part of the chapter) a particle of spin $J = 0$, V the vector state of which we want to study the polarization, and X an accompanying particle. The process has four degrees of freedom, represented by the angles Θ and Φ, describing the direction of V in the O rest frame, and ϑ and φ, the lepton emission angles in the V rest frame.

Figure 6.1 illustrates the definitions of these variables. The angles Θ and Φ are defined with respect to the polarization frame chosen for O (such as the GJ, CS, HX, and PX frames introduced in Chapter 2), referred to external physical directions (the colliding hadrons). For V we take as polarization axis the V direction in the O rest frame and, as a reference for the azimuthal anisotropy, the plane containing the polarization axes (z and z') of the two particles: we will refer to this frame as the "cascade helicity frame" (cHX).

In our specific case, the fact that O has zero angular momentum reduces considerably the complexity of the problem. Any $J = 0$ state, when it decays, emits its products isotropically. In fact, the spherical symmetry of a $J = 0$ wave function does not provide any possible reference for the definition of what an angular anisotropy could be. The calculation of the decay distribution involves the $\mathcal{D}^0_{LL'}(\Theta, \Phi)$ matrix, which has, actually, only one element, $\mathcal{D}^0_{00}$, constant and independent of the angles. As a result, the full angular distribution, $W(\cos\Theta, \Phi, \cos\vartheta, \varphi)$, is actually independent of $\cos\Theta$ and of Φ.

In several concrete cases it is also straightforward to write the $\cos\vartheta$ and φ dependence of W. We will consider a series of examples, where V is either a vector quarkonium or a Z boson and O is either a χ_0 quarkonium ($\chi_{c0} \to \mathrm{J}/\psi\,\gamma$ and $\chi_{b0} \to \Upsilon\,\gamma$), a B meson ($\mathrm{B} \to \mathrm{J}/\psi\,\mathrm{K}$), or a Higgs boson ($\mathrm{H} \to \mathrm{J}/\psi\,\gamma$, $\mathrm{H} \to \mathrm{Z}\,\gamma$). Some of these decays happen quite frequently in high-energy experiments; others are rare or even so-far unobserved processes. Together, they cover a large spectrum of possible observable manifestations of the polarization of V, thanks to the wide range of masses of the mother and daughter particles. In fact, and as we will see

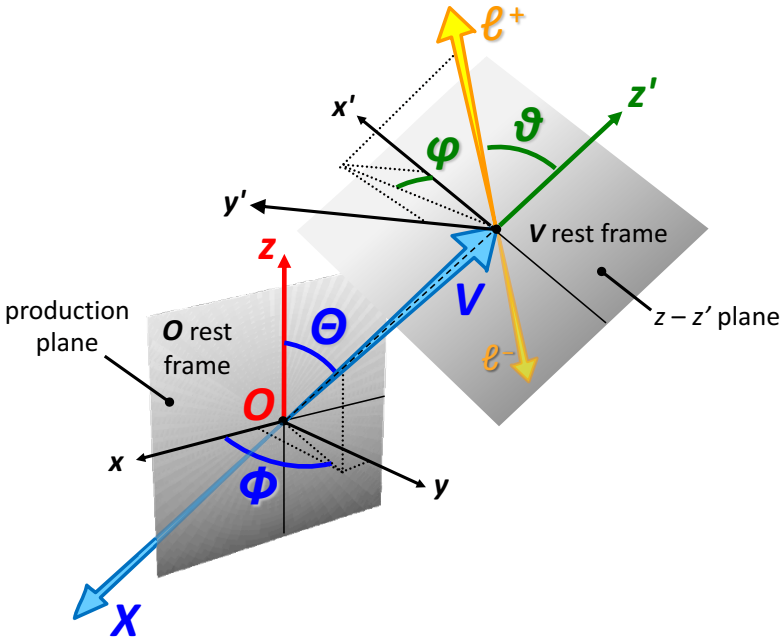

Fig. 6.1 Definition of the four angles used in the description of the cascade decay $O \to V + X$, $V \to \ell^+\ell^-$: the Θ and Φ angles are measured in the O polarization frame (x, y, z), defined as one of the usual frames (HX, CS, etc.) introduced in Chapter 2, while ϑ and φ are the dilepton emission angles in the V rest frame, with respect to the "cascade helicity" (cHX) system of axes (x', y', z').

in detail in Section 6.3, the results that can be observed in a real (or simulated) experiment are strongly dependent on the mass difference between O and V.

In all these examples the polarization of V, when measured in the cHX frame, is either fully transverse or fully longitudinal, depending on the accompanying daughter particle X (a photon or a kaon), as a pure consequence of angular momentum conservation: no role is played by the different interaction couplings involved.

The $O \to V + X$ decay in the O rest frame is illustrated in Fig. 6.2-top. The $V + X$ system has angular momentum $J = 0$ and, therefore, projection $J_z = 0$ on any z axis, so that, in general,

$$J_z^V + J_z^X + I_z^{V-X} = 0\,. \tag{6.1}$$

This relation includes a possible orbital angular momentum component $\mathbf{I}^{V-X}$ between the final states, which is, in particular, mandatory and well determined ($I = 1$) in the decay B($J = 0$) $\to$ J/ψ($J = 1$) K($J = 0$), where, otherwise, angular momentum conservation would be violated. The cHX axis z', defined by the common direction of the back-to-back V and X momenta, is a privileged axis to study the composition of angular momenta, because $\mathbf{I}^{V-X}$ is perpendicular to the linear momenta and $I_{z'}^{V-X}$ vanishes: only the individual spins of V and X have to be considered in the projected sum. The component $J_{z'}^X$ is well defined in all considered cases: it

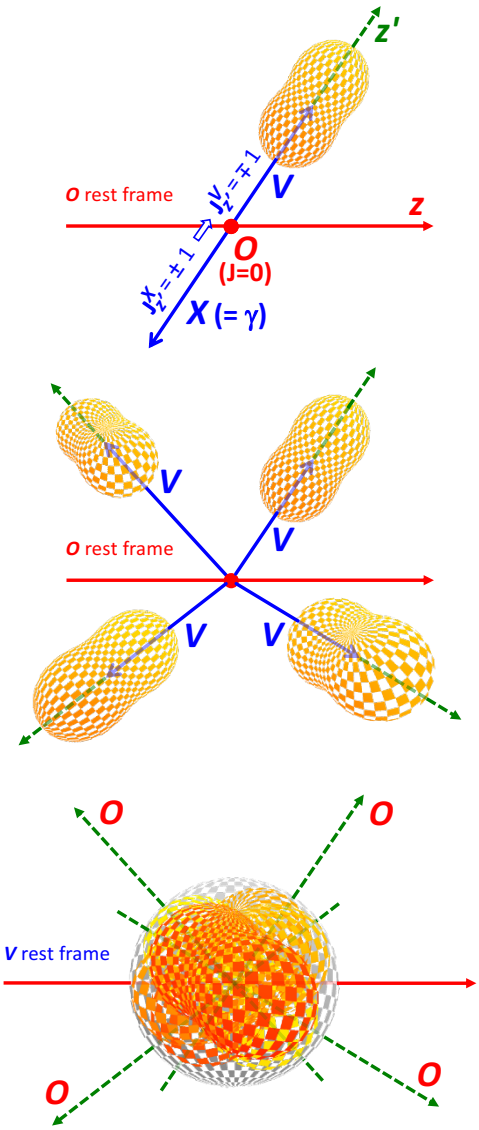

Fig. 6.2 How the vector particle V, produced in the $O \to V + X$ decay, acquires or loses its observable polarization, depending on the kind of measurement. Top: the process observed with respect to the O rest frame, in a measurement where both V and X are detected and the cHX axis z' is adopted as V polarization axis. For illustration, the case of a transverse polarization is shown, corresponding for example to $X = \gamma$ (transversely polarized photon): V is transversely polarized. Middle: the same kind of observation, for different directions of the outgoing V (different orientations of z'). Bottom: X is not observed or not used in the determination of the angular distribution; the measurement does not distinguish between directly and indirectly produced V and uses the same laboratory-referred frame as in inclusive studies. The average over all event configurations smears the shape of the V decay angular distribution towards the spherical symmetry.

can only be ±1 when X is a (transversely polarized) photon and 0 when X is a kaon or another $J = 0$ particle.

With these constraints, Eq. 6.1 implies, respectively, $J^V_z = \mp 1$ and 0 in the photon and kaon cases. As expected for a vector particle (Theorem 1.1), V is intrinsically polarized. The four-dimensional angular distribution is

$$W_{\mathrm{cHX}}(\cos\Theta, \Phi, \cos\vartheta, \varphi) \propto 1 + \lambda_0 \cos^2\vartheta\,, \tag{6.2}$$

where λ_0 is the "natural" polarization, $\lambda_0 = +1$ (photon) or -1 (kaon), and, as discussed above, there is no dependence on the Θ and Φ angles. To be measured, this distribution requires that the experiment reconstructs not only V but also X, using the momenta of both to determine the momentum and rest frame of O, needed for the definition of the cHX polarization axis.

The smearing effect that we will be studying arises when the V polarization measurement neglects (i.e. implicitly integrates out) the degrees of freedom of X, one possible reason being that X is not even observed and the $O \to V + X$ events are collected in the analysed data sample together with many other events where V represents *the* detected final state, independently of how it was produced.

To this category of measurement, which we will call "inclusive", belong, for example, most quarkonium ("prompt") production measurements, such as those published in Refs. [1–11], where J/ψ or Υ mesons are studied without distinguishing between directly produced states and those coming from the "feed-down" decays of χ_c or χ_b mesons: the analysed sample includes a fraction of such indirectly produced states, whose yields and (usually different) polarization properties must then be addressed, through hypotheses or analysis of further data, in the theoretical interpretation of the results.

The so-called "non-prompt" J/ψ (or ψ(2S)), produced in the decays of B mesons at an experimentally significant distance from the partonic interaction point, can, instead, be effectively distinguished from the prompt ones through suitable selection and subtraction procedures, as described hereafter, and are generally considered in separate measurements addressing their different production mechanisms (and different polarizations).

A second class of measurements, which we will refer to as "exclusive", is performed on the basis of event samples selected by fully reconstructing the final state. In particular, measurements of χ_c and χ_b cross sections (or cross-section ratios or polarizations), such as those reported in Refs. [12–19], reconstruct the photon emitted in the radiative decays, $\chi_c \to \mathrm{J}/\psi\,\gamma$ and $\chi_b \to \Upsilon\,\gamma$, and only select events where the final state has an invariant mass compatible with the χ_c or χ_b masses. Also in this case, the photon (X) momentum is, generally (and as assumed in our discussion), ignored in the angular analysis, i.e. it is not translated into values of $\cos\Theta$ and Φ.

Even when these variables are, in nature, uniformly distributed and the problem "looks" like a two-dimensional one (Eq. 6.2), acceptance and efficiency limitations in the detection of the involved particles can sculpt the four-dimensional distribution introducing correlations between the four angles. Integrating out the variables $\cos\Theta$ and Φ can be a necessity when the analysis cannot afford a four-dimensional anal-

ysis, typically because the data sample is too small. However, this analysis choice has consequences on the observable $\cos\vartheta, \varphi$ distribution, which we will illustrate in detail.

Considering the two kinds of measurements, inclusive and exclusive, allows us to address the following questions, here, for clarity of exposition, only formulated for the quarkonium case.

a) What are the polarizations of J/ψ or Υ mesons produced in the decays of χ_{c0} or χ_{b0} states, as they contribute to the inclusively observed prompt J/ψ or Υ production (that is, when radiative decay photons are not detected or are ignored)?

b) If, using the measured γ momentum, we exclusively select samples of J/ψ or Υ mesons coming from the decays of χ_{c0} or χ_{b0} states, and submit them to the same kind of analysis applied to the corresponding "inclusive" samples, what polarizations are we expected to measure and why?

We can already anticipate here that, contrary to what common sense may at first suggest, the two questions have different answers.

Of these two examples, the first one (a) can only be addressed theoretically or through simulated events: it cannot be investigated experimentally in a direct way, since restricting the analysis to the vector quarkonia coming from χ states requires that some selection is applied to $X = \gamma$, but this procedure is the one defining the second example (b).

When, instead, we consider the case of J/ψ mesons produced in decays of B mesons, the measurement of the corresponding polarization can actually be made also using "inclusive" samples. In fact, experiments often identify inclusive event samples dominated by $B \to J/\psi$ decays by selecting the "non-prompt" J/ψ mesons, i.e. the events in which the distance between the primary vertex (the proton-proton interaction point, where the B is produced), and the dimuon vertex, where the J/ψ is produced and immediately decays, is significantly larger than the uncertainty in the measurement of that distance. This method is justified by the relatively large decay length of B mesons (the $B^{\pm}$ lifetime is around 500 μm), with respect to the measurement resolution of most modern experiments, of around 10 μm.

In this case we can, therefore, ask the questions: what do we expect as an outcome of a real polarization measurement of J/ψ mesons produced in decays of B mesons, when using either an inclusive sample of non-prompt J/ψ mesons, or the exclusive events where the accompanying particle X (a kaon, for example) is identified? In both cases, it is meant that the angular degrees of freedom of the B decay are integrated out and the angular measurement is made in the two-dimensional $(\cos\vartheta, \varphi)$ space of the dilepton decay in the J/ψ rest frame.

Finally, we will also discuss the polarizations of the J/ψ or Z bosons emitted in radiative Higgs decays ($H \to J/\psi\,\gamma$ or $H \to Z\,\gamma$), measured with respect to the usual CS and HX frames, defined in terms of the momenta of the colliding protons without using the momentum of the daughter photon, that is, without referring, at each given event, to the rest frame of the specific Higgs boson that generated the observed particle.

We will discuss these questions gradually, until the end of this chapter, starting here with a first, simple and intuitive answer, quantitatively valid under conditions and limitations that will be studied in the next sections.

The idea is illustrated in Fig. 6.2. We know that V is emitted isotropically in the rest frame of the $J = 0$ particle O, as illustrated in the middle drawing. With a "Copernican" change of point of view, adopting as observation platform the rest frame of V (where the polarization measurement is made), we will see, event after event, O departing in all possible directions, a situation illustrated in the bottom drawing and described by uniformly distributed spherical coordinates $\cos\Theta$ and Φ. Along each of these individual directions (represented by the event-dependent z' cHX axis) we see a lepton decay distribution of shape $1 + \lambda_0 \cos^2\vartheta$, according to Eq. 6.2. With respect to a hypothetical "absolute" set of x, y, z axes fixed in space (for example, the laboratory axes), this distribution appears, each time, as rotated in a different direction. The convolution of all these rotated distributions leads to a spherical overall distribution. In other words, by referring to the "absolute" axes we lose the connection to the natural frame and the polarization orientation is fully "randomized", resulting in the apparent absence of any anisotropy of the decay distribution.

The intuitive concept that the decay distribution undergoes a full rotational smearing, concealing any underlying polarization, if the direction of the polarization axis is randomized with respect to the natural one, is formalized mathematically by Eq. 5.5. Here, $\cos\zeta$ and ω are the analogous of the spherical coordinates $\cos\Theta$ and Φ, describing how the observation frame (the "absolute" one in the present case) is rotated with respect to the natural one. All terms in $\sin(n\,\omega)$ or $\cos(n\,\omega)$, with $n = 1$ or 2, have zero average over the ω interval $[-\pi, +\pi]$, implying that λ_φ, $\lambda_\varphi^\perp$, $\lambda_{\vartheta\varphi}$, and $\lambda_{\vartheta\varphi}^\perp$ vanish. Concerning λ_ϑ, we notice that the uniform integration over the polar coordinate $\cos\zeta = \cos\Theta$ is actually not the only operation leading to a perfectly isotropic distribution. While there are in principle several ad hoc possibilities producing the same result, we consider here a case that will be seen as physically relevant in the subsequent discussion, namely a linear distribution of the kind $1/2\ (1 + B\cos\zeta)$ with $|B| \leq 1$ (normalized to unity over the $[-1, +1]$ range). In fact, the average of $\sin^2\zeta$ over this distribution is

$$\langle \sin^2\zeta \rangle = \frac{1}{2}\int_{-1}^{1} (1 - \cos^2\zeta)\,(1 + B\cos\zeta)\,\mathrm{d}\cos\zeta = \frac{2}{3}\,, \tag{6.3}$$

independently of B, leading to $\lambda_\vartheta = 0$ in Eq. 5.5: a constant distribution ($B = 0$) or a linear one ($0 < |B| \leq 1$), the latter option corresponding to a non-spherical smearing, both lead to the unpolarized scenario.

The actual reason why the linear $\cos\zeta$ distribution is equivalent to a flat one is that it corresponds to a flat distribution of $|\cos\zeta|$, and the sign of $\cos\zeta$ is not relevant for our present considerations (this argument would not be valid in studies of parity-violating effects).

This simple reasoning, leading to the prediction of unpolarized vector particles, does have counterparts in possible physical scenarios. However, depending on the

case, a fully isotropic smearing will be observed only in very specific kinematic conditions and/or with specific analysis choices. In fact, we have used two hypotheses that require case-by-case validation:

a) the laboratory-referred frames HX, CS, etc., are good approximations of an "absolute" frame;
b) the two-dimensional $(\cos\Theta, \Phi)$ distribution remains uniform, as it is in nature, in the data sample used for the measurement or, at most, its $\cos\Theta$ projection becomes linear.

How are these hypotheses affected by the experimental selections? The next sections address this problem and illustrate what kinds of observable distributions are expected in real experiments.

6.2 Kinematics of cascade decays

We have seen that the observation of an unpolarized vector particle becomes possible, at least conceptually, when the particle is produced from the decay of a $J = 0$ state O, in specific kinds of measurements where the observer is blind to the angular degrees of freedom of the O decay. The full smearing leading to a complete lack of measurable anisotropy, is, however, only an extreme case, occurring when, in the collected event sample, the (unobserved) $\cos\Theta$ distribution remains uniform as it is in nature, or becomes linear, the latter condition practically including, as approximations, cases where it is only slightly and smoothly shaped by experimental selections.

We are now going to study how the measurement itself, by sculpting the $\cos\Theta$ distribution, can perturb the spherical smearing naturally produced by the decay of a $J = 0$ particle, and actually find a more or less anisotropic dilepton distribution. The four-dimensional distribution W of Eq. 6.2 does not depend explicitly on $\cos\Theta$ and does not give any hint on how the dilepton distribution can be (more or less) smeared as a consequence of a (more or less) uniform randomization of the $\cos\Theta$ variable; in fact, it remains true that, even when such a randomization occurs, the V polarization along the cHX axis, built with the *per-event* knowledge of the O momentum, is immune to it and remains maximal and unsmeared.

In order to study the geometry of the smearing mechanism, it is convenient, therefore, to use an alternative configuration of the V polarization frame. Figure 6.3 shows the new definition, which, like the previous one, is adoptable, more generally, for the description of any two-step cascade decay. The x, y, z axes, with respect to which the emission angles Θ and Φ of the $O \to V + X$ decay are measured, are the same as in the previous definition: z is, for example, the polarization axis in the HX or CS frame of O. Instead, the x'', y'', z'' axes, the double-prime sign indicating the new references for the dilepton decay in the V rest frame, are now exact geometrical clones of the x, y, z axes, obtained by a simple, undistorted translation, not involving any Lorentz boosts of the physical references. In practice, the dimensionless unit

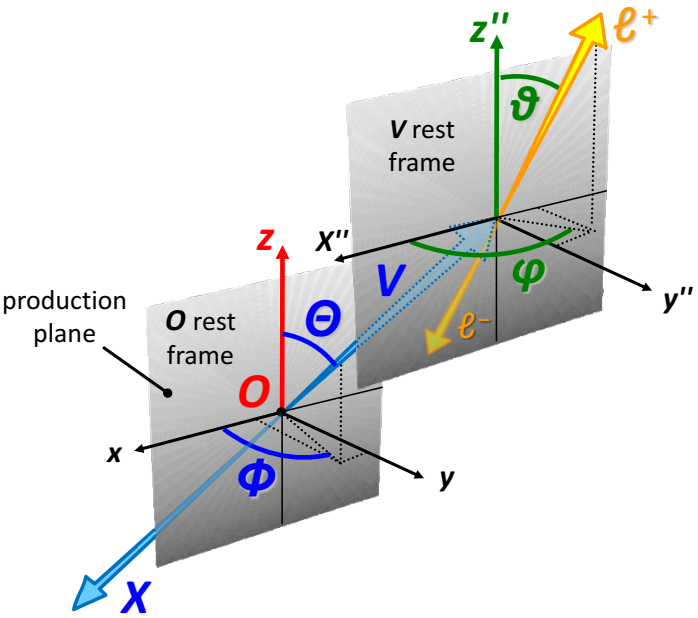

Fig. 6.3 An alternative definition of the polarization frame used in the description of the cascade decay $O \to V + X$, $V \to \ell^+\ell^-$: the x, y, z axes, and therefore the angles Θ and Φ, are the same as in the usual definition of Fig. 6.1, while ϑ and φ, dilepton emission angles in the V rest frame, are now defined with respect to a system of axes, x'', y'', z'', geometrically identical to x, y, z (the "cloned cascade frame", CC).

vectors of the x, y, z axes, defined in the O rest frame (O must, in principle, be reconstructed) are used with no modification as unit vectors of the x'', y'', z'' axes in the V rest frame.

This choice, hereafter referred to as the "cloned cascade frame" (CC) may sound physically abstract and perhaps counter-intuitive, but there is a limit in which the x'', y'', z'' axes simply reduce to the axes of the "ordinary" HX or CS frame (or any other frame adopted for x, y, z) of V, that is, the one "properly" defined in terms of beam directions Lorentz-boosted to the V rest frame: when the momenta of O and V in the laboratory are much larger than the mass difference between O and V, they become almost indistinguishable and the directions of, say, the HX axis in the O rest frame and the HX axis in the V rest frame tend to coincide (as is more quantitatively described later in this section).

We note that the definition of the CC frame requires the specification of the frame used for the decay of O, that is, of what frame is being "cloned": we can refer, for example, to the HX CC or CS CC frame. When this specification is absent, we will imply that we are using the HX frame as "master" frame.

For the decays $\chi_c \to \mathrm{J}/\psi\,\gamma$, $\chi_b \to \Upsilon\,\gamma$ or $\mathrm{B} \to \mathrm{J}/\psi\,\mathrm{K}$, given the relatively small differences between the masses of the mother and daughter particles, this condition is satisfied in most of the kinematic domain of the LHC measurements. In this limit,

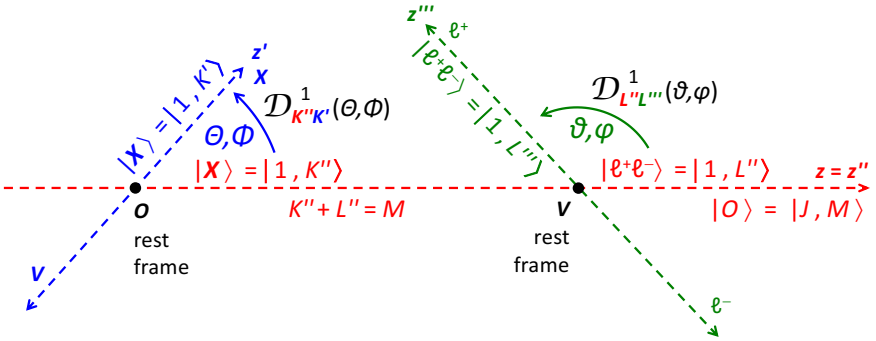

Fig. 6.4 Representation of the cascade decay $O \to V + X$, $V \to \ell^+\ell^-$, indicating the reference axes (CC frame), the decay angles, the angular momentum states of the involved particles, and the Wigner matrix elements used for their rotation. The red axis represents the common direction of the O and V polarization axes (z and z'', respectively) in the CC frame.

the determination of the x'', y'', z'' axes decouples from the knowledge of the O momentum and the polarization measurement in the CC frame can effectively be performed without observing the accompanying particle X and reconstructing the O rest frame.

To determine the expression of the four-dimensional angular distribution, we start by writing the amplitude of the process $O \to V+X$, following a procedure analogous to the one used in Section 1.7 to derive the dilepton distribution of a J/ψ.

Figure 6.4 summarizes the notations used for the angular momentum states of the involved particles, the axes and their rotations; for later use (Section 6.6), the diagram represents the general case where the mother particle O has angular momentum quantum number J.

As mentioned in the previous section, in the considered examples X has a definite angular momentum projection, which we indicate here with K', along the z' (cHX) axis, while there is, in general, also an orbital momentum component that now, with respect to the CC polarization axis z'', we will not be able to ignore. In order to use simple two-body angular momentum sum rules, we then attribute the orbital angular momentum to X: in practice, we consider X as a state that has, whatever its identity (a photon, a spin-0 kaon), total angular momentum $J = 1$, including the orbital part, as required so that its sum with the, also unitary, spin of V yields the zero angular momentum of O.

The Wigner matrix needed to rotate the angular momentum of X from the x', y', z' axes to the x'', y'', z'' axes is, therefore, $\mathcal{D}^1_{K'' K'}(\Theta, \Phi)$, where K'' is the $J_{z''}$ projection of X on the z'' axis:

$$|X; 1, K'\rangle_{z'} = \sum_{K''=0,\pm1} \mathcal{D}^1_{K'' K'}(\Theta, \Phi)\, |X; 1, K''\rangle_{z''} \,. \tag{6.4}$$

Since we will only be considering parity-conserving terms of the decay distribution, Θ and Φ indifferently denote the direction of V or of X, while to obtain correct

signs for the parity-violating terms, following the notations of Fig. 6.3 where it is the direction of V that defines Θ and Φ, the Wigner matrix for the rotation of X should read $\mathcal{D}^1_{K'' K'}(\pi - \Theta, \pi + \Phi)$.

Indicating with L'' the generic $J_{z''}$ projection of V on z'', the decay amplitude is given by

$$\begin{aligned} &\mathcal{A}(O \to V_{L''} + X_{K'}) \\ &= \sum_{K''=0,\pm1} {}_{z''}\langle V\, X;\ 1, L'',\ 1, K'' \,|\, \mathcal{B} \,|\, O; 0, 0\rangle_{z''}\ \mathcal{D}^{1*}_{K'' K'}(\Theta, \Phi) \\ &= \langle 1, L'',\ 1, -L'' \,|\, 0, 0\rangle\ \mathcal{D}^{1*}_{-L'' K'}(\Theta, \Phi)\ , \end{aligned} \tag{6.5}$$

where the operator $\mathcal{B}$, containing the dynamics of the decay, can, in general, impose relations between the angular momentum states of O, V, and X. In the cases here considered, the relevant physical constraints are two: a) along z'', the V and X particles have opposite angular momentum projections, being the two daughters of a $J = 0$ state, as expressed in the relation used in the second equality above:

$${}_{z''}\langle V\, X;\ 1, L'',\ 1, K'' \,|\, \mathcal{B} \,|\, O; 0, 0\rangle_{z''} \ \propto\ \delta_{K'', -L''}\ \langle 1, L'',\ 1, -L'' \,|\, 0, 0\rangle\ ; \tag{6.6}$$

b) the nature of X, being either a transversely polarized photon or another $J = 0$ particle (a condition that we will impose below, while summing over the squared amplitudes), effectively determines, by angular momentum conservation, a definite natural polarization of V.

The Clebsch–Gordan coefficient $\langle 1, L'',\ 1, -L'' \,|\, 0, 0\rangle$ is $\sqrt{3}/3$ or $-\sqrt{3}/3$, respectively for $L'' = 0$ or ±1. The amplitude of the two-step process can then be written by including a factor expressing the rotation of the dilepton angular momentum state, which has projection $L''' = \pm1$ along its own flight direction in the V rest frame (z''' axis), onto the z'' axis (where it has projection identical to the V one, L''), and summing over the possible L'' components of V:

$$\begin{aligned} &\mathcal{A}[\, O \to V + X_{K'},\ V \to (\ell^+\ell^-)_{L'''}] \\ &\propto \sum_{L''=0,\pm1} \langle 1, L'',\ 1, -L'' \,|\, 0, 0\rangle\ \mathcal{D}^{1*}_{-L'' K'}(\Theta, \Phi)\ \mathcal{D}^{1*}_{L'' L'''}(\vartheta, \varphi)\ . \end{aligned} \tag{6.7}$$

This latter expression can also be read, by comparison with Eq. 1.10, as the amplitude of the dilepton decay of V, when V has (Θ, Φ)-dependent angular momentum components (referred to z'') $a_{L''} = \langle 1, L'',\ 1, -L'' \,|\, 0, 0\rangle\ \mathcal{D}^{1*}_{-L'' K'}(\Theta, \Phi)$. The final expression of the angular distribution is obtained by squaring Eq. 6.7 and summing over $L''' = \pm1$ and over the relevant K' values, which depend on what the final state X is. In the cases we will consider, $K' = 0$ if X is a kaon (or other $J = 0$ particle), and $K' = \pm1$ if X is a photon. Therefore, V has a fully longitudinal natural polarization in the cHX frame, $\lambda_0 = -1$, in the first case and a fully transverse one, $\lambda_0 = +1$, in the second.

The resulting distribution for a generic natural polarization of V is:

$$\begin{aligned} & W_{\mathrm{CC}}(\cos\Theta, \Phi, \cos\vartheta, \varphi) \\ & \propto \frac{1}{3+\lambda_0}\Big(2 + \lambda_0\,(1 - \cos^2\Theta - \cos^2\vartheta + 3\cos^2\Theta\,\cos^2\vartheta\,) \\ & + \lambda_0\,\sin^2\Theta\,\sin^2\vartheta\,\cos 2(\varphi - \Phi) \\ & + \lambda_0\,\sin 2\Theta\,\sin 2\vartheta\,\cos(\varphi - \Phi)\Big)\,. \end{aligned} \tag{6.8}$$

Only the difference between azimuthal angles, $\varphi - \Phi$, enters this expression, which is, moreover, fully symmetric by exchange between the O and V decay angles: $(\Theta, \Phi) \rightleftharpoons (\vartheta, \varphi)$. It is, however, possible to rewrite the result giving emphasis to the dilepton part, by defining $(\cos\Theta, \Phi)$-dependent anisotropy parameters and obtaining the same usual expression of Eq. 1.16, with

$$\begin{aligned} \lambda_\vartheta &= \frac{-\lambda_0\,(1 - 3\cos^2\Theta)}{2 + \lambda_0\,(1 - \cos^2\Theta)}\,, \\ \lambda_\varphi &= \frac{\lambda_0\,\sin^2\Theta\cos 2\Phi}{2 + \lambda_0\,(1 - \cos^2\Theta)}\,, \quad \lambda_\varphi^\perp = \frac{\lambda_0\,\sin^2\Theta\sin 2\Phi}{2 + \lambda_0\,(1 - \cos^2\Theta)}\,, \\ \lambda_{\vartheta\varphi} &= \frac{\lambda_0\,\sin 2\Theta\cos\Phi}{2 + \lambda_0\,(1 - \cos^2\Theta)}\,, \quad \lambda_{\vartheta\varphi}^\perp = \frac{\lambda_0\,\sin 2\Theta\sin\Phi}{2 + \lambda_0\,(1 - \cos^2\Theta)}\,. \end{aligned} \tag{6.9}$$

The distribution becomes obviously isotropic if $\lambda_0 = 0$. We can also recognize from Eq. 6.8 that the average over a uniform (or linear) $\cos\vartheta$ distribution (giving $\langle\cos^2\vartheta\rangle = 1/3$) and over the azimuthal dimension leads to an isotropic $(\cos\Theta, \Phi)$ distribution, as expected from the decay of a $J = 0$ particle. Vice versa and more interestingly, the (uniform or linear) average over $\cos\Theta$ leads to an isotropic dilepton decay distribution of the vector particle V, providing a further illustration of the concepts discussed in the previous section. However, it is now apparent that, if the $\cos\Theta$ distribution is, for some reason, not uniform or linear, so that $\langle\cos^2\Theta\rangle \neq 1/3$, the resulting dilepton distribution measured in the CC frame will not be isotropic and the presence of a nonzero natural polarization λ_0 will somehow be revealed.

It is not difficult to realize that a measurement usually introduces sculpting effects on the $\cos\Theta$ distribution. If all V particles produced by the decay of O were included in the analysed data sample, the distribution would remain uniform, as it is naturally. In general, however, this is not possible in a real experiment, and not only because of the selection criteria applied to improve the quality of the signal reconstruction. The simple fact that we are *observing* a sample of V particles (instead of a sample of O particles) and we are, therefore, delimiting the range of their (transverse and/or longitudinal) momenta in the laboratory, reshapes the $\cos\Theta$ distribution. To understand how, we need to open a brief parenthesis on the relations between the relevant kinematic variables: the momenta of O and V in the laboratory, $\mathbf{P}$ and $\mathbf{p}$, with moduli P and p; the momentum of V in the rest frame of O, $\mathbf{p}'$, with

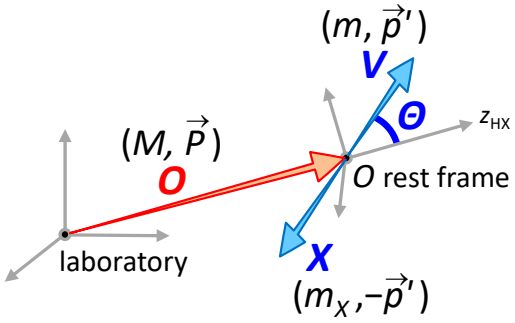

Fig. 6.5 Kinematic variables used in the description of the decay $O \to V + X$.

modulus p'; the masses M, m, and m_X of O, V, and X; and $\cos\Theta$. The notations are illustrated in Fig. 6.5, where the angle Θ is seen to be defined in the HX frame of O. In all relations until the end of this section, we imply $\Theta \equiv \Theta_{\rm HX}$.

The components of the V momentum perpendicular, $p_\perp$, and parallel, $p_\parallel$, to the direction of **P** transform from the O rest frame to the laboratory frame according to the Lorentz boost defined by $\beta = P/\sqrt{M^2 + P^2}$, so that:

$$p_\perp = p'_\perp = p' \sin\Theta \tag{6.10}$$

and

$$\begin{aligned} p_\parallel &= \frac{1}{\sqrt{1-\beta^2}} \left(p'_\parallel + \beta \sqrt{p'^2 + m^2} \right) \\ &= \sqrt{1 + \frac{P^2}{M^2}}\, p' \cos\Theta + \frac{P}{M} \sqrt{p'^2 + m^2}\,. \end{aligned} \tag{6.11}$$

The momentum p' is

$$p' = \frac{1}{2M} \sqrt{(M^2 + m^2 - m_X^2)^2 - 4M^2 m^2} \simeq \frac{M^2 - m^2}{2M}\,, \tag{6.12}$$

where the approximate equality corresponds to $m_X^2 \ll M^2 + m^2$, a relation satisfied in all the cases hereafter considered, either exactly ($X = \gamma$) or up to 1%-order corrections ($X = $ K in B decays).

For an easier illustration of the concept we will make the temporary assumption that we are considering high-momentum measurements, that is, the momenta of O and V in the laboratory are significantly bigger than their masses. This condition, which will not be used in the computations of the next section, can be considered to be satisfied, for example, in most charmonium measurements at the LHC. The relations seen in the remaining of this section are, therefore, applicable quantitatively to the decays $\chi_{c0} \to {\rm J}/\psi\,\gamma$ and ${\rm B} \to {\rm J}/\psi\,{\rm K}$, but not, in general, to the Higgs decays.

Equations 6.10 and 6.12 imply the general inequality $p_\perp < (M - m)\sin\Theta$ and, therefore,

$$p_\perp \ll p \quad \text{if} \quad M - m \ll p\,. \tag{6.13}$$

This means that, in the assumed approximation, we have $p \simeq p_\parallel$, so that the vectors $\mathbf{p}$ and $\mathbf{P}$ can be considered to be parallel. In this approximation, as previously mentioned, the CC frame becomes coincident with the corresponding laboratory-referred frame, for example the HX frame.

We can now quantify the effect of this approximation on a polarization measurement, considering that the angle $\delta_{\rm CC}$ between the two polarization axes is, by definition of such axes, the angle between the vectors $\mathbf{p}$ and $\mathbf{P}$, given by $\sin\delta_{\rm CC} = p_\perp/p$. Assuming that the decay distribution is of the kind $\propto 1 + \lambda_\vartheta^{\rm CC}\cos^2\vartheta$ in the HX-CC frame (that is, $\lambda_\vartheta^{\rm CC} \equiv \lambda_0$), the corresponding λ_ϑ value in the HX frame is (Eq. 2.13, setting λ_φ and $\lambda_{\vartheta\varphi}$ to zero)

$$\lambda_\vartheta^{\rm HX} \;=\; \lambda_\vartheta^{\rm CC}\,\frac{1 - \frac{3}{2}\sin^2\delta_{\rm CC}}{1 + \frac{1}{2}\lambda_\vartheta^{\rm CC}\sin^2\delta_{\rm CC}} \;\simeq\; \left[1 - \frac{3 + \lambda_\vartheta^{\rm CC}}{2}\sin^2\delta_{\rm CC}\right]\lambda_\vartheta^{\rm CC}\,, \tag{6.14}$$

where the approximate equality is valid in the limit of a small angle. Therefore,

$$\left|\lambda_\vartheta^{\rm HX} - \lambda_\vartheta^{\rm CC}\right| \;\simeq\; \frac{3 + \lambda_\vartheta^{\rm CC}}{2}\left|\lambda_\vartheta^{\rm CC}\right|\sin^2\delta_{\rm CC} \;\le\; \frac{3 + \lambda_\vartheta^{\rm CC}}{2}\left|\lambda_\vartheta^{\rm CC}\right|\left(\frac{M - m}{p}\right)^2\,. \tag{6.15}$$

For example, the relative deviation, $\left|(\lambda_\vartheta^{\rm HX} - \lambda_\vartheta^{\rm CC})/\lambda_\vartheta^{\rm CC}\right|$, of a λ_ϑ measurement in the HX frame from its CC expectation is at most of order 2–4% (depending on λ_ϑ) for the polarization of J/ψ mesons from B decays at $p_{\rm T} = 10$ GeV and rapidity $y = 1$, and decreases with increasing $p_{\rm T}$ and $|y|$.

We will now assume that the condition $\mathbf{p} \parallel \mathbf{P}$ is satisfied. Taking then $p_\parallel$ in Eq. 6.11 as expression for p, with

$$\sqrt{p'^2 + m^2} = \frac{M^2 + m^2}{2M} \quad \text{and} \quad \sqrt{1 + \frac{P^2}{M^2}}\,\frac{p'}{P} \simeq \frac{p'}{M}\,,$$

the first relation deriving from Eq. 6.12 and the second from the assumption that $P \gg M$, we find that

$$\mathbf{p} \;\simeq\; \mathbf{P}\; f(\cos\Theta)\,, \tag{6.16}$$

$$\text{with} \quad f(\cos\Theta) \;=\; \left(\frac{1 - \cos\Theta}{2}\,\frac{m^2}{M^2} \;+\; \frac{1 + \cos\Theta}{2}\right), \tag{6.17}$$

where we note the linear dependence on $\cos\Theta$.

This vector relation can be rewritten, remaining formally identical, with $\mathbf{p}$ and $\mathbf{P}$ replaced by their moduli, or their transverse or longitudinal components. The mathematical passages throughout this section will use the symbols p and P to denote either of the three possibilities. The one relevant for the case under study is the variable with respect to which the polarization parameters λ_ϑ, λ_φ and $\lambda_{\vartheta\varphi}$ in the CC

frame (that is, in its corresponding laboratory-referred frame) are observed. In our illustrative studies we will consider hypothetical measurements made as a function of p_{T}. Correspondingly, all the following relations should be considered with the substitutions $p \to p_{\mathrm{T}}$, $P \to P_{\mathrm{T}}$.

Equation 6.17 can be read as follows: if we consider a sample of events where O is always produced with the same laboratory momentum, of modulus (or component) P, the laboratory momentum (component) p of V is distributed uniformly between the values $m^2/M^2\, P$ and P, corresponding to the extremes of the natural uniform distribution of $\cos\Theta$ between -1 and $+1$.

Having a sample of events distributed within a defined narrow interval around a value of P is not a realistic situation for the considered examples, where the experiment may not even reconstruct O and, in general, does not perform the measurement as a function of P. Instead, the experiment observes V and at each event determines its momentum (component) p, so that the sample is characterized by a distribution of p values. However, while fixing P leads to a uniform $\cos\Theta$ distribution, fixing p does not. In fact, for a narrow interval in p, neither the $\cos\Theta$ nor the P distributions are uniform, their ratio being

$$\frac{\mathrm{d}N}{\mathrm{d}\cos\Theta} \Big/ \frac{\mathrm{d}N}{\mathrm{d}P} \equiv \left|\frac{\mathrm{d}P}{\mathrm{d}\cos\Theta}\right| = \begin{cases} \frac{1}{2}\, p \left(1 - (m/M)^2\right) f(\cos\Theta)^{-2} \\ \frac{1}{2}\, p^{-1} \left(1 - (m/M)^2\right) P^2 \end{cases} , \tag{6.18}$$

where the dependence on either $\cos\Theta$ or P has been made explicit.

From this relation we see that, given a value of p, the $\cos\Theta$ distribution could only be uniform (constant $\mathrm{d}N/\mathrm{d}\cos\Theta$) if the sample were chosen with a P distribution of the kind $\mathrm{d}N/\mathrm{d}P \propto P^{-2}$ (and it would be possible to obtain a uniform P distribution, constant $\mathrm{d}N/\mathrm{d}P$, only if $\cos\Theta$ would be distributed as $\mathrm{d}N/\mathrm{d}\cos\Theta \propto f(\cos\Theta)^{-2}$). But the P distribution is obviously not chosen by us: on the contrary, it is precisely what physically determines the p distribution of the event sample under analysis.

In summary, given a collected sample of V particles, how the $\cos\Theta$ distribution of the studied event sample departs from a constant distribution depends on the underlying shape of the unobserved P distribution, that is, on the shape of the observed p distribution. To figure out how, we start by writing the "original" two-dimensional $(P, \cos\Theta)$ distribution as

$$\frac{\mathrm{d}N}{\mathrm{d}P\, \mathrm{d}\cos\Theta} \propto \left(\frac{M}{P}\right)^{\rho} , \tag{6.19}$$

where there is no $\cos\Theta$ dependence (constant distribution) and the P dependence is parametrized with a power-law function, an always reliable shape approximation in a sufficiently narrow kinematic domain. Equation 6.19 means that, in measurements made as a function of the B momentum, the $\cos\Theta$ distribution would remain flat (apart from other perturbing effects) and, thus, a fully smeared J/ψ polarization should be seen (P-independent and negligible λ parameters).

We want to find the corresponding two-dimensional $(p, \cos\Theta)$ distribution, which is the one relevant for the description of an experimental data sample where p, and

not P, is the focus of the measurement. In the variable replacement

$$P \to p = P\, f(\cos\Theta)\,, \quad \cos\Theta \to \cos\Theta \tag{6.20}$$

the measure changes as

$$\mathrm{d}P\, \mathrm{d}\cos\Theta = 1/f(\cos\Theta)\, \mathrm{d}p\, \mathrm{d}\cos\Theta\,, \tag{6.21}$$

so that Eq. 6.19 is transformed into

$$\frac{\mathrm{d}N}{\mathrm{d}p\, \mathrm{d}\cos\Theta} \propto \left(\frac{m}{p}\right)^{\rho} f(\cos\Theta)^{\rho-1}\,. \tag{6.22}$$

Apart from finding an unchanged power-law dependence on momentum, we see from this expression and from the $f(\cos\Theta)$ definition (Eq. 6.17) that the effective $\cos\Theta$ distribution will, in general, depart from a flat or linear shape. Examples of $\cos\Theta$ distributions are shown in Fig. 6.6-left for the cases of the decays $\mathrm{B} \to \mathrm{J}/\psi\,\mathrm{K}$ (top) and $\chi_{c0} \to \mathrm{J}/\psi\,\gamma$ (bottom), for some chosen values of ρ. In their analytical description, the two decays differ only for the value of m/M, which fully determines the shape of $f(\cos\Theta)$. The corresponding $|\cos\Theta|$ distributions,

$$\frac{\mathrm{d}N}{\mathrm{d}\,|\cos\Theta|} \propto \frac{\mathrm{d}N}{\mathrm{d}\cos\Theta}(\cos\Theta) + \frac{\mathrm{d}N}{\mathrm{d}\cos\Theta}(-\cos\Theta)\,, \tag{6.23}$$

are shown in the right panels. As mentioned above, the latter distributions are the ones relevant for the effect under study: whether or not they are flat, and to what degree, determines if we will see a fully smeared or only attenuated polarization in the HX or CS frame approximating the CC frame. The cases $\rho = 1$ and $\rho = 2$ lead, for both decays, to a flat $|\cos\Theta|$ distribution and are not shown in the figure.

The deviation from a flat distribution is larger for larger values of $|\rho - 1|$. It is important to understand that ρ is the (locally defined) "slope" of the p distribution of the collected sample of V particles, affected by experimental acceptance and efficiency effects. Even if the measurement of the dilepton angular distribution implies that the dilepton acceptance and efficiency are taken into account and/or corrected for, and even if the correction of the dilepton events brings the p distribution close to its natural shape, the $\cos\Theta$ distribution, defined in the O rest frame and additionally affected by the acceptance and reconstruction efficiency for X, is, by hypothesis, not observed and cannot, obviously, be corrected. It is, therefore, the "raw" experimental distribution of p that determines the shaping of the $\cos\Theta$ distribution.

For example, as a consequence of the lepton selection criteria (minimum p_{T} requirement) we can expect to see a turn-down shape towards the lowest detected values of p, meaning that ρ can be negative at low p (number of events increasing with p), passing through zero at the maximum of the distribution and changing to positive values at higher p. Correspondingly, with varying p the shape of the $\cos\Theta$ distribution will change, according to Eq. 6.17, from decreasing to increasing, leading to varying degrees of smearing of the polarization observed in the CC (that is, HX or CS) frame.

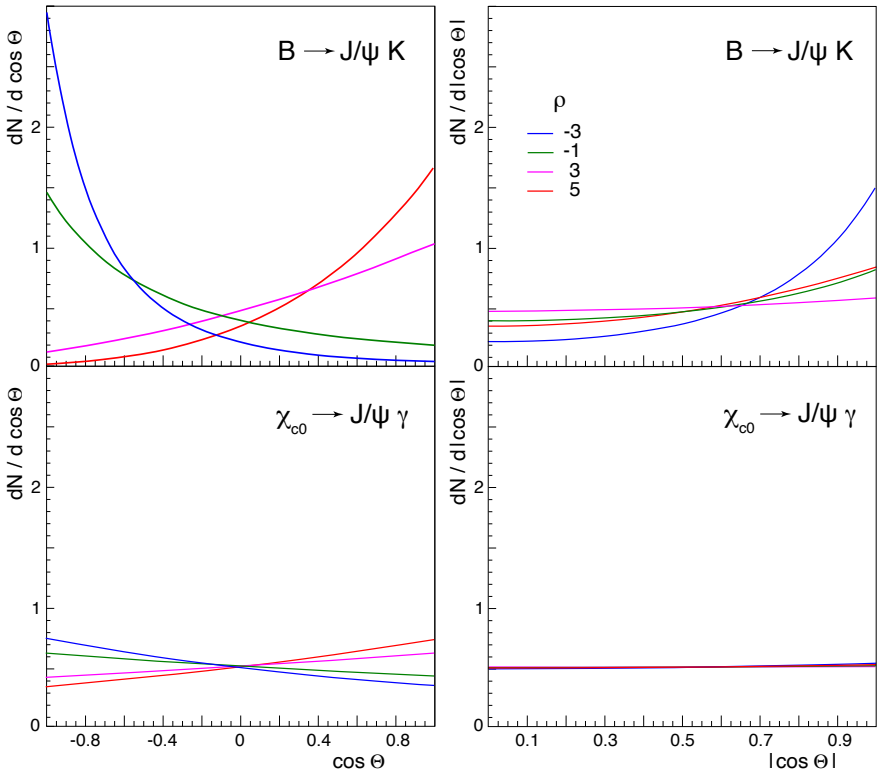

Fig. 6.6 Examples of the underlying $\cos\Theta$ and (corresponding) $|\cos\Theta|$ distributions for the decays B $\rightarrow$ J/ψ K and $\chi_{c0} \rightarrow$ J/$\psi\,\gamma$, when the experiment selects samples of J/ψ mesons having p distributions $\propto (p/m)^{-\rho}$, for different values of ρ.

Effectively, therefore, the smearing of the polarization is strongly influenced by purely experimental features of the measurement, which may be difficult to be accounted for. This fact can lead to disagreements between experiments performing the same measurement with different detectors and selection criteria, as illustrated in the next section.

Equation 6.17 shows another factor that influences the strength of the smearing: the dependence of f on $\cos\Theta$ tends to vanish in the limit $m/M \rightarrow 1$. We expect, for example, a significantly stronger polarization smearing for J/ψ mesons from $\chi_{c0} \rightarrow$ J/$\psi\,\gamma$ than from B $\rightarrow$ J/ψ K, given the proximity of the χ_{c0} and J/ψ masses, as shown by the comparison between the upper and lower panels of Fig. 6.6.

The above description is appropriate for measurements made at a high momentum-to-mass ratio. In particular, in the decay from χ_{c0} the condition of Eq. 6.13, leading to $\mathbf{p} \parallel \mathbf{P}$, is practically always satisfied and the "ordinary" J/ψ HX or CS axis, adopted in the measurement, becomes coincident with the corresponding CC axis over the entire momentum range of the measurement; moreover, for $p_{\mathrm{T}} \gtrsim 10$ GeV

and even at mid rapidity, the analytical relation of Eq. 6.17 is almost exact and the previous discussion should faithfully reproduce the reality. In the case of B decays, a slightly higher threshold in p_{T} and/or $|y|$ is necessary.

Instead, this description does not apply to the typical events produced by decays of the much heavier Higgs boson. The decay $\mathrm{H} \rightarrow \mathrm{J}/\psi\,\gamma$ is the one departing the most from the assumed approximations. It remains true that a smearing of the natural polarization is expected, because the direction of the z axis of the J/ψ HX frame (the observation frame) is certainly not fully correlated with the emission direction of the J/ψ in the Higgs rest frame (natural polarization axis). However, the sizeable J/ψ momentum $p' \simeq M/2 \simeq 62.5$ GeV in the Higgs rest frame must play an important role, determining different observations when the laboratory momentum p is much smaller than, or much larger than, or comparable to p': a complex smearing pattern is expected.

In general, realistic descriptions of the considered decays, moving away from the kinematic approximations mentioned in this section, are important to predict more accurately not only the effects of differences in the masses of the mother and daughter particles but also the transitions between scenarios where the smearing is more or less effective, depending on the laboratory momentum of V and on how the events are selected in the analyses (of measured or simulated event samples). This is the subject of the next section.

6.3 A wide spectrum of possible observations

In this section we will illustrate, using simulated events, a range of possible smearing effects occurring in the polarization measurement of a vector particle produced from the decay of another particle. As described in the previous section, the effects depend, among other things, on the distribution of the V momentum component with respect to which the polarization is measured. In what follows, we have chosen the transverse component, p_{T}. Since the kinematics of V are a direct reflection of those of the mother particle O, to produce a realistic event sample we must use realistic p_{T} distributions for the considered mother particles. The distributions are obtained by interpolating existing quarkonium, B meson and Higgs-boson cross section measurements from LHC experiments, shown in Fig. 6.7 as a function of p_{T}/M. The B meson cross section measured by CDF is also shown, as it will be used for the corresponding prediction in Section 6.5.

As illustrated in the left panel, the quarkonium data, available for seven states (including χ_{c1} and χ_{c2}), do not show deviations from a "universal" p_{T}/M spectrum. This observation allows us to assume, at least for illustration, that this universal shape also characterizes the χ_{c0} and χ_{b0} distributions, for which no data exist. Since a finite-p_{T} V can come from the decay of a "zero"-p_{T} O, especially if the mass difference (that is, p') is large, as in the Higgs decays, it is important that the mother particle is generated in the simulation down to low p_{T}. Extrapolated shapes are used for this purpose, but it must be kept in mind that these are only empirical guesses

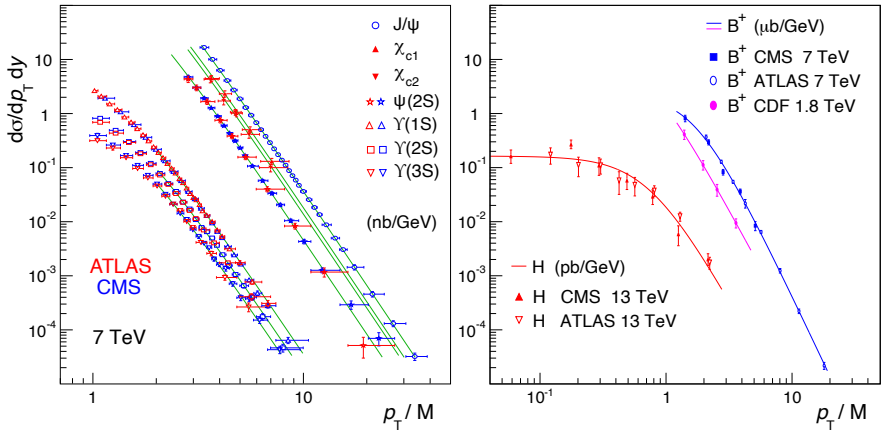

Fig. 6.7 Left: Prompt quarkonium double-differential cross sections, $\mathrm{d}\sigma/\mathrm{d}p_\mathrm{T}\,\mathrm{d}y$, measured at midrapidity, in pp collisions at $\sqrt{s}$ = 7 TeV, by CMS (blue markers) [1, 2] and ATLAS (red markers) [5, 12, 20]. All the green curves have identical shapes and represent the result of a fit to all quarkonium cross sections of $p_\mathrm{T}/M > 2$ [21]. Right: Midrapidity double-differential cross sections for the production of B^+ mesons at $\sqrt{s}$ = 1.8 TeV (pink circles) and at $\sqrt{s}$ = 7 TeV (blue markers), and Higgs bosons at $\sqrt{s}$ = 13 TeV (red markers), measured by CDF [22], ATLAS (open symbols) [23, 24] and CMS (closed symbols) [25, 26]. The curves represent empirical parametrizations.

made in an illustrative context. In the event generation, O decays isotropically into $V + X$ and V to $\mu^+\mu^-$ according to the distribution of Eq. 6.2 in the cHX frame. No approximations are made in the generation of the decay distributions.

We start by analysing the case of J/ψ production from B decays, for which both the "inclusive" and "exclusive" kinds of measurement are realistic experimental options. The inclusive case corresponds to measurements which select samples of J/ψ mesons from $\mathrm{B} \to \mathrm{J}/\psi\, X$ decays by applying a threshold on the distance between the primary and dimuon vertices, thus presumably rejecting all the "prompt" events. Ideally, this selection has no effect on the momentum of the accompanying particle X. Instead, the exclusive measurement selects events where X is identified as (for example) a kaon and its momentum enters, therefore, the domain of acceptance of the detector, here parametrized with the rapidity and p_T selections $|y_\mathrm{K}| < 2.5$ and $p_\mathrm{T}^\mathrm{K} > 1.3$ GeV, representative of those applied in typical analyses of the LHC experiments.

For the modelling of the inclusive scenario we are making a series of simplifying hypotheses that need to be clearly specified. First, we assume that X is a $J = 0$ particle (kaon, pion, eta meson, etc.), conferring a definite "natural" polarization to the J/ψ, longitudinal along the cHX axis, as discussed in Section 6.1, just as in the exclusive case. In reality, $\mathrm{B} \to \mathrm{J}/\psi\, X$ decays include cases where X is a second vector particle or a multi-body system (possibly having an invariant mass that can be significantly larger than the "small" mass of a kaon), and, in the lack of the strong $J(X) = 0$ constraint, the resulting natural polarization can become

less than fully longitudinal: the simulation provides, in this case, an upper limit for the *magnitude* of the observed polarization. Additionally, inclusive non-prompt production actually includes more complex decay chains, where the B meson first decays into a χ_{c1}, χ_{c2} or $\psi(2S)$ meson, which then decays into a J/ψ. Also this kind of further complexity, leading to a reduction in the observed polarization, will be neglected in our illustration.

As a further, more technical note we clarify that we are assuming that the J/ψ is produced in the B decay as a ${}^3S_1$ $c\bar{c}$ state, already having the quantum numbers of the final colour-neutral hadron (core hypothesis of the "colour singlet model", see Section 6.4). However, it can also happen that the J/ψ exits the decay through an intermediate coloured $c\bar{c}$ state,

However, it can also happen that the J/ψ exits the decay through an intermediate coloured $c\bar{c}$ state, possibly having an angular momentum configuration different from the final one (for example, ${}^1S_0$); in this case, the subsequent gluon emission(s) necessary to produce the observable meson will tend to attenuate its observed polarization, so that λ_0 will, also for this kind of contributing mechanism, deviate from its extreme value, -1.

All these simplifications are functional to the purpose of this section, where we want to illustrate the difference between two kinds of observation methods (inclusive vs. exclusive) on the observed polarization, applied to the same underlying process; it is, therefore, important that the physical cascade process is modelled in exactly the same way in the two cases. In Section 6.5 we will revise these assumptions in a more realistic description of the non-prompt case, also in the light of some basic notions, presented in Section 6.4, about the existing hypotheses on the mechanisms of J/ψ production.

The resulting polarization parameters of the J/ψ dilepton decay distribution, λ_ϑ, λ_φ, and $\lambda_{\vartheta\varphi}$, in the HX and CS frames, as well as $\tilde{\lambda}$, are shown in Fig. 6.8 for the inclusive and exclusive measurements. Both cases reveal a strong smearing of the natural longitudinal polarization (represented by the flat green line at $\lambda_\vartheta = -1$). The residual polarizations are, however, quite significant and, furthermore, p_T-dependent. The dashed and dotted lines illustrate the effect of performing the measurement on a sample where the decay muons are required to have minimum p_T values of 5 and 10 GeV, respectively. The application of these thresholds, inspired by selection criteria applied in some typical LHC analyses, leads to non-negligible variations of the obtained patterns.

We note that all the curves considered in the present chapter become asymptotically constant at very high p_T, where, in comparison, the relevant physical scales determining the natural polarization (the masses of mother and daughter particles) become indefinitely small. This also happens because the p_T distributions assumed in our simulation have a definite asymptotical power-law behaviour. The high-p_T flatness of the parameters can be disrupted whenever the p_T distribution changes its power-law slope for whatever reason not considered here, for example because a different production mechanism of the mother particle starts dominating, or in the proximity of a kinematic end point, or as a consequence of experimental selections affecting the high-p_T spectrum. It can be seen, in particular, that the lepton

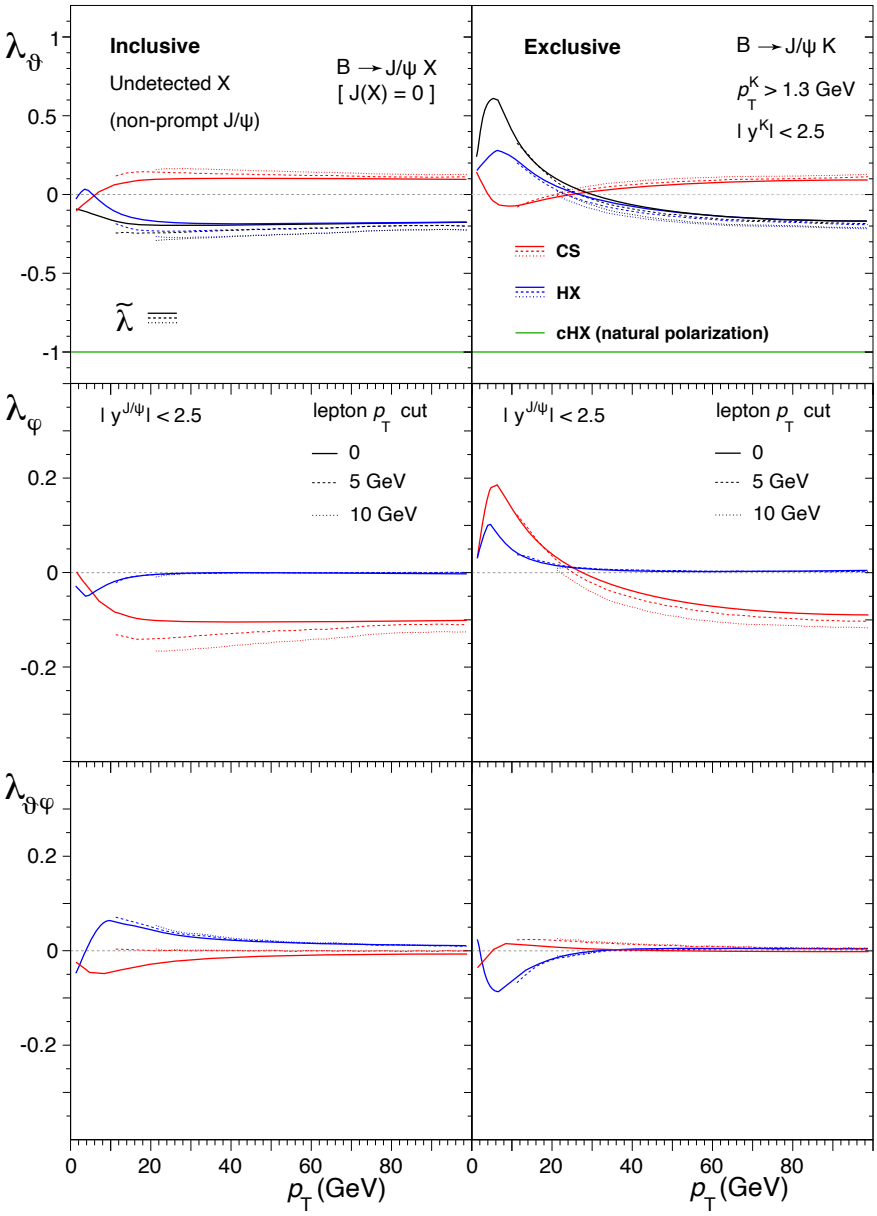

Fig. 6.8 The frame-dependent anisotropy parameters λ_ϑ, λ_φ, and $\lambda_{\vartheta\varphi}$ (top to bottom rows), as well as the frame-invariant parameter $\tilde{\lambda}$ (top row), of the dilepton decay distribution of inclusively observed "non-prompt" J/ψ mesons (left) and of J/ψ mesons observed in fully reconstructed exclusive B decays (right), requiring the detection of the daughter K meson. The results are shown in the HX (blue) and CS (red) frames, as functions of the J/ψ p_T, with no further selection (solid) and when minimum p_T values are required in the analysis for the decay muons (dashed and dotted). The green line represents the natural polarization of the generated events, $\lambda_0 = -1$.

selections and the momentum requirements on X in the exclusive case extend the non-flat behaviour to higher p_{T} values in comparison to the inclusive curves with no experimental selections.

The observed effects can be interpreted in the light of the analytical description made in the previous section. For this purpose we consider the J/ψ p_{T} range 25–30 GeV, where the high-momentum approximation, adopted in that discussion, is well satisfied. Figure 6.9-top shows the p_{T} distribution in the considered interval, well reproduced by a power-law function with best-fit exponent $\rho = 4.7 \pm 0.4$.

The fitted central value of the exponent can be univocally converted (Eqs. 6.17, 6.22 and Fig. 6.6) into the prediction of the $\cos\Theta$ distribution, $f(\cos\Theta)^{\rho-1}$, always meant here, as in the previous section, to be measured in the HX frame. As shown in the middle panel of Fig. 6.9, this prediction is in good agreement with the simulated data for the inclusive case, where no selections are applied to the data. The $|\cos\Theta|$ distribution (shown in the bottom panel of the same figure) is not flat, implying that the smearing effect is only partial and motivating the nonzero observed polarization.

Also the difference between the two experimental approaches can be explained in terms of the $\cos\Theta$ distribution. As seen in Fig. 6.10-top, where the exclusive and inclusive cases are shown by the red and blue histograms, respectively, the additional selection on the K momentum, in particular on p_{T}, further sculpts the distribution in the exclusive measurement, removing events close to $\cos\Theta = +1$. This is, in fact, the configuration where the J/ψ and K are emitted, respectively, forward and backward with respect to the B meson direction and, therefore, where the kaon is most likely to have a laboratory momentum too small to pass the acceptance threshold, so that the event is rejected. The $|\cos\Theta|$ distribution, shown in the middle panel, becomes less sharply unbalanced towards high values when the K momentum selection is applied, that is, its average becomes closer to the average of a uniform distribution, meaning that a fuller smearing should be expected. In fact, a smaller anisotropy is seen in Fig. 6.8, between 25 and 30 GeV, with respect to the inclusive case.

Figure 6.10 also shows, in the bottom panel, how the corresponding $\cos\vartheta$ distributions can be reproduced by integrating the angular distribution W (Eq. 6.8) over $\cos\Theta$. The integration would lead to a flat $\cos\vartheta$ distribution if the $\cos\Theta$ distribution were flat (or linear), while the resulting $\cos\vartheta$ modulation (different in the two cases) is a reflection of how non-uniform the $\cos\Theta$ distribution is. The slightly longitudinal polarization observed in the inclusive case is turned by the K selection criteria into a practically unpolarized result, a coincidence ($\langle\cos^2\Theta\rangle$ turns out to be close to $1/3$ even if the $\cos\Theta$ distribution is not flat nor linear) caused by the fact that inside the considered p_{T} interval the polarization is changing from transverse to longitudinal (as can be seen in Fig. 6.8).

Figures 6.11–6.13 illustrate the effects of requiring minimum p_{T} values on the muons used in the J/ψ reconstruction, referring to the inclusive case. As discussed in Section 2.13 and shown in Fig. 2.18, such requirements strongly sculpt the dilepton distribution. Figure 6.11-left shows the $\cos\vartheta$ distribution, in the HX frame, before (blue) and after (green and red) applying selection cuts on the p_{T} of the muons; the corresponding "acceptance ratios", representing the fraction of events that survive those selection cuts, are presented in Fig. 6.11-right.

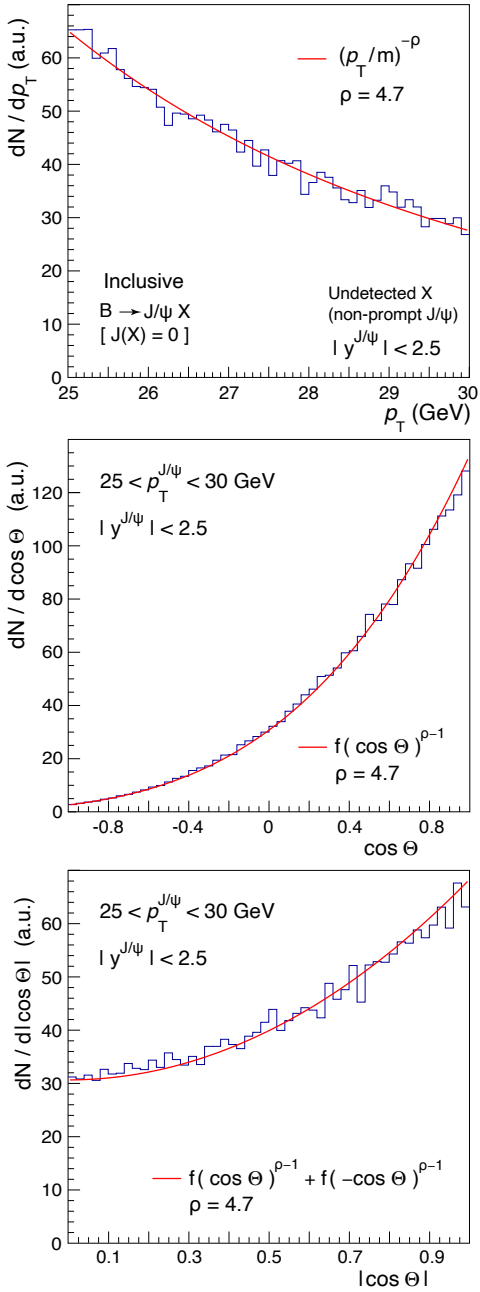

Fig. 6.9 The J/ψ p_{T} distribution (top), as well as the cos Θ (middle) and $|\cos\Theta|$ (bottom) distributions, of simulated B $\rightarrow$ J/ψ X events with unobserved X, for $25 < p_{\mathrm{T}}^{\mathrm{J}/\psi} < 30$ GeV. The exponent ρ, determined by fitting the p_{T} distribution, provides a good analytical description of the angular distributions.

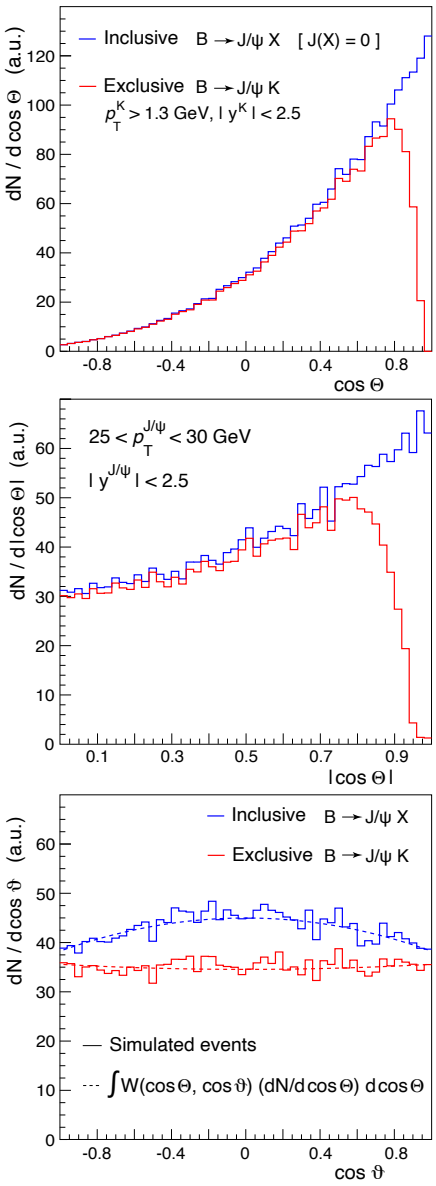

Fig. 6.10 The underlying distributions of $\cos\Theta$ (top) and $|\cos\Theta|$ (middle), in the B HX frame, and the corresponding measured distributions of $\cos\vartheta$ (bottom), in the J/ψ HX frame, for simulated B $\to$ J/ψ X events in the range $25 < p_T^{J/\psi} < 30$ GeV. The blue distributions correspond to measurements using a sample of non-prompt J/ψ events, where X remains unobserved, while the red ones represent analyses of exclusively reconstructed B $\to$ J/ψ K decays, with selection cuts applied on the K momentum. The curves (dashed lines) reproducing the shapes of the $\cos\vartheta$ distributions are obtained by integrating the full angular distribution W (Eq. 6.8) over $\cos\Theta$, taking into account the modulation in the latter distribution.

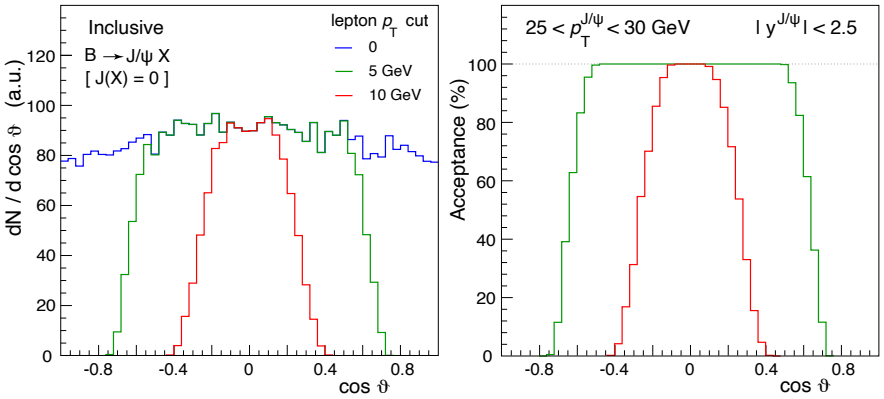

Fig. 6.11 The cos ϑ distribution in the J/ψ HX frame (left), applying (green and red) or not (blue) selection cuts on the p_T of the muons, and corresponding "acceptance ratios" (right), representing the fractions of events surviving the two considered muon p_T cut values.

Naturally, an accurate correction procedure must be applied for the recovery of the physical result. The dashed and dotted lines in Fig. 6.8 indicate the results that an experiment would obtain *after* such corrections have been successfully applied in the data-analysis procedure: they represent the *physical* polarization of the selected sample of J/ψ mesons and their values will always remain, irrespectively of how strong the applied selections are, within the boundaries of the physical domain of the polarization parameters.

Interestingly, however, we see that the obtained polarization result still reflects residual traces of how the sample was selected. This also implies that two experiments applying different selection criteria will obtain different physical results. We could even say, therefore, that there is no such thing as *the* polarization of J/ψ mesons from B decays, at a given collision energy and in given kinematic conditions: the experiment-dependent event selection criteria must concur to an extended definition of the "kinematic domain". This is, actually, a general feature of analyses where the polarization of an indirectly-produced particle is studied ignoring the event-by-event correlations between the mother's and the daughter's decay angles.

Before continuing with the discussion of this interesting and delicate problem, it is worth pausing to explain that these "corrected results" were determined using Eq. 6.9, with the (cos Θ, Φ)-dependent quantities replaced by average values calculated using the events around each considered p_T value. The dilepton decay parameters in the HX (CS) frame are obtained from these relations when the B decay angles in the HX (CS) frame are used for cos Θ and Φ. This procedure assumes that the CC frame can be replaced by the ordinary HX (CS) frame, an approximation valid in the high-momentum limit, with associated uncertainty quantified by Eq. 6.15 (and not applicable, for example, in the study of Higgs decays).

To clarify and explain why experiments applying different selection criteria will obtain different physical results we need to study how the sculpting of the (J/ψ de-

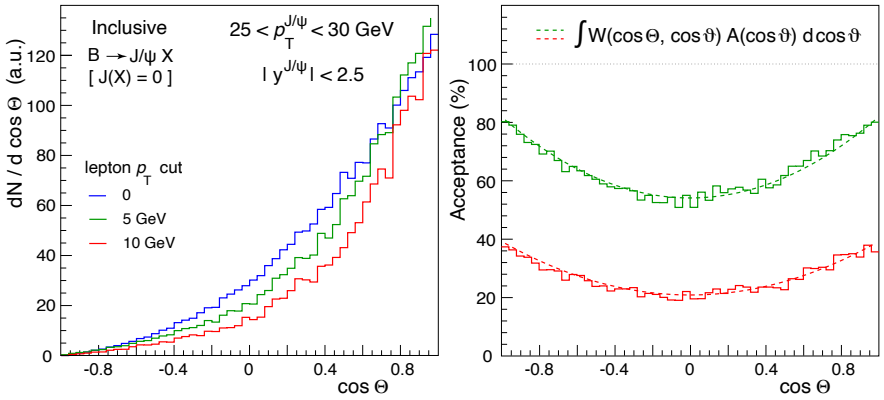

Fig. 6.12 Left: The cos Θ distributions (in the B HX frame) for simulated B $\rightarrow$ J/ψ X events with unobserved X and $25 < p_{\mathrm{T}}^{\mathrm{J}/\psi} < 30$ GeV, before (blue) and after (green and red) rejecting events with muon p_{T} smaller than some cut value. The distributions are arbitrarily normalized, to emphasize the shape differences. Right: Corresponding "acceptance ratios", representing the fractions of events surviving the muon selections. See the text for details on the superimposed curves.

cay) cos ϑ distribution affects the (B decay) cos Θ distribution. The concept is the same as illustrated above for the "inverse" effect of how different cos Θ modulations determine different resulting cos ϑ distributions: the two distributions are intimately correlated and any experiment-induced modification of one will have an effect on the other.

We remind that, in the considered high-momentum limit, the variables cos ϑ defined in the CC and HX frames (being cos Θ here defined in the HX frame) are effectively equivalent, so that the dilepton decay angles appearing in Eq. 6.8 can be calculated in the HX frame.

Figure 6.12-left compares the cos Θ distributions obtained before (blue) and after (green and red) muon selections. They are arbitrarily normalized so that the effect on the shapes can be more easily seen: removing low p_{T} muons induces a loss of events that is more pronounced as cos $\Theta \rightarrow 0$, and the higher is the cut threshold, the bigger is the event loss. The net result, symmetric in cos Θ, is best represented by the acceptance ratios, shown in Fig 6.12-right.

To confirm that it is the sculpting of the observed dilepton cos ϑ distribution that causes this shaping of the unobserved cos Θ distribution, we use the acceptance ratios $A(\cos\vartheta)$ shown in Fig. 6.11-right as weights in the integration of the four-dimensional angular distribution W (Eq. 6.8) over cos ϑ. While we know that a full and uniform cos ϑ coverage would lead to a uniform cos Θ distribution (in the absence of all other effects mentioned above), using the distribution of the actually accepted dimuon events, $A(\cos\vartheta)$, to perform the average over cos ϑ leads to the green and red curves shown in the right panel of Fig. 6.12, which reproduce perfectly well the the shapes of the acceptances as functions of cos Θ. Indeed, we can

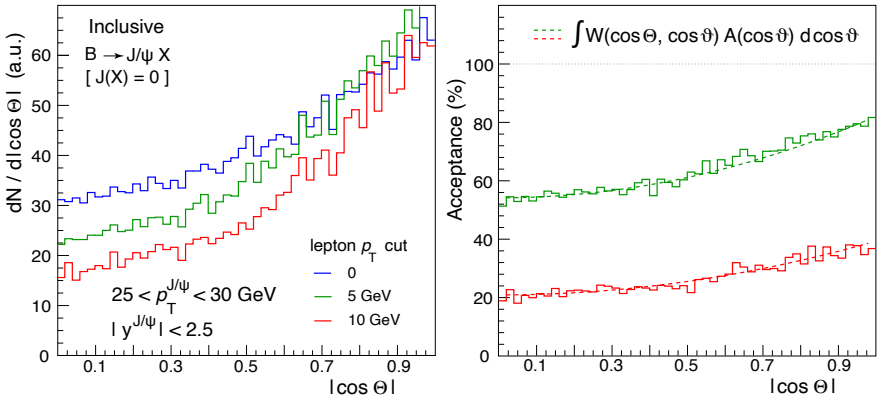

Fig. 6.13 Left: The $|\cos\Theta|$ distributions (in the B HX frame) for simulated $B \to J/\psi\, X$ events with unobserved X and $25 < p_T^{J/\psi} < 30$ GeV, before (blue) and after (green and red) rejecting events with muon p_T smaller than some cut value. The distributions are arbitrarily normalized, to emphasize the shape differences. Right: Corresponding "acceptance ratios", representing the fractions of events surviving the muon selections. See the text for details on the superimposed curves.

conclude that the $\cos\Theta$ modulations induced by the muon selections are a direct reflection of the sculpting of the $\cos\vartheta$ distribution.

As clearly shown by the $|\cos\Theta|$ distributions, and even more visibly by their ratios, both shown in Fig. 6.13, the muon selections accentuate the unevenness of the B decay angular distribution, therefore decreasing the smearing effect and increasing the magnitude of the observed polarization, just as seen in Fig. 6.8. The only way to remove the dependence of the measurement outcome on the event selections specifically applied by the experiment is to adopt a fully four-dimensional analysis approach, taking into account acceptance correlations between the angular variables $(\cos\Theta, \Phi)$ and $(\cos\vartheta, \varphi)$. This is not possible, by definition, when X is not observed (inclusive case) or when the angular analysis is anyhow restricted to its dilepton "projection", as in our definition of the exclusive scenario.

The conclusion of this discussion is that both kinds of measurement should report a full and reproducible definition of the dilepton and single-lepton kinematic phase space where the analysis is made. Two different experimental measurements (or a measurement and a theory prediction) can only be reliably compared if those kinematical constraints are carefully taken into account. In fact, the exact comparison between two results may require detailed simulations of the experimental conditions, including any specific event selections that may affect the $\cos\Theta$ distribution.

As a variation on the theme, Fig. 6.14 shows the result of a simulation of non-prompt $\psi(2S)$ mesons (right panels), made in the same conditions as the J/ψ simulation (left panels). The comparison between the two cases, focusing on the low-p_T region, illustrates the important role of the mother-daughter mass difference. With the decrease of the momentum of the charmonium in the B rest frame, $p' \approx (M_B^2 - M_\psi^2) / (2\, M_B)$, from $p' \simeq 1.7$ GeV for the J/ψ to $\simeq 1.3$ GeV for the $\psi(2S)$,

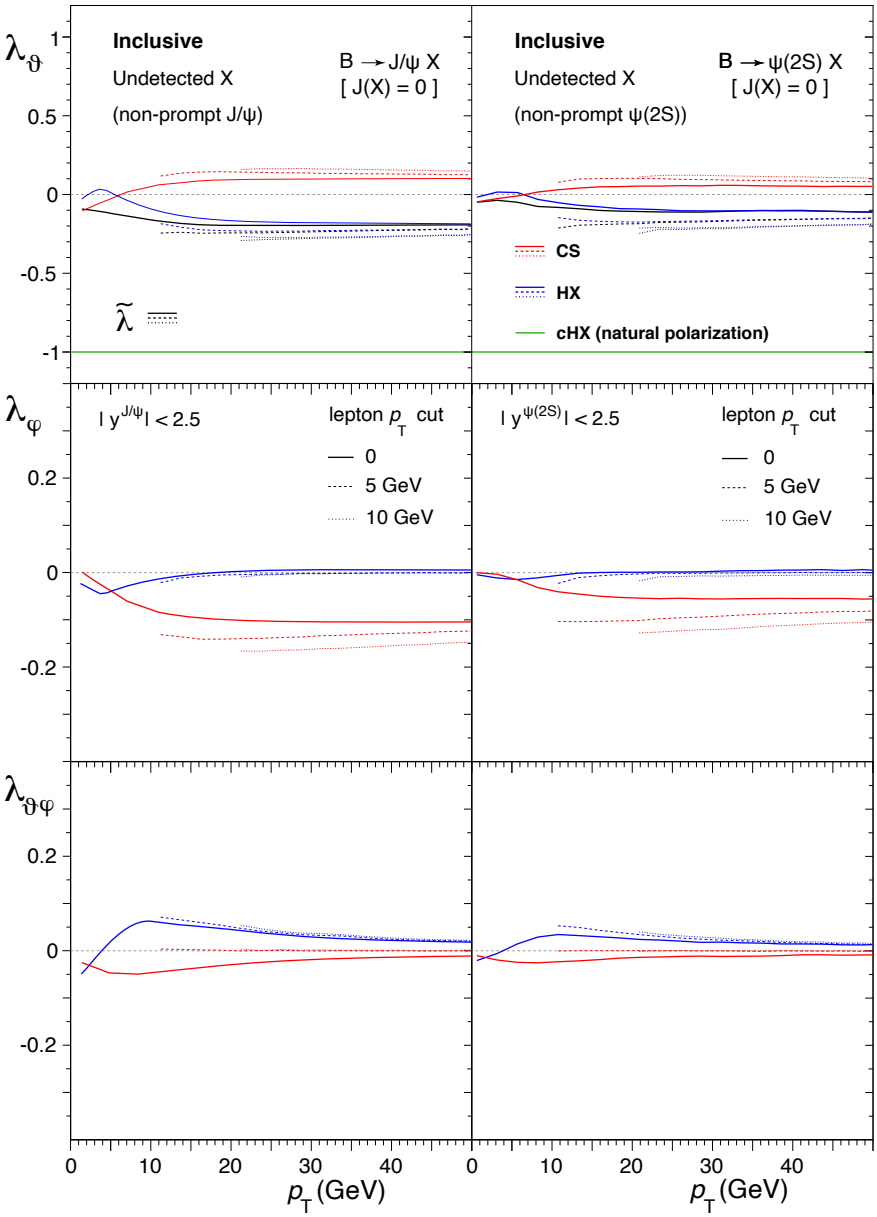

Fig. 6.14 The frame-dependent anisotropy parameters λ_ϑ, λ_φ, and $\lambda_{\vartheta\varphi}$ in the HX and CS frames (top to bottom rows), as well as the frame-invariant parameter $\tilde{\lambda}$ (top row), of the dilepton decay distribution for the inclusive observation of "non-prompt" J/ψ (left) and ψ(2S) (right). The curves (blue, red, and green; solid, dashed and dotted), shown as functions of the p_{T} of the J/ψ or ψ(2S), have the same meaning as those shown in Fig. 6.8. Comparing the non-prompt J/ψ (left) and ψ(2S) (right) patterns illustrates the sensitivity of the results to the difference between the masses of the mother (B mesons) and daughter (J/ψ or ψ(2S)) particles.

the smearing increases significantly and the magnitude of the observed ψ(2S) polarization is only about half of that seen in the J/ψ case.

We turn now to the case of the cascade process $\chi_{c0} \rightarrow \mathrm{J}/\psi\,\gamma$, with $\mathrm{J}/\psi \rightarrow \ell^+\ell^-$, where ℓ represents a muon or an electron. Inclusive and exclusive scenarios are formally defined as previously, except for the selection of the photon in the exclusive case, for which the lower p_{T} threshold of 0.4 GeV is used, as a realistic emulation of typical data analyses in the LHC experiments.

Conceptually, the "inclusive" case no longer represents a realistic measurement, since it is not possible to measure the polarization of J/ψ mesons emitted in χ_{c0} decays without applying selections on the photon momentum to obtain an event sample dominated by χ_{c0} decays. However, the scenario remains interesting, since it depicts the polarization of the (small) fraction of J/ψ mesons coming from χ_{c0} decays in all existing J/ψ polarization measurements, which always address the total "prompt" production, including undistinguished contributions from the feed-down decays of heavier charmonium states. The results for the two scenarios are shown in Fig. 6.15. The differences with respect to the $\mathrm{B} \rightarrow \mathrm{J}/\psi\,X$ case are the input p_{T} distribution, the natural polarization in the cHX frame (transverse, in this case) and, most importantly, the significantly smaller mass difference between mother and daughter particles. In fact, a practically full smearing happens in the inclusive scenario, as anticipated from the almost flat $\cos\Theta$ distributions seen in Fig. 6.6, as a consequence of the sole reduction in mass difference: χ_{c0} decays do give an unpolarized contribution to the inclusive prompt J/ψ production. However, the selection of events with minimum photon p_{T} leads to a slight polarization, according to the mechanism described above for the B decays.

The difference between the χ_{c0} feed-down contribution to inclusive J/ψ polarization and the measured polarization of J/ψ coming from χ_{c0} decays may be at first sight counter-intuitive, but becomes comprehensible as a consequence of the two different selection criteria applied to the $\chi_{c0} \rightarrow \mathrm{J}/\psi\,\gamma$ events. Even if small, the difference is conceptually non-negligible.

While radiative χ_{c0} decays actually play a minor role in J/ψ production, because of their small branching ratio, the decays from χ_{c1} and χ_{c2} produce a fraction of order 25% of the observed J/ψ mesons [27]. It should not be forgotten that a mismatch between the contribution to inclusive polarization and the exclusive polarization of J/ψ from χ_{c1} and/or χ_{c2} has to be expected and should, in principle, be taken into account when "subtracting" the latter from the total inclusive result to deduce the polarization of the directly produced J/ψ mesons. This problem will be addressed in the next sections.

One may wonder what happens if we change the masses of *both* the mother and the daughter particles. As shown in Fig. 6.16 for the exclusive measurement, going from the charmonium to the bottomonium system, which implies an increase in the masses by a factor of three, does not lead to significantly different smearing patterns. The relevant parameter is not the absolute mass of each of the two particles but rather the mass difference or, more precisely, the p' value, which remains in this case rather similar, only changing from 0.30 to 0.39 GeV. The inclusive case is

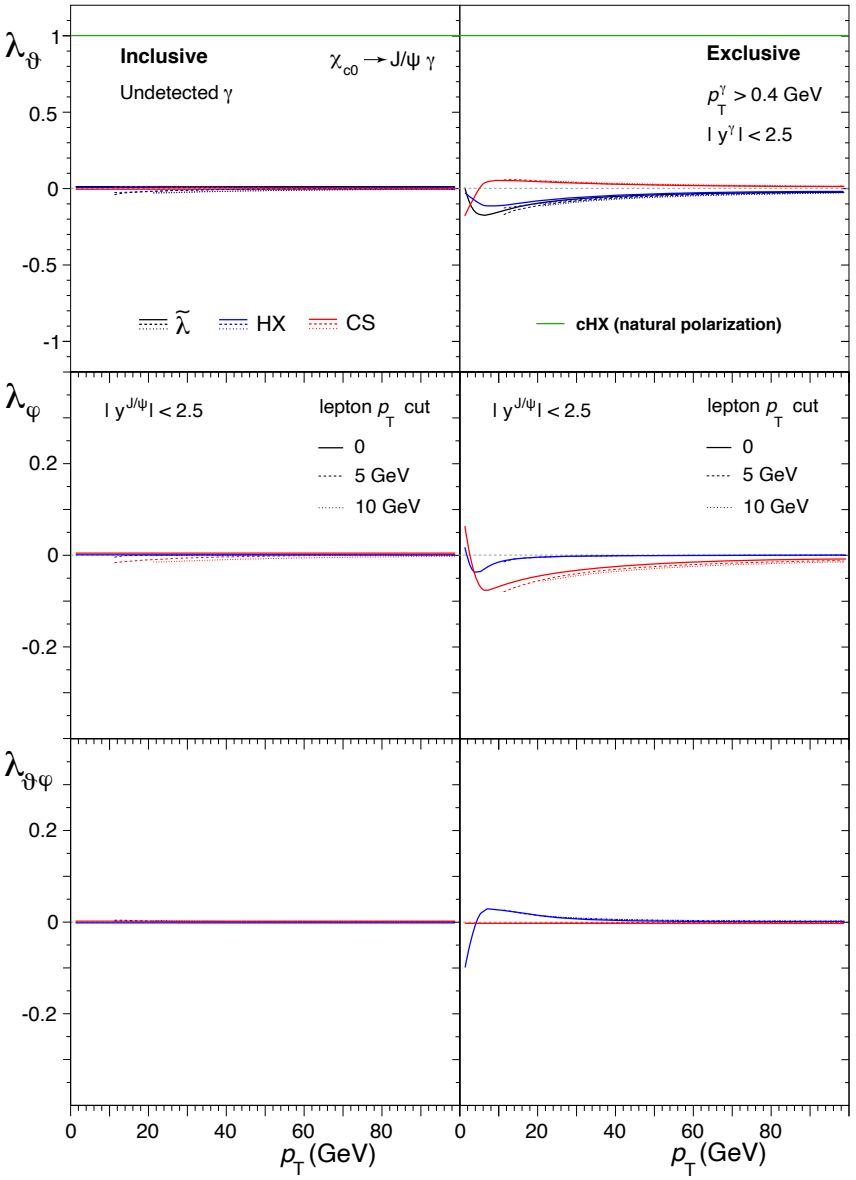

Fig. 6.15 The frame-dependent anisotropy parameters λ_ϑ, λ_φ, and $\lambda_{\vartheta\varphi}$ in the HX and CS frames (top to bottom rows), as well as the frame-invariant parameter $\tilde{\lambda}$ (top row), of the dilepton decay distribution of J/ψ mesons produced in the radiative decays of χ_{c0} mesons, as functions of the J/ψ p_T. The curves (blue, red, and green; solid, dashed and dotted), shown as functions of the p_T of the J/ψ, have the same meaning as those shown in Fig. 6.8, the natural polarization of the generated events being $\lambda_0 = +1$. The inclusively observed J/ψ mesons (left) show essentially no polarization, while those selected by fully reconstructing the exclusive decays (right), requiring the detection of the radiated photon, do not suffer from a full rotational smearing and, hence, lead to a slight, p_T-dependent polarization.

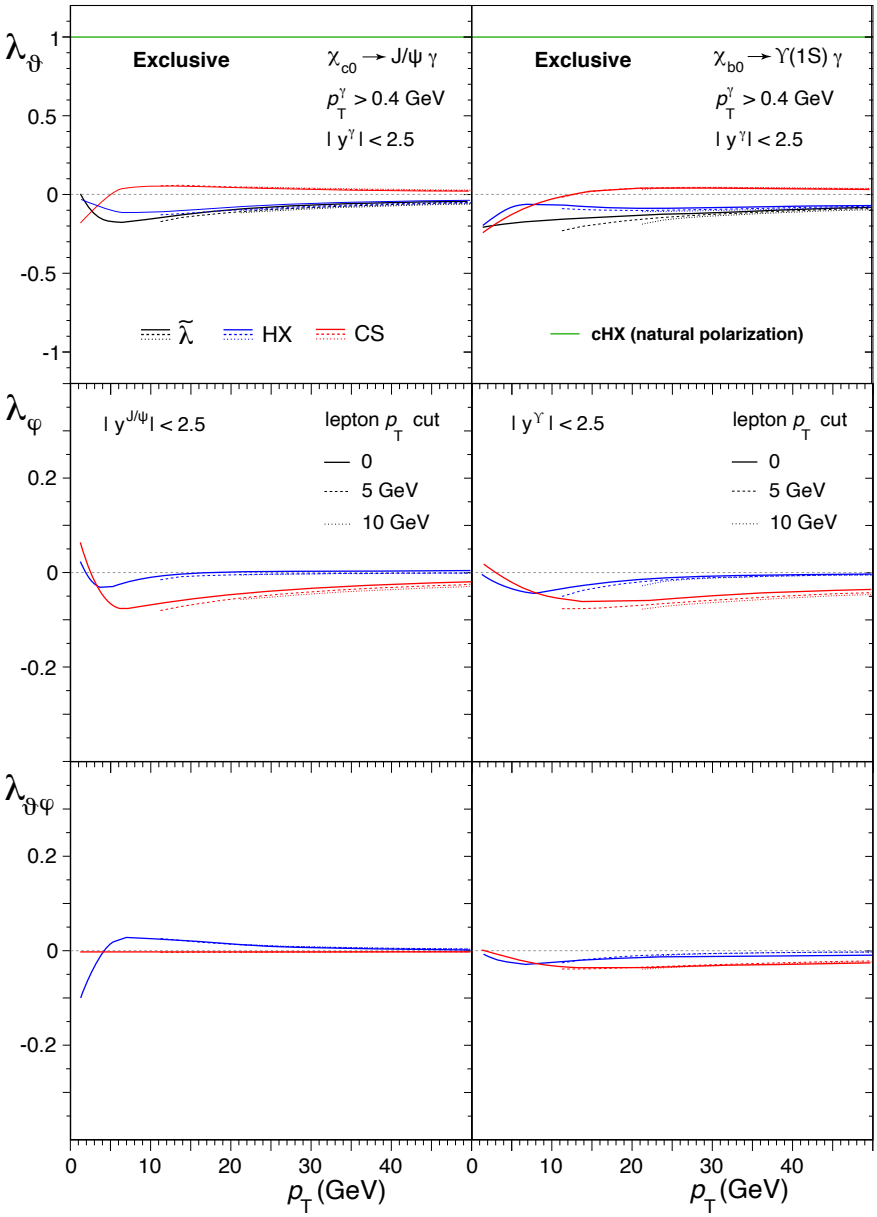

Fig. 6.16 The frame-dependent anisotropy parameters λ_ϑ, λ_φ, and $\lambda_{\vartheta\varphi}$ in the HX and CS frames (top to bottom rows), as well as the frame-invariant parameter $\tilde{\lambda}$ (top row), of the dilepton decay distribution of J/ψ (left) and Υ(1S) (right) mesons observed in fully reconstructed exclusive radiative decays of χ_{c0} and χ_{b0} mesons, respectively. The curves (blue, red, and green; solid, dashed and dotted), shown as functions of the p_T of the J/ψ or Υ(1S), have the same meaning as those shown in Fig. 6.15. Comparing the J/ψ and Υ(1S) patterns illustrates the sensitivity of the results to the difference between the masses of the mother and daughter mesons.

omitted in the comparison given its simplicity: the contribution of $\chi_{b0}(1P)$ decays to inclusive $\Upsilon(1S)$ production remains fully unpolarized.

Finally, Fig. 6.17 shows the results of an exclusive simulation of the decays $H \to J/\psi\,\gamma$ and $H \to Z\,\gamma$, with the requirement that the photon has a minimum p_T of 15 GeV, a realistic value for analyses of experimental data. While in the previous examples p' was smaller than the minimum dilepton momentum accessible to the experiment, now its value falls inside the measured p_T spectrum ($p' \simeq 62$ and 29 GeV, respectively), creating complex polarization patterns. The most significant polarization magnitude is seen, with a resonance-like effect, for $p_T \simeq p'$, as well as in the limit $p_T \to 0$ for the $H \to J/\psi\,\gamma$ case. The decay with larger mass difference produces the less smeared polarization, even approaching the fully transverse limit of the natural one, as shown by the variable $\tilde{\lambda}$, which combines the polar and azimuthal anisotropies.

The decay with larger mass difference produces the less smeared polarization, even approaching the fully transverse limit of the natural one, as shown by the variable $\tilde{\lambda}$, which combines the polar and azimuthal anisotropies. The decay $H \to \Upsilon\,\gamma$ leads to a Υ polarization of a magnitude similar to that of the J/ψ, given the negligible decrease in p' value.

6.4 The unique case of J/ψ production

We have discussed how the observation of an unpolarized (or almost unpolarized) vector particle is indeed possible: the particle must be produced *indirectly*, in the decay of a heavier $J = 0$ particle, which the experiment is unable to fully reconstruct or decides to not take into account in a multi-dimensional angular study, to minimize the complexity of the analysis. The cancellation between oppositely polarizing production processes remains an alternative possibility as explanation of an unpolarized observation, even if it is not only improbable, but also reasonably limited to a restricted transition domain between kinematic regions where individual processes dominate. Most often, different production mechanisms tend to be charactrized, for example, by different p_T distributions. In fact, the existence of concurring processes having exactly opposite polarizations and otherwise indistinguishable kinematic properties should rather be interpreted as the existence of deeper underlying symmetries than those conjectured in the production model.

There is one case where a vector particle appears to be produced unpolarized, even when produced *directly*: the J/ψ meson, as observed by LHC experiments [32]. While at first sight this phenomenon seems to pose a serious challenge to the considerations exposed above, in reality, and as we will see in this section, it provides the most paradigmatic example of what we have discussed in the previous sections.

In fact, the "promptly produced" J/ψ mesons (i.e. after subtracting the contribution from B meson decays) are mostly produced directly: the feed-down decays of the $\psi(2S)$ and χ_c states are responsible for, respectively, around 8 and 25% of the J/ψ yield [27], and the corresponding polarizations are known or constrained exper-

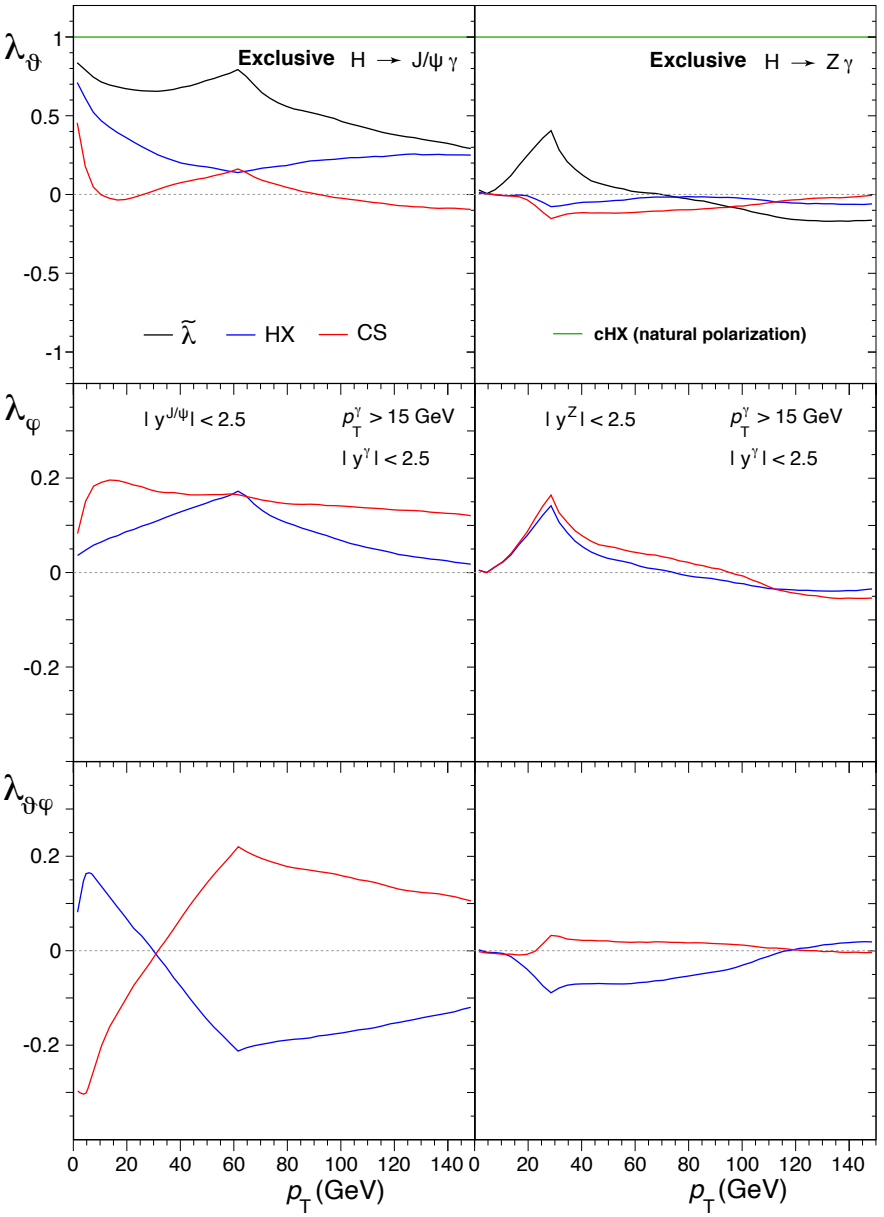

Fig. 6.17 The frame-dependent anisotropy parameters λ_ϑ, λ_φ, and $\lambda_{\vartheta\varphi}$ in the HX and CS frames (top to bottom rows), as well as the frame-invariant parameter $\tilde{\lambda}$ (top row), of the dilepton decay distribution of J/ψ mesons (left) and of Z bosons (right) produced in the decays of Higgs bosons, and selected by fully reconstructing the exclusive decays. The parameters are shown as functions of the p_{T} of the J/ψ or Z.

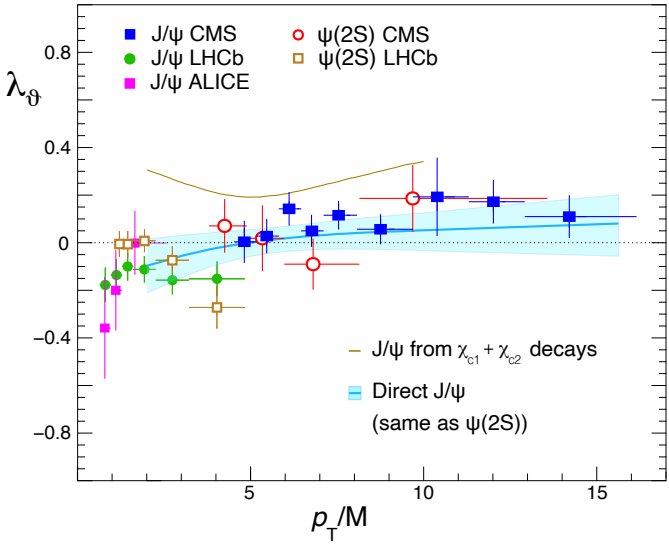

Fig. 6.18 Measurements of J/ψ and ψ(2S) polarizations (λ_ϑ in the HX frame) from LHC experiments [28–31]. The band represents the best-fit result for the polarization of the *directly* produced J/ψ, obtained in a global analysis of charmonium data [32], including χ_c cross sections [12–14] and constraints on the polarization of the J/ψ mesons emitted in χ_c decays [19].

imentally. Moreover, its radial excitation, the ψ(2S) state, is always produced directly, presumably by the same partonic processes as the direct 1S state, and shows a similar polarization pattern: above a certain p_{T} both states are very close to the unpolarized conditions, with no significant kinematic dependence.

Figure 6.18 shows the J/ψ and ψ(2S) polarizations measured by LHC experiments [28–31], as well as the result of a global data fit analysis [32] that also uses experimental constraints on the polarizations of J/ψ mesons emitted in χ_{c1} and χ_{c2} decays [19], providing a reasonably precise determination of the *direct* J/ψ polarization: above $p_{\mathrm{T}}/m \simeq 3$ the J/ψ is produced unpolarized over a wide range of laboratory momentum, making the hypothesis of a polarization cancellation implausible.

The mechanism behind the production of vector quarkonia has always been a matter of debate. The conceptually simplest idea, that a $c\bar{c}$ pair is produced by the parton scattering process as an already colour-neutral state in the "right" spin-angular-momentum configuration $^3S_1$ ("colour singlet' model" [35]), underestimates by a large factor the J/ψ and ψ(2S) production yields seen in hadron collider experiments. This data-to-theory discrepancy was originally seen in the mid-1990's by CDF [36, 37]. Figure 6.19 provides a more modern illustration of this observation by showing the data-theory comparison for the two states, as measured at the LHC [1, 20] and as computed in perturbative QCD at next-to-leading order [33, 34].

While for the J/ψ case part of the large discrepancy can be attributed to the contribution from (prompt) feed-down decays of heavier quarkonia, which corresponds to around one third of the total prompt cross section and is not considered in the cal-

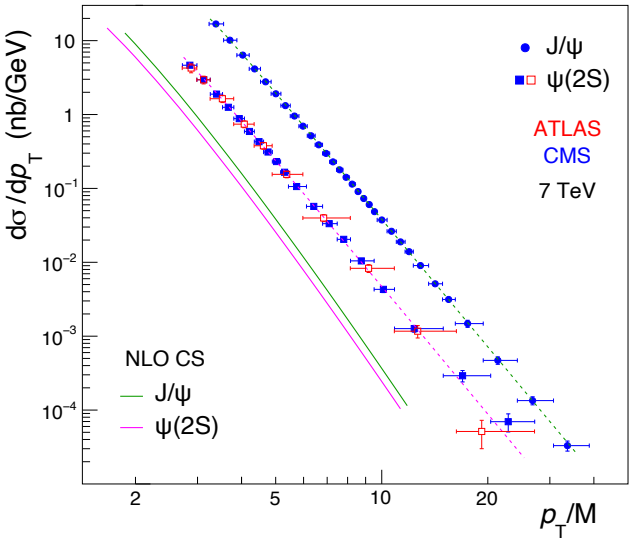

Fig. 6.19 The J/ψ and ψ(2S) production cross sections, as measured at the LHC [1, 20] compared with the next-to-leading order (NLO) predictions of the colour-singlet model [33, 34].

culated curves, the ψ(2S) comparison is free from those contaminations, justifying why the early results became known as "the CDF ψ(2S) anomaly". Clearly, there must exist additional sources of quarkonium production, besides colour-singlet production, dominating at least in high-energy collisions and at high p_T. Also in the mid-1990's, an improved and more general quarkonium production model was developed: the non-relativistic QCD (NRQCD) approach [38].

In NRQCD, the J/ψ (or the ψ(2S)) bound state is considered in its superposition of Fock states, consisting not only of a simple $c\bar{c}$ pair, but also of combinations of $c\bar{c}$ pairs with gluons (or light $q\bar{q}$ pairs):

$$\begin{aligned}\left|\psi\left({}^3S_1\right)\right\rangle \;=\; & a_{{}^3S_1^{[1]}}\left|c\bar{c}\left({}^3S_1^{[1]}\right)\right\rangle \\ & +\; a_{{}^3P_0^{[8]}}\left|c\bar{c}\left({}^3P_0^{[8]}\right)\,g\right\rangle \;+\; a_{{}^3P_1^{[8]}}\left|c\bar{c}\left({}^3P_1^{[8]}\right)\,g\right\rangle \;+\; a_{{}^3P_2^{[8]}}\left|c\bar{c}\left({}^3P_2^{[8]}\right)\,g\right\rangle \\ & +\; a_{{}^3S_1^{[8]}}\left|c\bar{c}\left({}^3S_1^{[8]}\right)\,gg\right\rangle \;+\; a_{{}^1S_0^{[8]}}\left|c\bar{c}\left({}^1S_0^{[8]}\right)\,gg\right\rangle \;+\; \ldots\end{aligned} \tag{6.24}$$

The first term, representing an already colour-neutral (singlet) state and having the spin and angular momentum quantum numbers of a vector particle, is the dominant one. In each term of the remaining expansion only the $c\bar{c}$-gluon(s) combination must be colour neutral; the $c\bar{c}$ pair itself is, in general, coloured ("octet" state) and can have any spin and angular momentum quantum numbers, provided that it combines with the gluon(s) into a ${}^3S_1$ state.

The colour-octet terms are suppressed by powers of v, the velocity of the c quark in the $c\bar{c}$ rest frame, which is assumed to be only moderately relativistic. In fact, the

kinetic energy $T \simeq mv^2$ of the bound state is estimated as $T \approx 0.4$–0.6 GeV from the energy splittings between radial and orbital angular momentum excitations of the quarkonium system, which are very similar for charmonium and bottomonium. For the J/ψ, the lightest of the vector quarkonia, v is the largest, at around 0.4.

The probability that the final-state hadron has been produced as the result of the transition from an initial octet $c\bar{c}$ state is evaluated to be of order v^4 smaller than the probability that it came from a singlet $c\bar{c}$. This means that, if in a given experiment $c\bar{c}$ pairs were produced with the same probability in the ${}^3S_1^{[1]}$ singlet as in any octet state, the production via colour-octet $c\bar{c}$ would be responsible for only a few percent of the observed J/ψ mesons, and an even smaller fraction should be expected for the three-times heavier Υ mesons coming from coloured $b\bar{b}$ pairs ($v^4 \approx 10^{-3}$).

These proportions are opposite to what is necessary to explain the LHC observation of cross sections one order of magnitude larger than the singlet-only ones. However, perturbative calculations confirm that the existence of colour-octet processes represents a solution to the problem: the partonic cross sections for the production of colour-octet $c\bar{c}$ pairs are orders of magnitude larger than the colour-singlet one and their inclusion completely overturns the proportion, leading to predicted quarkonium yields dominated by the octet processes.

Furthermore, octet mechanisms offer a potential and interesting solution to another problem of the colour-singlet model: the singlet channel alone leads to a practically fully polarized J/ψ [39], as is the case of all mechanisms producing vector particles directly, a prediction in clear contradiction with the quarkonium polarization measurements made at the LHC.

The production via colour-octet quark-antiquark states is a perfect example of what happens in a cascade process where the mother state is unobserved and, at the same time, the daughter's mass is only slightly smaller than the mother's. The mass difference between the octet state and the physical quarkonium must be, in fact, of the same order as the typical splittings of the mass spectrum (of the order of 0.5 GeV). If the mother happens to be a $J = 0$ state, a complete smearing of the polarization should be expected, in analogy with the $\chi_{c0} \to \mathrm{J}/\psi\,\gamma$ and $\chi_{b0} \to \Upsilon\,\gamma$ decays seen in the previous section (inclusive case). For example, the ${}^3P_0^{[8]} \to \mathrm{J}/\psi\, g$ transition is completely equivalent to the $\chi_{c0} \to \mathrm{J}/\psi\,\gamma$ decay and leads to an unpolarized J/ψ, considering that the gluon is not observed. The most relevant $J = 0$ octet state is, however, the ${}^1S_0^{[8]}$ one. Even if its transition to J/ψ has a more complex topology because it involves the emission of (at least) two gluons and the natural J/ψ polarization in the ${}^1S_0^{[8]}$ rest frame is not easily characterized, the resulting dilepton decay distribution is isotropic. In fact, it should be clear from the considerations in the previous sections that the full rotational smearing occurring for small mass differences with respect to a $J = 0$ mother state is a pure consequence of the flatness of the $|\cos\Theta|$ distribution and is independent of the value of λ_0. Above all, however, it is important to remember that the condition that the mother is a $J = 0$ state remains the most crucial one for the explanation of the observed unpolarized production. Other octet terms, for example the ${}^3S_1^{[8]}$ one, lead, instead, to a full polarization, transverse in this case. It is, therefore, important to determine which of the octet terms are actually significant.

Each individual octet contribution to the cross section includes a non-perturbative constant factor (the long-distance matrix element, LDME), representing the probability of transition from the considered coloured $c\bar{c}$ state to the J/ψ and considered to be "universal", that is, independent of the nature of the short-distance partonic process and equal, for example, in hadroproduction, photoproduction or in indirect production via decays of heavier particles. The LDMEs have not yet been theoretically calculated, and their values are currently determined in the very process of theory-data comparison, through global fit analyses [33, 40–46].

All octet LDMEs corresponding to the terms shown in Eq. 6.24 are equally "small", of order v^4 smaller than the singlet LDME (as discussed above with other words), and it would not be surprising if one of these "corrective" terms were actually dominating over the others: this could not be reasonably considered as a failure of the v hierarchy, which is only an order-of-magnitude expectation. However, a reliable answer to the question of how the octet terms actually compare to one another in magnitude is only recently and gradually coming to light. After several years of difficulties and contradictory or even puzzling results shown by theory studies of the experimental data [47], the results of recent global-fit analyses comparing NRQCD calculations with experimental measurements show that the ${}^1S_0^{[8]}$ octet mechanism is indeed the dominant contribution to direct J/ψ production in high-energy hadron colliders [21, 48–50].

While the explanation of the unique and puzzling observation of the unpolarized production of the J/ψ meson, as a directly produced vector particle, is the result of a long path of understanding, we could, a posteriori, look at the problem from a different perspective and realize that this polarization measurement has always been implying, by itself, an almost unequivocal physical indication: in the considered conditions, the J/ψ must have a "two-step" production mechanism, where the intermediate stage is a $J = 0$ state. This is a good example of how polarization measurements can provide deep insights into the underlying physics.

It remains true that the J/ψ case is rather special and results from concurrent causes. Despite being a "heavy quarkonium" state, the J/ψ is rather light and the v hierarchy does not penalize the octet terms with respect to the singlet ones as it could happen for heavier states. For example, it will be interesting to see if future high-precision polarization measurements for the Υ states will show the same p_{T}-independent lack of polarization or will rather denote the presence of more competing processes by showing a non-negligible kinematic variation. Above all, the overwhelming importance of partonic processes producing octet quark-antiquark pairs is a peculiarity of direct quarkonium production in hadron collider experiments.

This dominance of octet processes does not seem to be present in low-p_{T} measurements made in fixed-target experiments, which actually show significant polarizations of vector quarkonia, as seen in Section 5.4.

It is also reasonably absent in several cases of indirect production, a clear example being when the parent particle (with its constituents) and the accompanying particles have zero colour charge, as in the previously considered $\mathrm{H} \rightarrow \mathrm{J}/\psi\,\gamma$ case, so that the gluon emissions enabling the transformation of a coloured $c\bar{c}$ into the final observable state cannot be reabsorbed within the isolated process. For similar

reasons, the purely electromagnetic transitions from χ_c states do not involve intermediate octet states. In fact, in these examples (as considered in Section 6.3 and in the following Section 6.6), the J/ψ does have a strong natural polarization, potentially observable by choosing the cHX frame. The non-prompt production of J/ψ is a more complex case, as denoted by the several simplifying assumptions we adopted for its description in Section 6.3, and will be further discussed in the next section.

Another counterexample is the production of vector quarkonia in the electromagnetic process $e^+e^- \to Q\overline{Q}$ (with $Q = c, b$), where the quark-antiquark pair is formed through a virtual photon as a colour singlet state and is fully transversely polarized, as shown by the BES experiment [51]. In summary, the unpolarized production of J/ψ mesons in high energy proton-proton collisions is an exceptional observation resulting from exceptional circumstances.

6.5 Non-prompt charmonium production

In the comparison between the two measurement scenarios discussed in Section 6.3 for the polarization of J/ψ mesons emitted in B decays we assumed that the non-prompt J/ψ events, addressed by the "inclusive" measurement without observing or selecting a specific accompanying state X, are due to decays of the kind B $\to$ J/ψ K (with K possibly replaced by another relatively light $J = 0$ state), just as in the "exclusive" measurement, which explicitly selects these decays through additional requirements on the X = K candidates. In reality, non-prompt events result from a spectrum of different B decay channels. In this section we want to address this problem and provide a more realistic description of the phenomenon.

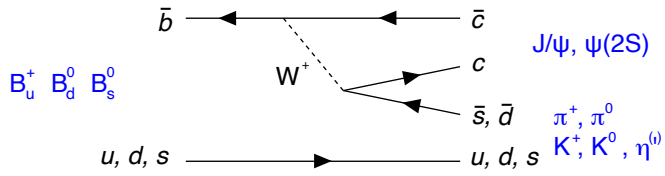

Fig. 6.20 Feynman diagram for the decay B $\to$ J/ψ X, with X = K, π or η.

In an exclusive two-body decay as, for example, B $\to$ J/ψ X, with X = K, π or η, it is reasonable to assume that the formation of the J/ψ bound state often happens through the colour-singlet mechanism, where the decay, represented in Fig 6.20, produces a $c\bar{c}$ state that is already a colour neutral $^3S_1$ state [52, 53]. In fact, the production of an intermediate coloured state (with possibly different quantum numbers) would imply its subsequent emission of soft gluons, necessary for the colour neutralization into a physical hadron; these gluons should then recombine with the spectator quark of the B meson, to form exactly the "right" accompanying particle X, for example a kaon: the probability that this happens should be relatively small.

However, intermediate octet $c\bar{c}$ states are also expected to contribute to the "cocktail" of decay configurations composing the sample of non-prompt events. These cases generally lead to "multi-body" final states, where X is a system of two or more particles (for example, two or more pions). Complex final states are also produced by multiple decay chains, of the kind $\mathrm{B} \to \chi_{c1}/\chi_{c2}/\psi(2\mathrm{S})\,X$, with, for example, $\chi_{c1}/\chi_{c2} \to \mathrm{J}/\psi\,\gamma$ and $\psi(2\mathrm{S}) \to \mathrm{J}/\psi\,\pi^+\pi^-$.

From the point of view of the expected J/ψ polarization, as it can be measured in an inclusive analysis, the variety of the processes described above can be reduced to two categories: the one of the two-body B decays where X is a single kaon (or another relatively light particle) and $J(X) = 0$ (or, more generally, the J/ψ has a natural longitudinal polarization), and the one represented by the ensemble of all the remaining $\mathrm{B} \to \mathrm{J}/\psi$ decays, mostly including multi-body configurations and complex cascade sequences. We will denote these two cases with the expressions "two-body" and "multi-body".

The relevant differences between the two kinds of processes can be summarised as follows. 1) While the J/ψ has a maximally longitudinal natural polarization ($J_{z'} = 0$ in the cHX frame) when it comes from the two-body decays (given how we defined them), the multi-body case represents a mixture of several decays, favouring, in general, all kinds of J/ψ $J_{z'}$ projections: a significantly reduced polarization magnitude is, hence, expected. 2) For the two-body case, the hypothesis that X is, for instance, a kaon or a pion determines the value of the J/ψ momentum p' in the B rest frame, which is one of the parameters determining how the natural polarization is "smeared" when observed, for example, in the J/ψ HX frame. In Eq. 6.12, the second, approximate relation shows that any relatively light X leads to the same $p' \simeq 1.7$ GeV. Instead, in multi-body decays the invariant mass m_X of the accompanying system assumes a distribution of values, possibly significantly larger than the mass of a kaon, and p' is smaller. Also this effect, increasing the uniformity of the smearing (as seen in Section 6.3 when the mother-daughter mass difference, hence p', are smaller), should lead to a smaller observable polarization.

To quantify the importance of these different properties, we will examine results reported by the CLEO [54] and BaBar [55] experiments, which measured the momentum distribution of J/ψ mesons, daughters of B^+ and B^0 mesons produced "almost at rest" in the decay of the $\Upsilon(4\mathrm{S})$ resonance. To interpret these measurements, shown in Fig. 6.21, we will first have a look at some kinematic relations. The B mesons have a momentum of only 0.33 GeV in the $\Upsilon(4\mathrm{S})$ rest frame, and, therefore, the J/ψ momentum (p) distribution measured in the $\Upsilon(4\mathrm{S})$ "laboratory" is a slightly smeared version of the one observed in the B rest frame (p'). The mathematical relations between p' and p, and between m_X and p, are shown in the top and middle panels of Fig. 6.22, where the blue dashed lines represent the hypothetical limit case where the B meson is produced exactly at rest, that is, $p = p'$ (and the relation between m_X and p is simply the one described by Eq. 6.12), while the coloured bands describe the effect of the momentum smearing produced by the small boost of the B meson in the laboratory. The red lines indicate the case of the specific decay $\mathrm{B} \to \mathrm{J}/\psi\,\mathrm{K}$. It can be seen that, for masses comparable to or lighter than the one of a kaon, the p range does not change significantly: we can assume, therefore, that

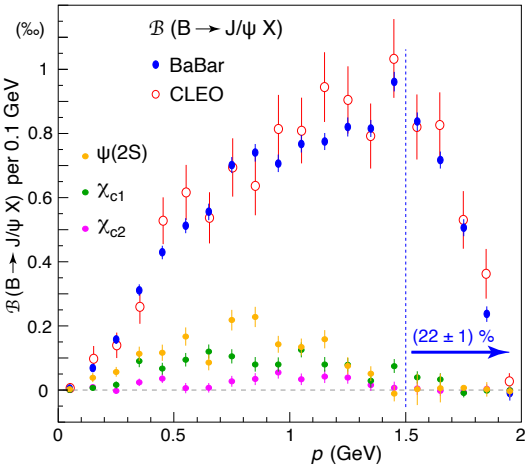

Fig. 6.21 Laboratory momentum distribution of J/ψ mesons emitted in decays of B mesons that are themselves produced by Υ(4S) decays. Besides the inclusive spectrum, the individual contributions (measured by BaBar) from the feed-down decays B $\to [\chi_{c1}|\chi_{c2}|\psi(2S)]\,X$ are also shown.

the ensemble of two-body decays, with $m_X \lesssim 0.5$ GeV, is responsible for the events with $p \gtrsim 1.5$ GeV. The measured p distribution (Fig. 6.21) shows that a large part of the spectrum covers a domain complementary to this, clearly indicating the important role of multi-body decays. For example, the decay chains B $\to \chi_{c1} \to$ J/ψ, B $\to \chi_{c2} \to$ J/ψ, and B $\to \psi(2S) \to$ J/ψ, individually determined by BaBar and also shown in Fig. 6.21, contribute mostly to the region $p < 1.5$ GeV.

In these experimental conditions, very different from those of LHC measurements, it also happens that the polarization measured in the HX frame, that is, taking the direction of **p** as polarization axis, will tend to be very close to the one measured in the cHX frame, with polarization axis along **p′**, given the similarity of the two momenta. Figure 6.22-bottom shows how λ_ϑ is smeared in the HX frame with respect to the hypothetical natural polarization cases $\lambda_\vartheta^{\rm cHX} \equiv \lambda_0 = -1, -0.6$, and -0.2. The first case corresponds to our hypothesis for the two-body processes: the full longitudinal polarization for $p > 1.5$ GeV remains practically unsmeared. BaBar reported the values $\lambda_\vartheta^{\rm HX} = -0.196 \pm 0.044$ for $p < 1.1$ GeV and -0.592 ± 0.032 for $p > 1.1$ GeV. The former value, in the low-p region, refers to multi-body configurations, with no contamination from two-body ones. In Fig. 6.22-bottom we see that the polarization smearing for the case closest to this, $\lambda_\vartheta^{\rm cHX} = -0.2$, leads to a difference $\lambda_\vartheta^{\rm HX} - \lambda_\vartheta^{\rm cHX}$ of order 0.01 on average, considering that the bulk of the events has $0.4 < p < 1.1$ GeV. We will, therefore, assume the range from -0.25 to -0.15 for the average natural polarization of the J/ψ mesons produced in multi-body decays.

As a cross check, we can try to interpret the result in the high-p region, which reflects a mixture of two-body and multi-body events. Assuming, for simplicity, that all the events in the range $p > 1.5$ GeV are due to two-body processes, we derive that these processes contribute $(40 \pm 1)\%$ of the events in the $p > 1.1$ GeV region.

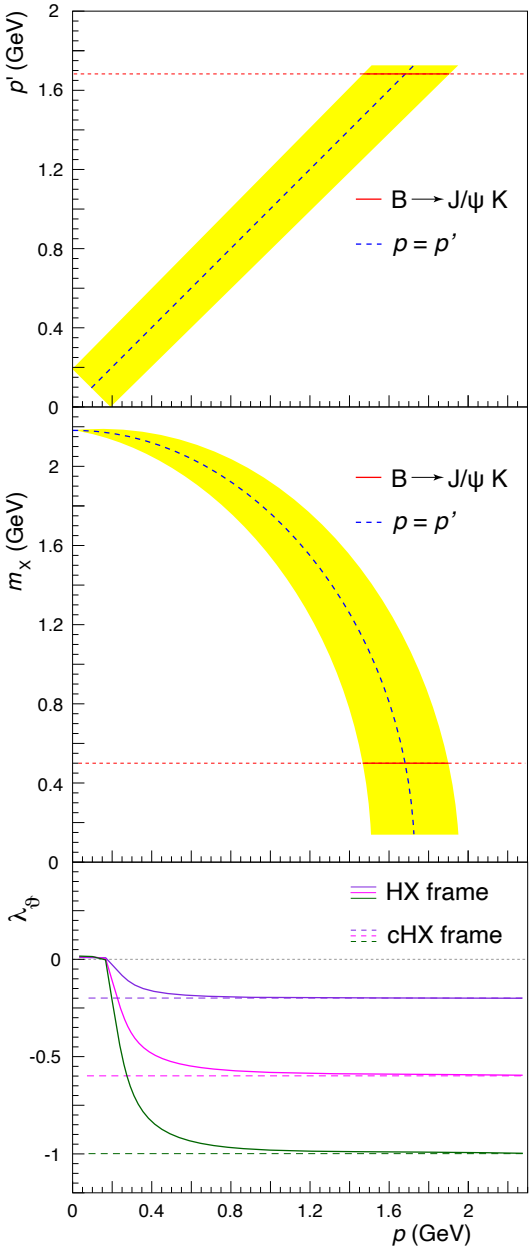

Fig. 6.22 Relations between kinematic variables used in the description of the process $B \to J/\psi X$. Top: momentum smearing from the B rest frame (p') to the $\Upsilon(4S)$ rest frame (laboratory, p). Middle: invariant mass of the X system as a function of p. The $p = p'$ limit is indicated by the blue dashed line, while the red line describes the $B \to J/\psi$ K case. Bottom: polarization smearing from the cHX to the HX frame, for three different natural polarizations: $\lambda_\vartheta^{\mathrm{cHX}} \equiv \lambda_0 = -1$ (green), -0.6 (pink), and -0.2 (purple).

Assuming $\lambda_\vartheta^{\mathrm{cHX}} = \lambda_\vartheta^{\mathrm{HX}} = -0.592 \pm 0.032$ for the average natural polarization of the mixture in the broader range (where the smearing is completely negligible, as seen in Fig. 6.22-bottom) and taking $\lambda_\vartheta^{\mathrm{cHX}}$ between -0.25 and -0.15 for the subsample of multi-body decays, the sum rule of Eq. 1.17, inverted, leads to a value between -1.1 and -0.9 for the two-body polarization, which is in perfect agreement with our assumption that this category of processes leads to fully longitudinal J/ψ mesons.

We will now convert this information, derived from measurements made at the Υ(4S) resonance, into realistic expectations for the non-prompt J/ψ polarization as measurable in a high-energy collider experiment. Here the B meson, generally produced with a large laboratory momentum, emits the J/ψ almost collinearly (Eq. 6.13), so that the HX axis adopted for the observation of the dilepton decay loses its correlation to the natural (cHX) one, and a significantly smeared polarization is observed, as we saw in Section 6.3.

From the spectra measured by BaBar and CLEO, shown in Fig. 6.21, and assuming that the transition from multi-body to two-body events happens at $p \simeq 1.5$ GeV, we see that the fraction of two-body events is $f_{2-\mathrm{body}} = (22 \pm 1)\%$. However, the relative contribution of two- and multi-body processes in (high-energy) hadron collisions is probably not the same as the one observed in the conditions of BaBar and CLEO, given that a different admixture of parent hadron species containing b quarks (additionally including B_s mesons and b baryons) contributes to the non-prompt J/ψ sample. Moreover, it should be kept in mind that, at least hypothetically, certain event selection criteria may alter the proportions between the two kinds of processes in the collected and/or analysed sample, given that, in general, a multi-body event should lead to a higher number of particles traversing the detector. It would be very interesting, in fact, to probe experimentally if the polarization of the non-prompt J/ψ mesons tends to become more significantly longitudinal when stricter selection criteria are applied to retain an event sample that corresponds more closely to the two-body decay limit. For these reasons, besides the realistic mixture using $f_{2-\mathrm{body}}$ we will also report the predictions for the two-body and multi-body individual cases. The measurement itself should be able to consider the two physical options and determine their relative contributions.

The two-body expectation is obtained, as was done in Section 6.3, assuming $\lambda_\vartheta^{\mathrm{cHX}} = -1$ and $m_X = m_K = 0.5$ GeV. For the multi-body case, from the p distribution of Fig. 6.21 and the m_X-to-p correlation shown in Fig. 6.22-middle, we deduce that the 1–2 GeV range of average m_X values is a good representation of the spectrum of physical possibilities. Taking into account that a higher m_X value leads to a more strongly smeared polarization in the experimental frames, we can define reasonable upper and lower margins for the observable polarization magnitude: they correspond, respectively, to the pairs of parameter values $\lambda_\vartheta^{\mathrm{cHX}} = -0.15$, $\langle m_X \rangle = 2$ GeV and $\lambda_\vartheta^{\mathrm{cHX}} = -0.25$, $\langle m_X \rangle = 1$ GeV. The only existing measurement in the case of hadron collisions was performed by CDF [56], which reported λ_ϑ in the HX frame as a function of p_{T}. As shown in Fig. 6.23, where the predictions reflect the specific conditions of the experiment ($|y| < 0.6$), the precision of the data is not sufficient to indicate if one or the other mechanism is predominant. The intermediate prediction assumes the same mixture of processes as in the Υ(4S)

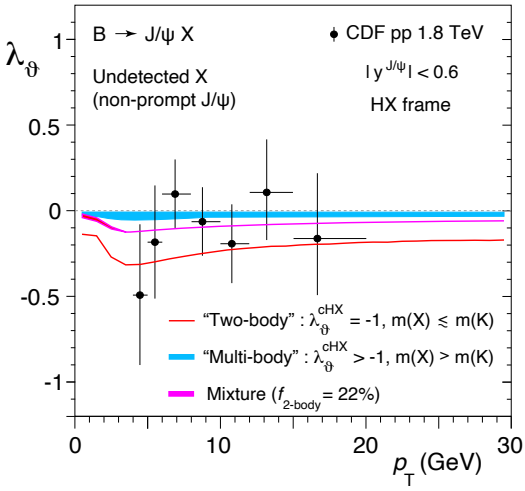

Fig. 6.23 The non-prompt J/ψ polarization (λ_ϑ in the HX frame) measured by CDF in $p\bar{p}$ collisions at $\sqrt{s} = 1.8$ TeV, as a function of p_T, in the rapidity range $|y| < 0.6$, compared to predictions assuming that the J/ψ is produced in "two-body" (red curve) or "multi-body" (blue band) B decays, the width of the band reflecting the variation of the relevant parameters, $\lambda_\vartheta^{\rm cHX}$ and $\langle m_X \rangle$. The pink band represents a mixture of the two kinds of processes, as motivated in the text. The B meson p_T distribution measured by CDF (Fig. 6.7) was used in the simulation. For improved visibility, curves including the small effects of the selection criteria applied to the decay leptons are not shown.

measurements. The multi-body prediction is compatible with the (octet-dominated) NRQCD calculations of non-prompt J/ψ polarization reported in Refs. [57, 58].

Figure 6.24 shows the predictions of all parameters, in the HX and CS frames, calculated for conditions typical of a LHC experiment, already considered in Section 6.3; in fact, the curves for the two-body case were already shown in Fig. 6.8 (we do not report again the lepton selection effects, which are invisible in the multi-body case). The J/ψ mesons produced in multi-body decays look practically unpolarized, This also means that this prediction is, in substance, insensitive to the assumptions made to obtain it: further adjustments in the input parameters $\lambda_\vartheta^{\rm cHX}$ and $\langle m_X \rangle$ are unlikely to change the conclusion that multi-body decays lead to a barely detectable degree of polarization. The almost p_T-independent difference with respect to the polarization of the two-body case, $\Delta\lambda_\vartheta^{\rm HX} \simeq 0.2$, is not negligible, so that some LHC experiments should be able to perform significant measurements of the relative importance of the two kinds of processes.

6.6 Decays from $J > 0$ particles and the "cloning" effect

Among the physical examples considered in Section 6.3, the decay $\chi_{c0} \to$ J/$\psi\,\gamma$, followed by J/$\psi \to \ell^+\ell^-$, illustrates in a paradigmatic way, by virtue of the small

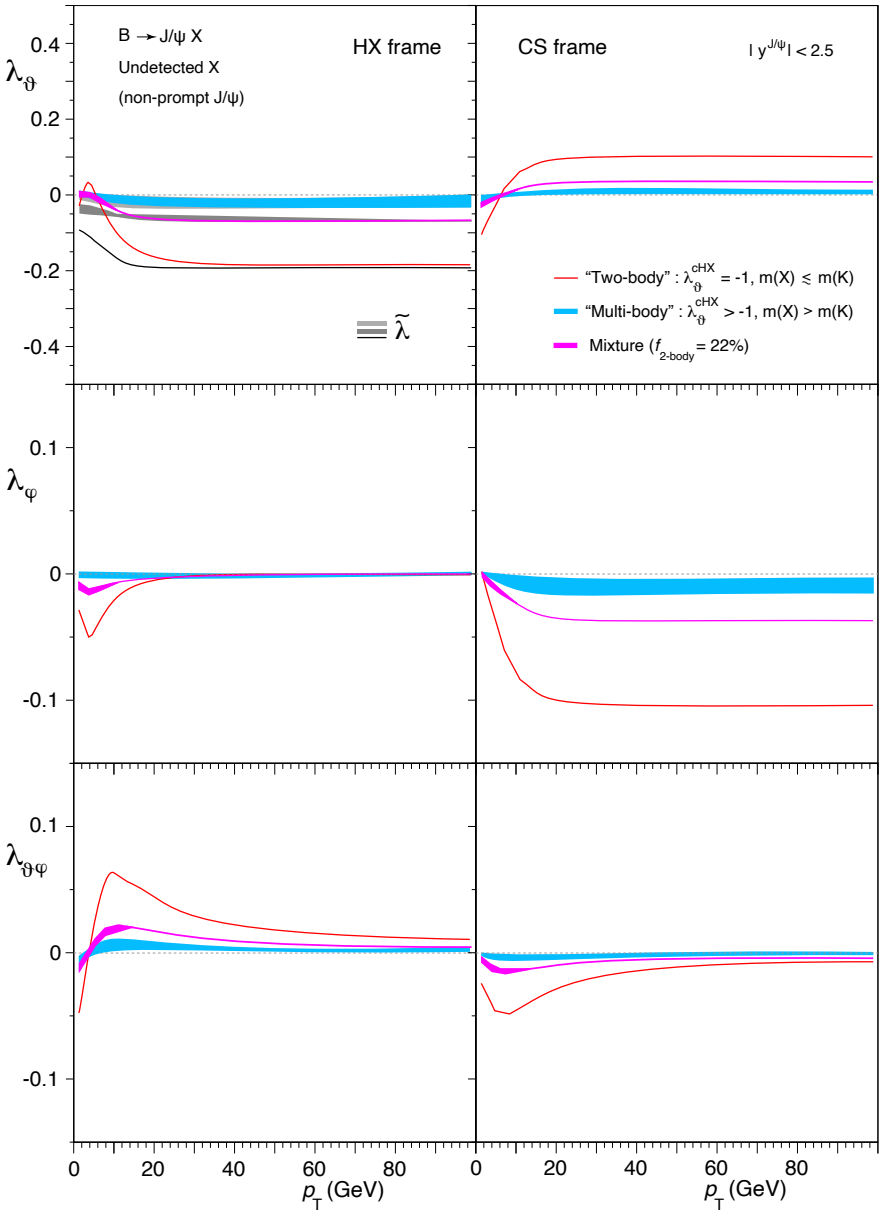

Fig. 6.24 The frame-dependent anisotropy parameters λ_ϑ, λ_φ, and $\lambda_{\vartheta\varphi}$ (top to bottom rows), as well as the frame-invariant parameter $\tilde{\lambda}$ (top row), of the dilepton decay distribution of inclusively observed "non-prompt" J/ψ mesons, in the two complementary assumptions that the J/ψ is produced in "two-body" B decays (same curves as in Fig. 6.8) or in "multi-body" B decays (blue bands, their widths representing the variation of the relevant input parameters, $\lambda_\vartheta^{\mathrm{cHX}}$ and $\langle m_X \rangle$). The pink bands represent a mixture of these two kinds of processes, as motivated in the text. The results are shown in the HX (left) and CS (right) frames, as functions of the J/ψ p_{T}.

mass difference between the χ_{c0} and J/ψ mesons, the randomization effect leading to a zero-polarization contribution in the inclusive dilepton observation. In this section we address its $J = 1$ and 2 counterparts, the χ_{c1} and $\chi_{c2} \to \mathrm{J}/\psi\,\gamma$ decays, as prototype cases to illustrate how the previous considerations can be extended to a wider category of cascade processes, by releasing the crucial $J = 0$ condition. Just as seen in the $J = 0$ case, the following discussion also applies to the bottomonium counterparts, $\chi_{b1,2} \to \Upsilon\,\gamma$.

We should reasonably expect to see, in these cases, a generally polarized vector quarkonium, reflecting the J_z state of the χ. In fact, the first step is to generalize Eq. 6.7, by introducing the sum over the amplitudes a_M defining the angular momentum state of the mother particle O with respect to the system of axes (x, y, z) of Fig. 6.3, with M representing the eigenvalues:

$$|\,O\,\rangle = \sum_{M=-J}^{+J} a_M\,|\,J,\,M\,\rangle_z\ . \tag{6.25}$$

Figure 6.4 provides a visual aid also for the description of this case. The general amplitude for the description of the two-step process is

$$\begin{aligned}\mathcal{A}\Big[\,O \to V + X_{K'},\ V \to (\ell^+\ell^-)_{L'''}\Big]\ \propto\\ \sum_{M=-J}^{+J} a_M \sum_{L''=0,\pm1} \sum_{K''=0,\pm1} {}_{z''}\langle V\,X; 1, L'',\ 1, K''\,|\,\mathcal{B}|\,O; J, M\rangle_{z''}\\ \times\,\mathcal{D}^{1*}_{K''\,K'}(\Theta,\Phi)\,\mathcal{D}^{1*}_{L''\,L'''}(\vartheta,\varphi)\ ,\end{aligned} \tag{6.26}$$

where $\mathcal{B}$ represents the underlying dynamics of the decay. In the radiative transition we are studying, we just have to take into account that the $J_{z''}$ projections of V (L'') and X (K'') must sum to M, because the z'' and z axes represent the same direction in the definition of the CC frame:

$$\begin{aligned}\mathcal{A}\Big[\,O \to V + X_{K'},\ V \to (\ell^+\ell^-)_{L'''}\Big]\ \propto\\ \sum_{M=-J}^{+J} a_M \sum_{L''=0,\pm1} \sum_{K''=0,\pm1} \langle 1, L'',\ 1, K''\,|\,J, M\,\rangle\,\delta_{L''+K'',\,M}\\ \times\,\mathcal{D}^{1*}_{K''\,K'}(\Theta,\Phi)\,\mathcal{D}^{1*}_{L''\,L'''}(\vartheta,\varphi)\ .\end{aligned} \tag{6.27}$$

Moreover, the squared amplitude must be summed over $K' = \pm1$ ($J_{z'}$ projection of X = photon over the cHX z' axis of Fig. 6.1; corresponding to setting $\lambda_0 = +1$ in the formulas for the $J = 0$ case) and $L''' = \pm1$ (dilepton decay of V).

In reality, we are making an approximation in the derivation of the anisotropies of the χ_c and subsequent J/ψ decays. In these transitions the photon emission is sensitive to the internal electromagnetic charge structure of the quarkonium state. As a result, the photon can effectively have an orbital angular momentum component and, therefore, a total angular momentum of up to $J_\gamma = 2$ (in $\chi_{c1} \to \mathrm{J}/\psi\,\gamma$) and up to $J_\gamma = 3$ (in $\chi_{c2} \to \mathrm{J}/\psi\,\gamma$). To account for the contributions of these higher

J_γ values, the total amplitude should be calculated summing also over J_γ, using the corresponding photon $\mathcal{D}$ matrix and the Clebsch–Gordan coefficients for $J \to (J = 1) + J_\gamma$, and the partial amplitudes would now have a dependence on J and J_γ, contained in the matrix elements of $\mathcal{B}$. However, these effects can be neglected, since they only cause a small change of the values of the anisotropy parameters [59] and do not have a significant influence in the illustrative considerations that follow.

The resulting expression of the four-dimensional angular distribution for the most generic χ_{c1} angular momentum state of Eq. 6.25, depending on the complex amplitudes a_M, can be found in Appendix B. The corresponding χ_{c2} distribution is not included in that appendix because its much more complex expression extends over almost two pages, without offering particularly original insights into the properties of the observable polarization. Here we report the much simpler distributions produced by the χ_{c1} and χ_{c2} mesons when they are pure eigenstates of J_z, i.e., $|J,\, M\rangle_z$:

$$W_{\mathrm{CC}}(\cos\Theta, \Phi, \cos\vartheta, \varphi) \propto \tag{6.28}$$

$$\begin{cases} (1+\cos^2\Theta)(1+\cos^2\vartheta) - \sin^2\Theta\,\sin^2\vartheta\,\cos2(\varphi-\Phi) & \text{for } \chi_{c1}\,,\ M=0\,, \\ 1-\cos^2\Theta\cos^2\vartheta - \frac{1}{4}\sin2\Theta\,\sin2\vartheta\,\cos(\varphi-\Phi) & \text{for } \chi_{c1}\,,\ M=\pm1\,, \\ 9\,(1+\cos^2\Theta\cos^2\vartheta) - 7\,(\cos^2\Theta+\cos^2\vartheta) + \\ \sin^2\Theta\,\sin^2\vartheta\,\cos2(\varphi-\Phi) - 2\sin2\Theta\,\sin2\vartheta\,\cos(\varphi-\Phi) & \text{for } \chi_{c2}\,,\ M=0\,, \\ 1-\cos^2\Theta\cos^2\vartheta + \frac{1}{4}\sin2\Theta\,\sin2\vartheta\,\cos(\varphi-\Phi) & \text{for } \chi_{c2}\,,\ M=\pm1\,, \\ (1+\cos^2\Theta)(1+\cos^2\vartheta) & \text{for } \chi_{c2}\,,\ M=\pm2\,. \end{cases}$$

As already noticed for the $J = 0$ case, the distribution is in all cases invariant by exchange between $(\cos\Theta, \Phi)$ and $(\cos\vartheta, \varphi)$. The origin of the symmetry is in fact visible in the amplitude of Eq. 6.28, where L'' and K'' are completely equivalent as running variables of two identical sums (with the Clebsch–Gordan coefficient reflecting the commutative property of the sum) and, therefore, exchanging the upper and lower case angles is equivalent to exchanging L''' with K'. As long as the square amplitude is summed over the same set of values for L''' and K' (±1, in this case), the exchange has no effect on the final result.

Figure 6.25 gives an intuitive illustration of the symmetry. The adopted frame (Fig. 6.3) has *one* set of axes providing the reference directions for both angular distributions, the one of the photon (and J/ψ) emission in the χ_c rest frame and the one of the dilepton emission in the J/ψ rest frame. In this situation, it is evident from the figure that exchanging the "names" of γ and $\ell^+\ell^-$ (i.e., the blue and green colours), two equivalent objects from the point of view of angular momentum, only modifies the individual event configuration, but not the resulting event distribution.

Equation 6.28 can be translated into a form that uses the coefficients of the dilepton distribution (similarly to what was done in Eq. 6.9), as measured in the CC frame (coinciding, in the case considered, with the corresponding laboratory-referred frame, HX or CS) and as functions of Θ and Φ. The λ_ϑ, λ_φ, $\lambda_\varphi^\perp$, $\lambda_{\vartheta\varphi}$, and $\lambda_{\vartheta\varphi}^\perp$ parameters are reported in Table 6.1, including the χ_{c0} case (Eq. 6.9 with $\lambda_0 = +1$).

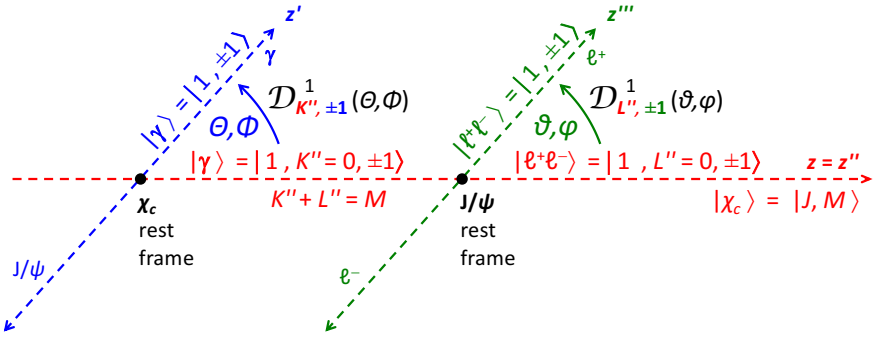

Fig. 6.25 Illustration of the origin of the $(\Theta, \Phi) \rightleftarrows (\vartheta, \varphi)$ exchange symmetry for the angular distribution of the cascade decay $\chi_{cJ} \to \mathrm{J}/\psi\,\gamma$, followed by $\mathrm{J}/\psi \to \ell^+\ell^-$.

Table 6.1 The (Θ, Φ)-dependent J/ψ decay anisotropy parameters for the cascade process $\chi_{cJ} \to \mathrm{J}/\psi\,\gamma$, $\mathrm{J}/\psi \to \ell^+\ell^-$, when the χ_{cJ} is an eigenstate of J_z with eigenvalue M.

	χ_{c0}	χ_{c1}		χ_{c2}		
	$(M=0)$	$M=0$	$M=\pm1$	$M=0$	$M=\pm1$	$M=\pm2$
λ_ϑ	$\frac{-1+3\cos^2\Theta}{3-\cos^2\Theta}$	$+1$	$-\cos^2\Theta$	$\frac{-7+9\cos^2\Theta}{9-7\cos^2\Theta}$	$-\cos^2\Theta$	$+1$
λ_φ	$\frac{\sin^2\Theta\cos 2\Phi}{3-\cos^2\Theta}$	$\frac{-\sin^2\Theta\cos 2\Phi}{1+\cos^2\Theta}$	0	$\frac{\sin^2\Theta\cos 2\Phi}{9-7\cos^2\Theta}$	0	0
$\lambda^\perp_\varphi$	$\frac{\sin^2\Theta\sin\Phi}{3-\cos^2\Theta}$	$\frac{-\sin^2\Theta\sin 2\Phi}{1+\cos^2\Theta}$	0	$\frac{\sin^2\Theta\sin 2\Phi}{9-7\cos^2\Theta}$	0	0
$\lambda_{\vartheta\varphi}$	$\frac{\sin 2\Theta\cos\Phi}{3-\cos^2\Theta}$	0	$-\frac{\sin 2\Theta\cos\Phi}{4}$	$-\frac{2\sin 2\Theta\cos\Phi}{9-7\cos^2\Theta}$	$\frac{\sin 2\Theta\cos\Phi}{4}$	0
$\lambda^\perp_{\vartheta\varphi}$	$\frac{\sin 2\Theta\sin\Phi}{3-\cos^2\Theta}$	0	$-\frac{\sin 2\Theta\sin\Phi}{4}$	$-\frac{2\sin 2\Theta\sin\Phi}{9-7\cos^2\Theta}$	$\frac{\sin 2\Theta\sin\Phi}{4}$	0

If the distribution is integrated over $\cos\Theta$ and Φ uniformly, that is, in the absence of modulations created by experimental selections as those discussed in Section 6.3, it can be seen that all azimuthal terms vanish (not a surprising result, as we are in the special case when the χ_{cJ} is in a pure J_z state) and λ_ϑ in the CC frame assumes (being $\langle\cos\Theta\rangle = 1/3$) nonzero values, except for the χ_{c0} case. In particular, we see that the J/ψ mesons produced in decays of χ_{c1} mesons with $M = 0$ or of χ_{c2} mesons with $M = \pm2$ are fully transverse ($\lambda_\vartheta = +1$), those from decays of χ_{c1} or χ_{c2} mesons with $M = \pm1$ are half transverse and half longitudinal ($\lambda_\vartheta = -1/3$), and those from decays of χ_{c2} mesons with $M = 0$ are $2/3$ longitudinal and $1/3$ transverse ($\lambda_\vartheta = -3/5$). As anticipated, the "smearing" effect leading to the unpolarized observation

only happens when the mother particle has $J = 0$, while the decay from a polarized $J > 0$ particle produces, in general, a polarized daughter reflecting the mother's polarization.

There is no obvious pattern of correspondence between the χ_{cJ} and J/ψ polarizations. However, a common denominator can be recognized in how the *shape* of the distribution is "propagated" from mother to daughter. In fact, the previously mentioned $(\Theta, \Phi) \leftrightharpoons (\vartheta, \varphi)$ exchange symmetry implies that the integrated distributions $W(\cos\Theta, \Phi)$ and $W(\cos\vartheta, \varphi)$ are functionally identical: the two-body decay distribution $\chi_{cJ} \to \mathrm{J}/\psi\,\gamma$ can be written exactly as in Eq. 1.16, replacing the lower-case angles with the upper-case ones and using the coefficients of Table 6.1 with the opposite replacement of symbols. Integrating uniformly over $\cos\vartheta$ and φ, we obtain that both the χ_{c1} with $M = 0$ and the χ_{c2} with $M = \pm 2$ decay into J/$\psi\,\gamma$ with a $\cos\Theta$ distribution of polar parameter $\lambda_\Theta = +1$, the χ_{c1} or χ_{c2} with $M = \pm 1$ produce a distribution with $\lambda_\Theta = -1/3$ and the χ_{c2} with $M = 0$ has $\lambda_\Theta = -3/5$. Comparing these numbers with those reported a few lines above, we see that the anisotropy parameters are the same for the decays of mother and daughter, even if the polarization states are very different. Also the χ_{c0} decay fits this interpretation: both the decay $\chi_{c0} \to \mathrm{J}/\psi\,\gamma$ and the following $\mathrm{J}/\psi \to \ell^+\ell^-$ are isotropic. What unifies all these cases is, therefore, that the shape of the two-body distribution is "cloned" from the mother's to the daughter's decay, as illustrated in Fig. 6.26.

Just as seen for the "smearing" effect in Section 6.3, deviations from the "cloning" condition are expected in real experiments. For χ_{c1} and χ_{c2}, as for χ_{c0}, the J/ψ CC frame is well approximated by, for example, the HX one (when the HX frame is chosen for the χ_c), at least in LHC experiments, where the laboratory momenta of the involved particles are always much larger than their masses. Therefore, the four-dimensional angular distributions reported above can effectively be measured defining $\cos\vartheta$ and φ as the angular variables in the experimental J/ψ HX frame. Consequently, no large "anti-smearing" (or, rather, "anti-cloning") effects as those seen in Higgs decays (especially close to the limits $p_\mathrm{T} \simeq p'$ and $p_\mathrm{T} \ll M$, not relevant in here) should be observed.

What can still moderately perturb the cloning effect in the χ_c decays is the shaping of the $\cos\Theta$ distribution induced by experimental selections in the exclusive observations where the photon is reconstructed. However, as seen in Table 6.1, several of the anisotropy parameters for J/ψ from χ_{c1} and χ_{c2} are $\cos\Theta$-independent (λ_ϑ for $M = \pm 1$ as well as λ_φ and/or $\lambda_{\vartheta\varphi}$ in several cases), so that deviations from an exact cloning should be moderate. In particular, no visible deviations exist in inclusive observations, as already seen for the χ_{c0} case.

Figures 6.27 and 6.28 show, respectively for the χ_{c1} and χ_{c2}, the resulting J/ψ anisotropy parameters for exclusive measurements in the HX frame (blue curves) or in the CS frame (red curves), when the χ_c mesons are produced with J_z projections $M = 0, \pm 1$ and ± 2 (panels from left to right) along the HX axis. The solid, dashed and dotted curves represent the effect of applying threshold values of 0.4, 1 and 2 GeV, respectively, on the p_T of the detected photon. The differences with respect to the cloned parameter values, represented by the green (HX frame) and magenta (CS frame) curves, corresponding to the inclusive measurements, are relatively small.

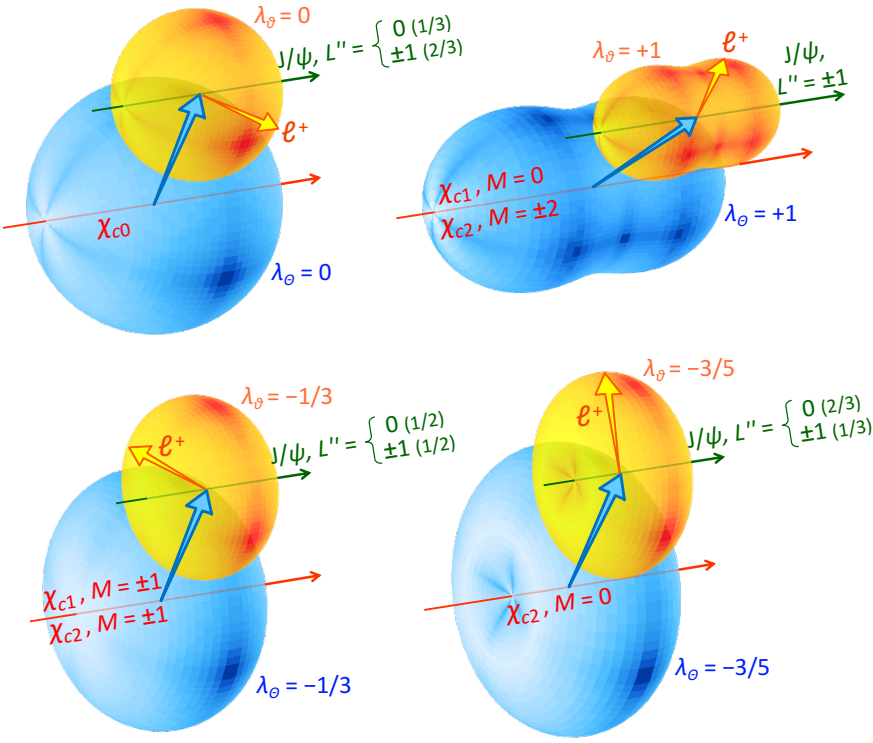

Fig. 6.26 Illustration of the "cloning" effect: the $\chi_{cJ} \to \mathrm{J}/\psi\,\gamma$ decay and the subsequent $\mathrm{J}/\psi \to \ell^+\ell^-$ decay have identical distributions of the products' directions.

Nevertheless, they are not zero, meaning that the polarization parameters determined in an exclusive measurement of J/ψ mesons produced in χ_c decays are not always identical to those describing the contribution of χ_c feed-down to inclusive prompt J/ψ production.

In particular, we even see values of $\tilde{\lambda}$ larger than +1 towards low p_{T} in the χ_{c1} case for $M = 0$. This is a spurious effect of the requirement that the photon p_{T} must be larger than 0.4 GeV, which, besides removing configurations with $\cos\Theta$ close to +1 (for any p_{T} value), as mentioned in Section 6.3, also sculpts the azimuthal distribution of the J/ψ emission direction when p_{T} is small, rejecting events with Φ around ±180°, for which the photon is emitted at $\Phi \to 0°$, that is, towards the beam direction. This leads to negative values of the average $\langle \cos 2\Phi \rangle$ and, therefore, to a positive λ_φ, according to the corresponding formula in Table 6.1. Since λ_ϑ remains unchanged, being independent of the J/ψ emission angles, this experimentally induced azimuthal component results in an increase of $\tilde{\lambda}$ beyond +1. This is not an unphysical effect (in fact, $\tilde{\lambda}$ has no upper limit, unlike λ_ϑ); it is created by the selection of a peculiar (but physical) subset of events.

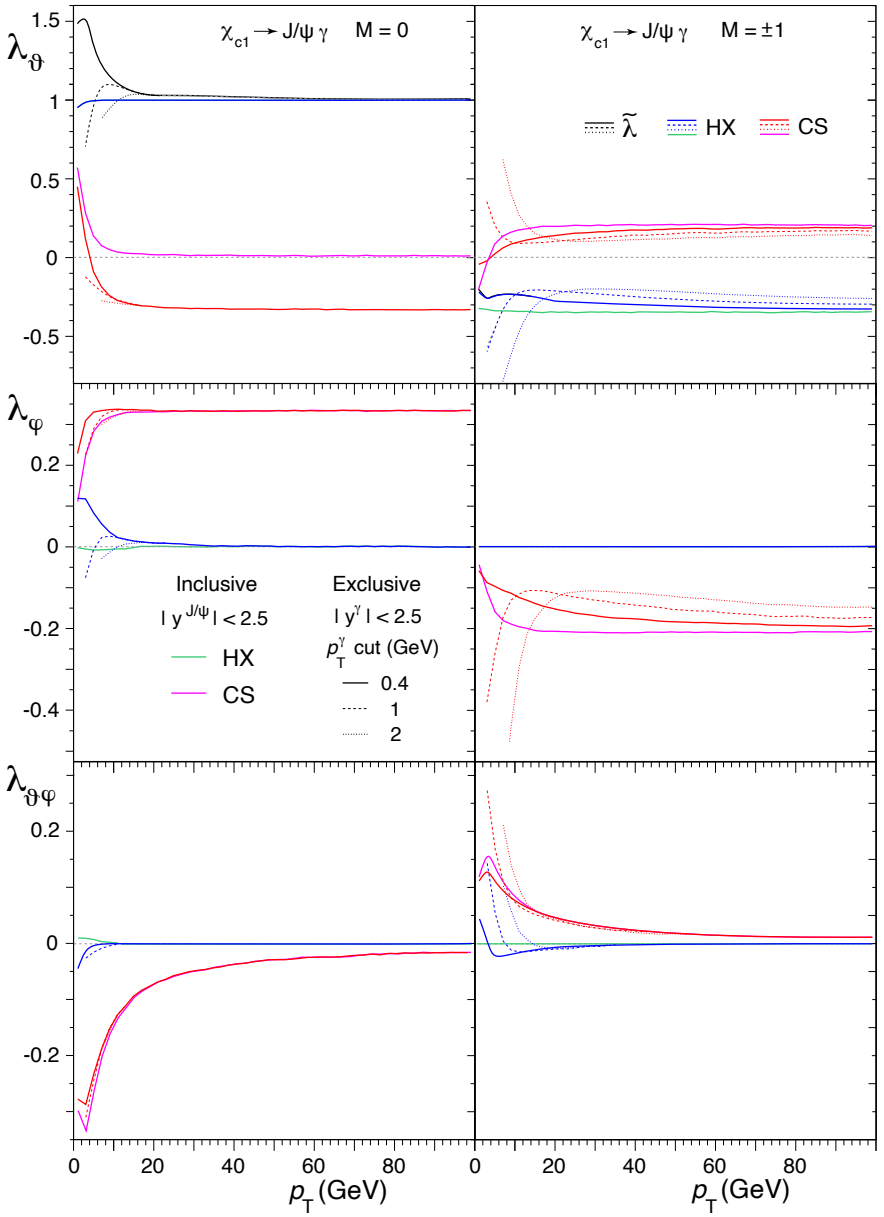

Fig. 6.27 The frame-dependent anisotropy parameters λ_ϑ, λ_φ and $\lambda_{\vartheta\varphi}$ (top to bottom rows), in the HX (blue) and CS (red) frames, as well as the frame-invariant parameter $\tilde{\lambda}$ (top row), of the dilepton decay distribution of J/ψ mesons observed in fully reconstructed exclusive radiative decays of χ_{c1} mesons produced with J_z projections $M = 0$ (left) and $M = \pm 1$ (right) along the HX axis. The solid, dashed and dotted curves correspond to increasing cuts on the photon p_T. The corresponding curves for inclusive measurements, where the cloning effect occurs almost exactly, are also shown, in green (HX) and magenta (CS).

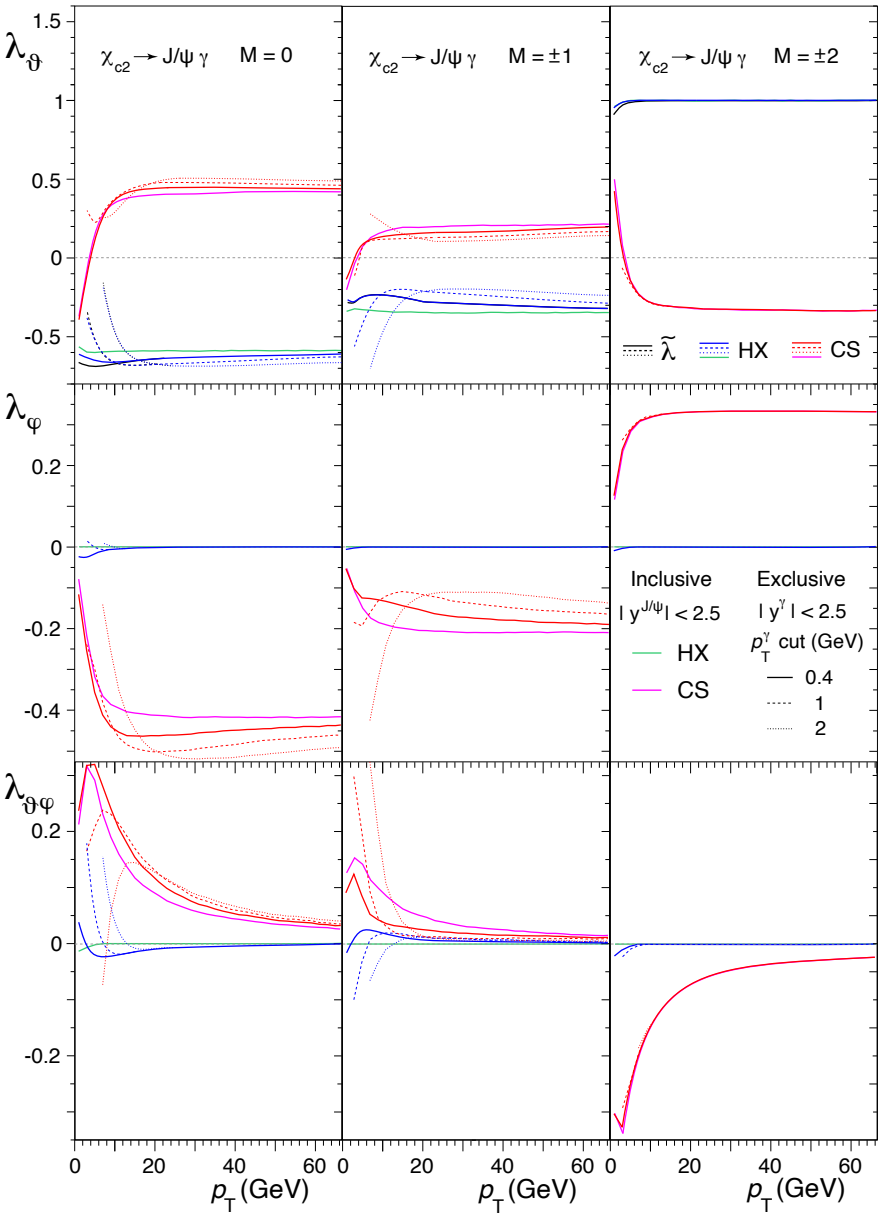

Fig. 6.28 The frame-dependent anisotropy parameters λ_ϑ, λ_φ and $\lambda_{\vartheta\varphi}$ (top to bottom rows), in the HX (blue) and CS (red) frames, as well as the frame-invariant parameter $\tilde{\lambda}$ (top row), of the dilepton decay distribution of J/ψ mesons observed in fully reconstructed exclusive radiative decays of χ_{c2} mesons produced with J_z projections $M = 0$ (left), $M = \pm 1$ (centre), and $M = \pm 2$ (right) along the HX axis. The solid, dashed and dotted curves correspond to increasing cuts on the photon p_T. The corresponding curves for inclusive measurements, where the cloning effect occurs almost exactly, are also shown, in green (HX) and magenta (CS).

The difference between the results of inclusive and exclusive observations has to be taken into account when sufficiently precise measurements of the polarization of J/ψ mesons produced in χ_c decays are used in a subtraction procedure to extract the polarization of the directly produced J/ψ, as was done to obtain the band in Fig. 6.18.

Similarly, accurate comparisons of exclusive measurements with theoretical predictions must account for the impact of the experimental selections on the photon (and leptons), either by applying the same selection criteria in the theoretical calculations or by performing a full-dimensional acceptance correction of the experimental data.

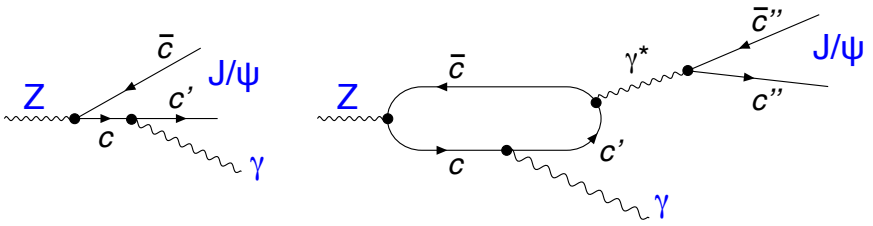

Fig. 6.29 Diagrams describing the decay Z $\rightarrow$ J/$\psi\,\gamma$. The same processes, replacing the c quarks with b quarks, also describe the analogous decay Z $\rightarrow \Upsilon\,\gamma$.

As in the $J = 0$ case, a more variegated scenario is expected when the mother particle has a much larger mass. As a prototype example of this case we consider the decay Z $\rightarrow$ J/$\psi\,\gamma$, which is formally analogous to the radiative decay of the χ_{c1} meson. In fact, as can be seen in Fig. 6.29, in the diagrams describing the processes [63–65] the Z boson transforms into an initial $c\bar{c}$ pair; one of the quarks then radiates a photon and the pair turns into the final J/ψ. The diagram on the right side, representing a higher-order process, adds a further step, where the quarks annihilate into a virtual photon, which transforms into a J/ψ, but the momentum (**P**) and angular momentum (**J**) of the J/ψ are the same as those of the pair that has just produced the photon. In both processes we hence have an initial $c\bar{c}$ state having the same **P** and **J** as the Z and a post-radiation one having the same **P** and **J** as the J/ψ: from the point of view of energy and angular-momentum conservation among the involved particles, the process is identical to an electromagnetic transition between "quarkonium" states, $c\bar{c} \rightarrow c'\bar{c}\gamma$. The four-dimensional angular distribution in the CC frame has, therefore, the same expression for the Z and χ_{c1} decays, for all polarization cases. Figure 6.30 shows the p_{T} distribution used for the generation of the simulated Z events.

The Z polarization is well measured, as seen in Sections 4.3 and 5.2, and can in principle be used to completely determine $W(\cos\Theta, \Phi, \cos\vartheta, \varphi)$ and, therefore, obtain one definite prediction for the polarization of the J/ψ mesons produced in Z decays. The necessary formulas, depending on a completely generic polarization state of the mother particle, are reported in Appendix B, for this and analogous decays where the J/ψ is replaced by another vector particle (ϕ, ρ) decaying into

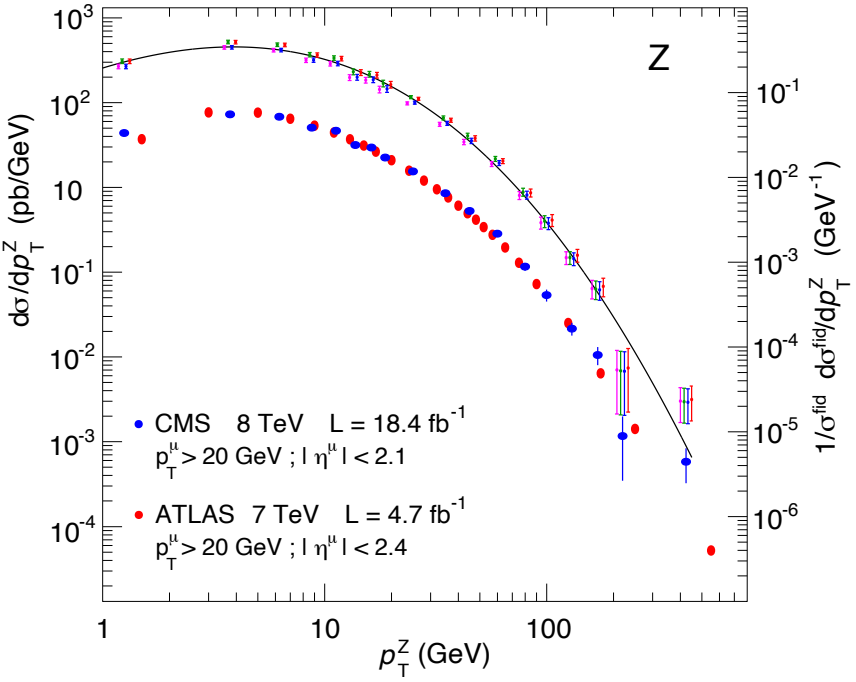

Fig. 6.30 The Z boson fiducial normalized p_{T}-differential cross section, $1/\sigma^{\mathrm{fid}}\mathrm{d}\sigma^{\mathrm{fid}}/\mathrm{d}p_{\mathrm{T}}$ (right y-axis), measured by ATLAS [60] (red bullets) and CMS [61] (blue bullets), in the phase space domain defined by the single muon cuts $p_{\mathrm{T}}^{\mu} > 20$ GeV and $|\eta^{\mu}| < 2.4$ (ATLAS) or 2.1 (CMS). The corresponding absolute fiducial cross sections, in pb/GeV (left y-axis), were obtained using the σ^{fid} value reported (for $|y^{\mathrm{Z}}| < 2$) by CMS [62]. The curve represents the absolute acceptance-corrected p_{T}-differential cross section that we used in the generation of simulated events. It provides a faithful interpolation of four sets of data points (slightly shifted horizontally for visibility reasons), acceptance-corrected assuming four different Z polarization scenarios. While the procedure usually depends on the assumed polarization, the results obtained in the four scenarios are almost identical, the residual differences being negligible for our purposes.

either $\ell^+\ell^-$ (or $\pi^0\gamma$) or $\pi^+\pi^-/\mathrm{K}^+\mathrm{K}^-$, and/or where W is the decaying boson, for example in $\mathrm{W}^{\pm} \to \rho^{\pm}\gamma$, with $\rho^{\pm} \to \pi^{\pm}\pi^0$ (or $\to \pi^{\pm}\gamma$).

Here, for simplicity, and for immediateness of comparison with the χ_{c1} case, we still consider the two distinct hypotheses of pure polarization states, $M = 0$ and ± 1, both in the HX frame. The anisotropy parameters expected as a function of the J/ψ p_{T} for exclusive measurements in the HX and CS frames are shown in Fig. 6.31. In this case, with the experimental frame deviating substantially from the CC frame, given the large p' value ($p' \simeq 46$ GeV), we see more complex patterns: the cloning phenomenon is visibly disrupted. However, the different λ_{ϑ}, λ_{φ} and $\lambda_{\vartheta\varphi}$ values and p_{T} dependences still univocally characterize the $M = 0$ and ± 1 cases. The analogous decay $\mathrm{Z} \to \Upsilon\gamma$ leads to very similar results, given the only slightly smaller p' value.

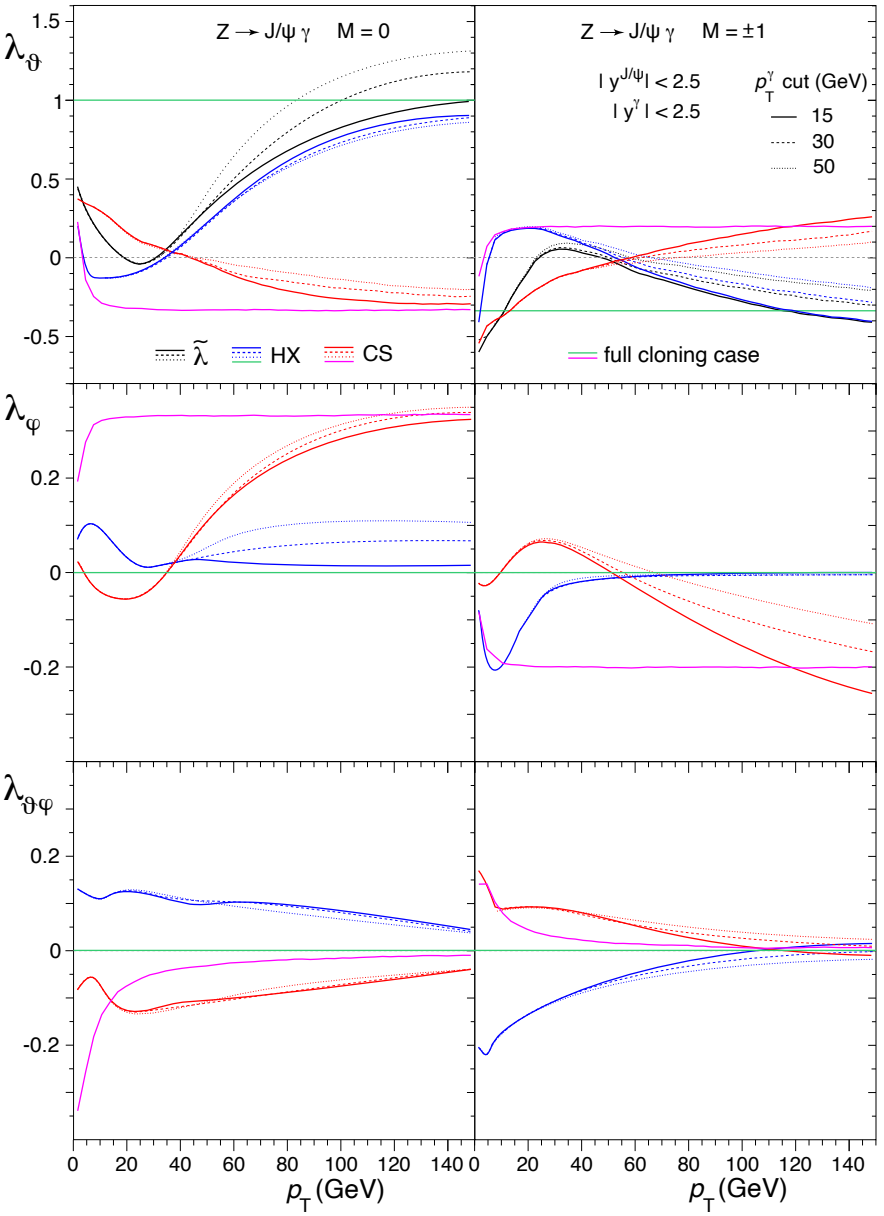

Fig. 6.31 The frame-dependent anisotropy parameters λ_ϑ, λ_φ and $\lambda_{\vartheta\varphi}$ (top to bottom rows), in the HX (blue) and CS (red) frames, as well as the frame-invariant parameter $\tilde{\lambda}$ (top row), of the dilepton decay distribution of J/ψ mesons observed in the decays of Z bosons produced with J_z projections $M = 0$ (left) and $M = \pm 1$ (right) along the HX axis. The results corresponding to an exact cloning effect are also shown, in green (HX) and magenta (CS). The solid, dashed and dotted curves correspond to increasing cuts on the p_T of the accompanying decay photon, also detected by the experiment.

6.7 The importance of the reference frame

In our discussion of the cascade decays we have adopted, as a reference for the dilepton decay of V, the CC frame, represented in Fig. 6.3, instead of the one more usually found in the literature, and perhaps a priori more intuitive, which is the cHX frame, defined in Fig. 6.1. This choice has allowed us to illustrate in an almost "visual" way, through the concepts of smearing and cloning, how the polarization properties are transferred from mother to daughter particle. The discussion would remain somehow incomplete without a brief account of what happens when, instead, we choose the cHX frame.

To address this point, we will determine the polarization of the J/ψ produced in the decays $\chi_{cJ} \to \mathrm{J}/\psi\,\gamma$ for $J = 0, 1, 2$, using the cHX frame. For simplicity, we limit the illustration to the polar anisotropy. This allows us to avoid dealing with rotations and $\mathcal{D}$-matrices and follow a simple shortcut, only considering the possible combinations of angular momentum projections $J_{z'}$ of J/ψ (L') and γ (K') along their common emission direction in the χ_c rest frame, represented by the z' axis, that is, the cHX axis, as illustrated in Fig. 6.32.

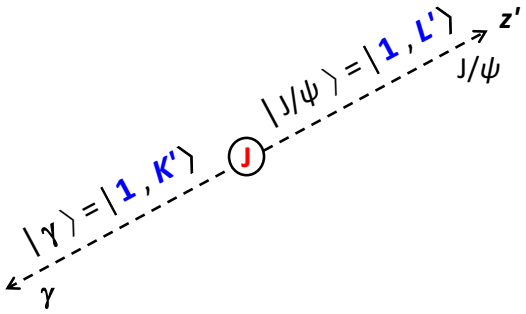

Fig. 6.32 The decay $\chi_{cJ} \to \mathrm{J}/\psi\,\gamma$ seen in the χ_{cJ} rest frame, where J/ψ and γ have angular momentum projections L' and K' along their common direction (z' axis).

The relative probabilities of these combinations are expressed by the corresponding Clebsch–Gordan coefficients, squared. The numbers are listed in Table 6.2 for the generic decay of a $J = 0$, 1 or 2 particle into two $J = 1$ particles.

The configurations where $K' = 0$ correspond to the forbidden case of a longitudinally polarized photon and must be excluded for the present examples. In the case of the decay $\chi_{c0} \to \mathrm{J}/\psi\,\gamma$, we find, as expected, that in the only two remaining configurations the J/ψ has $L' = +1$ and -1: it is, like the photon, transversely polarized along z', so that $\lambda_\vartheta = +1$: this reproduces the result amply discussed in the previous sections (Eq. 6.2).

We consider now the $\chi_{c1} \to \mathrm{J}/\psi\,\gamma$ case. Taking $J = 1$ and excluding the forbidden configurations where $K' = 0$, besides $L' + K' = \pm 2$, we find that in the four allowed ones the J/ψ has 50% probability of being transverse ($L' = +1$ or -1) and 50% of

Table 6.2 The squared Clebsch–Gordan coefficients weighing the angular momentum configurations of the decay $|J,\, L' + K'\rangle \to |1,\, L'\rangle + |1,\, K'\rangle$, with $J = 0$, 1, and 2, along the z' axis.

L'	K'	$L' + K'$	weight = C^2		
			$J = 0$	$J = 1$	$J = 2$
+1	+1	+2	–	–	1
+1	0	+1	–	1/2	1/2
+1	−1	0	1/3	1/2	1/6
0	+1	+1	–	1/2	1/2
0	0	0	1/3	0	2/3
0	−1	−1	–	1/2	1/2
−1	+1	0	1/3	1/2	1/6
−1	0	−1	–	1/2	1/2
−1	−1	−2	–	–	1

being longitudinal ($L' = 0$): therefore, its dilepton distribution along z' is

$$w(\cos\vartheta) \propto \frac{1}{2}\frac{1+\cos^2\vartheta}{4} + \frac{1}{2}\frac{1-\cos^2\vartheta}{2} \propto 1 - \frac{1}{3}\cos^2\vartheta\,, \tag{6.29}$$

that is, $\lambda_\vartheta = -1/3$. This result is *independent* of the polarization state of the χ_{c1}. For the χ_{c2} decay, by summing the relevant coefficients in the table we find that the J/ψ is 70% transverse and 30% longitudinal with respect to the z' axis,

$$w(\cos\vartheta) \propto \frac{7}{10}\frac{1+\cos^2\vartheta}{4} + \frac{3}{10}\frac{1-\cos^2\vartheta}{2} \propto 1 + \frac{1}{13}\cos^2\vartheta\,, \tag{6.30}$$

that is, $\lambda_\vartheta = +1/13$, irrespectively of the χ_{c2} polarization state. In summary, by adopting the cHX axis for the observation of the J/ψ decay distribution, the measurement remains completely blind to the χ_c polarization. This is a result of the implicit integration we made over the emission angles Θ, Φ of the J/ψ itself in the χ_c rest frame. In fact, the full information on the χ_c polarization state remains available in the four-dimensional distribution $W(\cos\Theta, \Phi, \cos\vartheta, \varphi)$ of the cascade $\chi_{cJ} \to \mathrm{J}/\psi\,\gamma$ with $\mathrm{J}/\psi \to \ell^+\ell^-$, which can of course be determined, with a method analogous to the one used in Section 6.6, adopting the cHX axis for the J/ψ.

Anyhow, in the light of these examples, the results seen in Section 6.6 imply a clear advantage in the use of the CC frame: with this choice the dilepton anisotropy alone, even after integration over $\cos\Theta$ and Φ, is fully sensitive to the χ_c polarization, because it "clones" the polarization-dependent anisotropy of the J/$\psi\,\gamma$ emission

in the χ_c rest frame. The difference between the results obtained with the two frame choices is illustrated in Fig. 6.33.

This crucial advantage of the CC frame remains present also when the cloning effect is disrupted by the deviation of the HX from the CC frame at typical p_T values and by the effects of exclusive selection cuts, as in the measurement of the J/ψ polarization in the decay $Z \to J/\psi\,\gamma$, discussed in the previous section. In fact, the calculation of the J/ψ dilepton distribution in the cHX frame leads to the same polarization-insensitive result as in the χ_{c1} case, $\lambda_\vartheta = -1/3$. Instead, even if the cloning is now visually unrecognizable (Fig. 6.31), the λ_ϑ, λ_φ and $\lambda_{\vartheta\varphi}$ patterns in the HX (or CS) frame remain very different in the $M = 0$ and $M = \pm 1$ cases, allowing for a clear discrimination between Z polarization cases.

The title of this section alludes to the previous discussion of Chapter 2 about the dependence of a polarization measurement on the reference frame and how it is convenient to test more than one frame in the search for possibly simpler (and, therefore, more physically revealing) "patterns". However, it is important to remark that, in that case, we were considering polarization frames (HX, CS, GJ, PX) that are mutually related by simple spatial rotations around the y axis and, for this reason, the measurement in one frame could always be translated into a corresponding result in any other frame, provided that all anisotropy parameters are measured and effects caused by integrations over kinematic intervals (e.g. p_T and/or rapidity bins) can be neglected. In the present case, the choice between cHX and CC frames for the measurement of the J/ψ polarization is irreversible, at least if only the dilepton distribution is measured (and, of course, if the analysis is not repeated with the other choice): it is not possible to transform mathematically the measurement made in the cHX frame to the CC frame, as can be understood by the simple fact that only the destination frame gives an anisotropy that depends on the χ_c polarization, while this information is irrecoverably occulted in the frame of origin. In fact, the relation between the cHX and CC frames at fixed p_T and rapidity is not a rotation, but the convolution of a continuous series of event-dependent rotations, where the *shape* of the distribution changes and some of the original information it contained gets lost.

6.8 A counterexample for the cloning effect

We have presented the χ_c radiative decays as prototypes for the illustration of the cloning mechanism, which can be seen at work when the measurement adopts, for example, the HX frame, as an almost perfect replica of the CC frame: the dilepton decay in the J/ψ rest frame will be practically identical to the distribution of the J/ψ emission in the χ_c rest frame and, therefore, fully and univocally reflect the χ_c polarization in its HX frame (this is exactly true when higher order multiple radiations are neglected, as previously mentioned and as discussed in detail in Ref. [59]).

When the mother-daughter mass difference is large, as in the otherwise analogous $Z \to J/\psi\,\gamma$ decay, the cloning effect is no longer clearly recognizable as such in the "usual" HX frame. However, the J/ψ dilepton distribution continues to be a

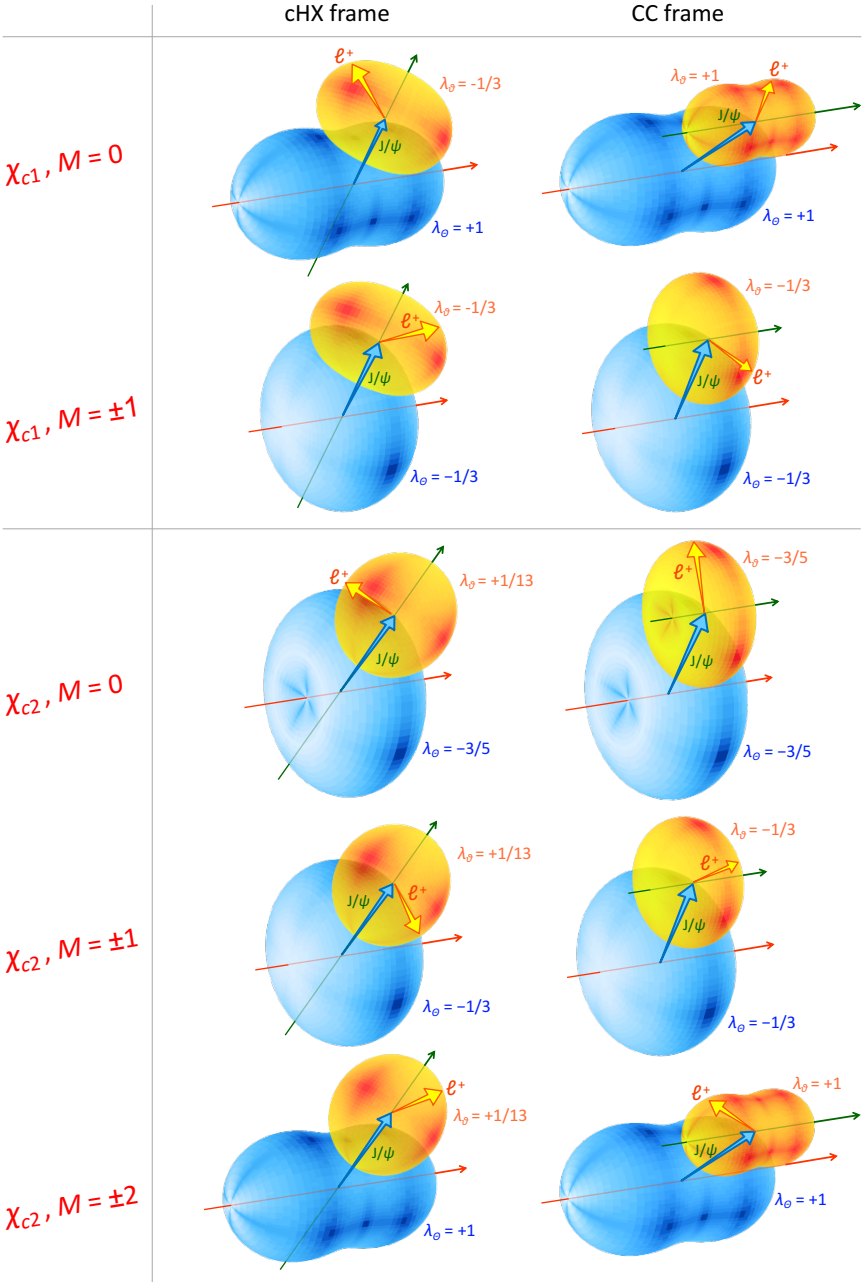

Fig. 6.33 Illustration of how the observation of the angular distribution of the decay $J/\psi \to \ell^+\ell^-$, subsequent to $\chi_{cJ} \to J/\psi\,\gamma$, is substantially different in the cHX and CC frames. In the CC frame the shape of the dilepton distribution is univocally correlated to the χ_{cJ} polarization state, making its measurement possible even when the decay distribution of the χ_{cJ} itself is not observed. Instead, in the CC frame the J/ψ polarization is blind to the χ_{cJ} polarization.

definite indicator of the Z polarization. Above all, it is important to remind that the cloning mechanism remains present in this decay and is, in principle, observable: it is sufficient to adopt for the J/ψ the exact CC frame, that is, to calculate the polarization direction in the Z rest frame and translate it with no change into the J/ψ rest frame.

It is now natural to wonder about what happens in the decays where this kind of cloning is absent: does in such cases the CC axis still provide its advantage in terms of sensitivity to the mother's polarizations? Fortunately, our $\chi_{cJ} \to \mathrm{J}/\psi\,\gamma$ "prototype" admits a very close counterpart, providing a particularly instructive answer. We simply have to release the constraint that the radiated photon is transversely polarized: we replace it with a virtual photon γ^*, which eventually produces a second, non-resonant, lepton-antilepton pair. The corresponding physical cases are the rarer decays $\chi_{cJ} \to \mathrm{J}/\psi\,\gamma^*$, where both J/$\psi$ and γ^* further decay into $\ell^+\ell^-$ pairs. The exchange symmetry $(\Theta, \Phi) \leftrightharpoons (\vartheta, \varphi)$ illustrated in Fig. 6.25 is broken by the replacement of γ with γ^*, since this latter admits a $J_{z'} = 0$ component along z' and ceases to be perfectly analogous to the J/ψ's $\ell^+\ell^-$ system as observed with respect to the z''' axis: no cloning is expected in this case.

The amplitude of the process is unchanged with respect to the one of Eq. 6.28. The difference in the observable angular distribution results from extending the sum of the squared amplitudes to include the $K' = 0$ term. The four-dimensional angular distribution for pure χ_{cJ} polarizations, corresponding to Eq. 6.28, becomes

$$W_{\mathrm{CC}}(\cos\Theta, \Phi, \cos\vartheta, \varphi) \propto \begin{cases} 1 + \cos^2\vartheta & \text{for } \chi_{c1}\,,\ M = 0\,, \\ 1 - \frac{1}{3}\cos^2\vartheta & \text{for } \chi_{c1}\,,\ M = \pm 1\,, \\ 1 - \frac{3}{5}\cos^2\vartheta & \text{for } \chi_{c2}\,,\ M = 0\,, \\ 1 - \frac{1}{3}\cos^2\vartheta & \text{for } \chi_{c2}\,,\ M = \pm 1\,, \\ 1 + \cos^2\vartheta & \text{for } \chi_{c2}\,,\ M = \pm 2\,. \end{cases} \tag{6.31}$$

These expressions are independent of the angles Θ and Φ, implying that the integration over ϑ (and φ) leads to a constant distribution: the J/ψ is emitted *isotropically* in the χ_c polarization frame. This means that the measurement of the two-body decay angular distribution of the χ_c is blind to its polarization state.

Additionally, we can recognize, with the method used in Section 6.7 (Fig. 6.32), that also the dilepton decay in the J/ψ cHX frame is isotropic for $J = 0$, 1 and 2 (the same is true, incidentally, for the one in the γ^* cHX rest frame): with no restriction on K', the summed Clebsch–Gordan weights (Table 6.2) become identical for the three configurations $L' = -1$, 0 and $+1$, in all three J cases. No trace of the χ_{cJ} polarization would be seen, therefore, in *either* integrated two-dimensional distribution by adopting the cHX frame. Only the four-dimensional distribution $W_{\mathrm{cHX}}(\cos\Theta, \Phi, \cos\vartheta, \varphi)$ will contain such information, in terms correlating the upper- and lower-case angles.

The CC frame continues, instead, to provide for the J/ψ decay the same distribution as in the $\chi_{cJ} \to \mathrm{J}/\psi\,\gamma$ case: the polar anisotropy parameters implied by Eq. 6.31,

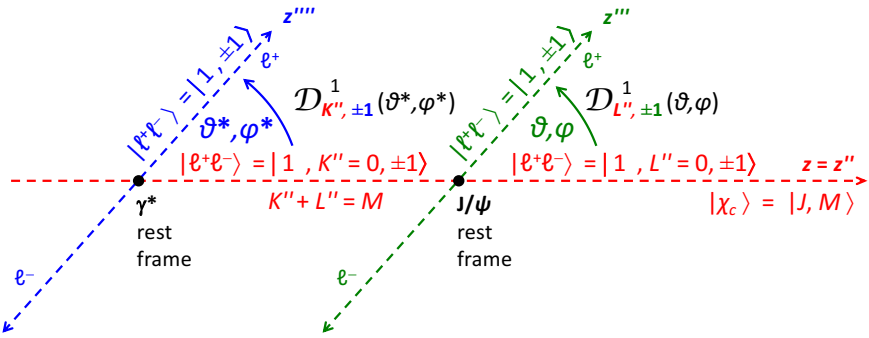

Fig. 6.34 Illustration of the $(\vartheta', \varphi') \rightleftharpoons (\vartheta, \varphi)$ exchange symmetry for the angular distribution of the cascade decay $\chi_{cJ} \to \mathrm{J}/\psi\, \gamma^*$, followed by $\mathrm{J}/\psi \to \ell^+\ell^-$ and $\gamma^* \to \ell^+\ell^-$.

$\lambda_\vartheta = -3/5$ (χ_{c2} for $M = 0$), $-1/3$ (χ_{c1} or χ_{c2} for $M = \pm 1$), and $+1$ (χ_{c1} for $M = 0$ or χ_{c2} for $M = \pm 2$) are the same as those found in Section 6.6 for the decays with a real photon.

Moreover, for understandable reasons of symmetry, that same polarization information is also carried by the additional dilepton distribution produced by the γ^* decay, when observed with respect to the CC axis. In fact, another clone symmetry can be discerned, as illustrated in Fig. 6.34, between the two dilepton systems, which are completely equivalent and exchangeable (they only differ for their invariant masses, which do not affect the determination of the angular distribution): the four dimensional angular distribution $W(\cos\vartheta, \varphi, \cos\vartheta', \varphi')$ is symmetric with respect to a change of the J/ψ decay angles (ϑ and φ) by those of the virtual photon (ϑ' and φ').

It is now immediate to determine the correlated distribution of the four angular coordinates $\cos\vartheta$, φ, $\cos\vartheta'$, and φ'. In fact, we can reuse the passages of Section 6.6 that lead to the derivation of the distribution of $\chi_{cJ} \to \mathrm{J}/\psi\, \gamma$, $\mathrm{J}/\psi \to \ell^+\ell^-$ (Eq. 6.28), replacing the rotation of the γ eigenstate from the z' to the z'' (CC) axis, by angles Θ and Φ, with the rotation of the second dilepton system, coming from the γ^* decay, from the z'''' axis (where lepton and antilepton are back-to-back) to the z'' axis, by angles ϑ' and φ'. Along z'''' the γ^* dilepton has allowed angular momentum projections ± 1, just like γ had along z'. Moreover, the involved Wigner matrices are exactly the same.

The replacement, therefore, does not change the functional dependence of the result on the angles: it only leads to the substitution of Θ, Φ with ϑ', φ'. This means that, with only a change of names of the angles, Eq. 6.28 represents the correlated angular distribution of the two dilepton systems of the J/ψ and γ^* decays, being the angles measured in the respective CC rest frames of the two particles. In particular, by integrating this four-dimensional distribution $W(\cos\vartheta, \varphi, \cos\vartheta', \varphi')$ over either $\cos\vartheta'$ and φ', or $\cos\vartheta$ and φ, to derive, respectively, the J/ψ decay distribution $w(\cos\vartheta, \varphi)$ or the γ^* one, $w(\cos\vartheta', \varphi')$, we obviously obtain the same result

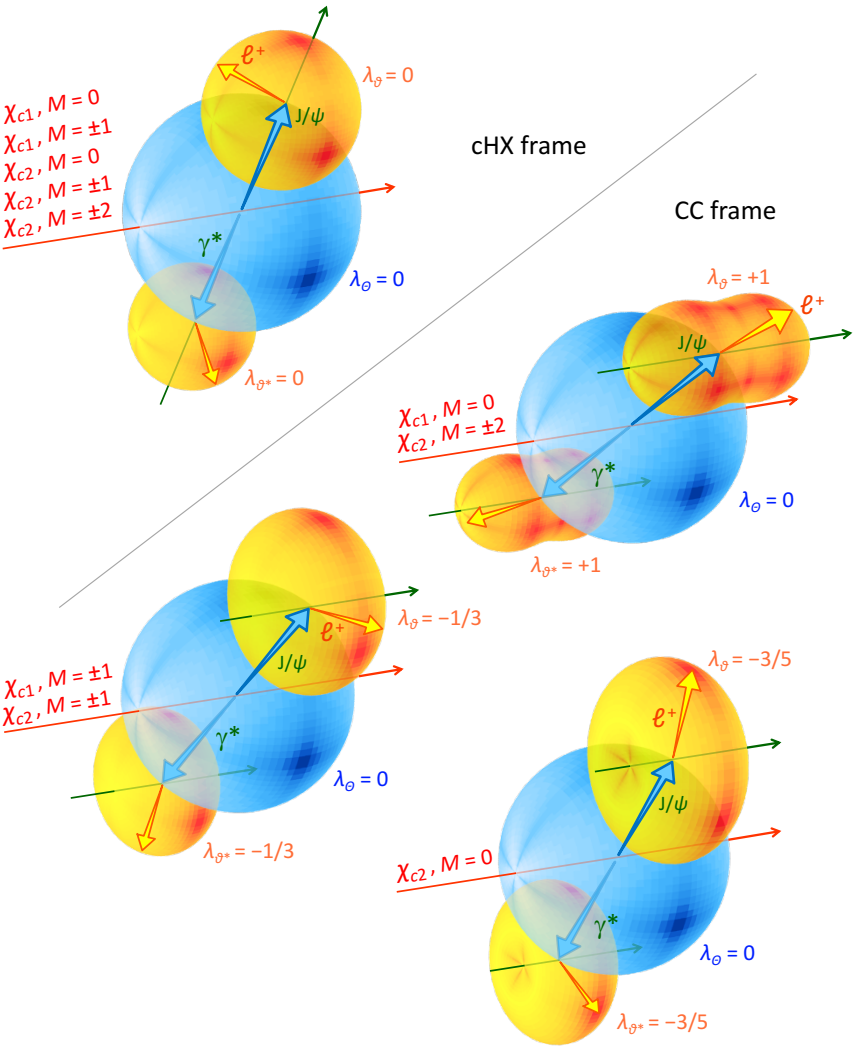

Fig. 6.35 Illustration of how the angular distribution of the decay $\chi_{cJ} \to \mathrm{J}/\psi\,\gamma^*$, with $\mathrm{J}/\psi \to \ell^+\ell^-$ and $\gamma^* \to \ell^+\ell^-$, is observed in the cHX and CC frames. The χ_{cJ} decay is isotropic in all cases and both frames. Concerning the dilepton distributions, all χ_{cJ} polarization cases lead to an undistinguished, fully isotropic result in the cHX frame, while both J/ψ and γ^* decay distributions in the CC frame univocally reflect the χ_{cJ} polarization state, being two identical replicas of the $\mathrm{J}/\psi \to \ell^+\ell^-$ distribution in the $\chi_{cJ} \to \mathrm{J}/\psi\,\gamma$ case (Fig. 6.26).

as when we integrate the distribution $W(\cos\Theta, \Phi, \cos\vartheta, \varphi)$ of the $\chi_{cJ} \to \mathrm{J}/\psi\,\gamma$ case over $\cos\Theta$ and Φ.

Figure 6.35 gives a pictorial summary of how the measurements in the cHX and CC frames differ for integrated two-dimensional distributions: in the cHX frame

every distribution is isotropic, independently of the χ_c polarization; in the CC frame both the distribution of the J/ψ decay and that of the γ^* are exactly the same as in the dilepton distribution in the $\chi_{cJ} \to \mathrm{J}/\psi\,\gamma$ case (Fig. 6.33), and both fully reflect the χ_c polarization.

We have exploited the close parallelism between the two alternative χ_{cJ} decays, $\chi_{cJ} \to \mathrm{J}/\psi\,\gamma$ and $\chi_{cJ} \to \mathrm{J}/\psi\,\gamma^*$, to further illustrate the concept of cloning and the roles of different frame definitions, taking advantage of existing and experimentally observed decay channels. The latter decay channel may, however, not be a good alternative for the measurement of the χ_c polarization. First, because the event sample would certainly be much smaller than the $\chi_{cJ} \to \mathrm{J}/\psi\,\gamma$ sample, given the lower branching fraction. Second, because it remains necessary to carefully evaluate the effects of the integration over $\cos\vartheta'$ and φ' in the presence of experimental selections.

As previously described in detail, the selection criteria applied to the photon lead to sculpting effects on the $(\cos\Theta, \Phi)$ distribution in the $\chi_{cJ} \to \mathrm{J}/\psi\,\gamma$ case, thereby creating slight deviations from the full-cloning expectation. In exactly the same way, the selections applied to the lepton pair produced by the γ^* will affect the observed J/ψ dilepton distribution (and vice-versa), since the functional correlation between $(\cos\vartheta', \varphi')$ and $(\cos\vartheta, \varphi)$ is the same as the one between $(\cos\Theta, \Phi)$ and $(\cos\vartheta, \varphi)$. This problem should not be more easily addressed in the γ^* decay case, because the invariant mass of the γ^* is very small, of the order of only 1 MeV, so that the two resulting leptons will be produced with very low laboratory momenta, making their detection a big challenge.

6.9 Recapitulation

In this chapter we have studied the dilepton decay distribution of a vector particle V produced indirectly, in the decay $O \to V + X$ of a heavier particle O, to answer the following question: what polarization does V inherit in this two-step production process?

We started by developing in detail the description of the vector particle production from the decay of a $J = 0$ particle, including cases like $\chi_{c0} \to \mathrm{J}/\psi\,\gamma$, $\chi_{b0} \to \Upsilon\,\gamma$, $\mathrm{B} \to \mathrm{J}/\psi\,\mathrm{K}$, $\mathrm{H} \to \mathrm{J}/\psi\,\gamma$, and $\mathrm{H} \to Z\,\gamma$. In certain experimental and kinematic conditions, these processes represent extreme examples of polarization "smearing", potentially leading to the extraordinary observation of a fully unpolarized vector particle. In fact, V is intrinsically polarized along the direction of its emission in the O rest frame (the cHX frame, Fig. 6.1) having, for example, a natural polarization $\lambda_0 = +1$ when X is a real photon and $\lambda_0 = -1$ when X is a $J = 0$ particle.

However, in "inclusive" studies, where the production of V is observed by reconstructing only its dilepton decay, and not the underlying $O \to V + X$ step, the dilepton distribution is necessarily referred to the directions of the colliding beams, taking for example the HX axis as polarization axis. Given that V is emitted isotropically in the O rest frame, in the V rest frame the directions of the HX and cHX axes

are distributed in a spherically uniform way with respect to one another, leading, in principle, to a fully smeared dilepton distribution as seen with respect to the HX axis (Fig. 6.2).

The four-dimensional distribution of the V emission angles Θ, Φ in the O rest frame and the dilepton emission angles ϑ, φ in the V rest frame is given by Eq. 6.2 in the cHX frame and by Eq. 6.8 in the "cloned cascade" (CC) frame of Fig. 6.3, where the V polarization axis is a geometrical clone of the O polarization axis and approximates the HX or CS axis (the same chosen for O) when the laboratory momentum of V is large with respect to the $O - V$ mass difference (Eq. 6.15). In this latter frame we see that the uniform integration over the angular variables of either step of the cascade leads indeed to a constant. However, when the integration is not uniform, the result is, in general, an anisotropic two-dimensional distribution.

It actually happens that the measurement process disrupts the spherical symmetry of the smearing, by sculpting the $\cos\Theta$ distribution. If, for example, V is reconstructed in intervals of its p_{T}, the $\cos\Theta$ distribution ceases to be uniform and assumes a shape depending on the slope of the p_{T} distribution within the considered interval (Eqs. 6.17 and 6.22, Fig. 6.9). The effect increases with the mass difference between O and V, as shown in Fig. 6.6, comparing the cases $\mathrm{B} \to \mathrm{J}/\psi\,\mathrm{K}$ and $\chi_{c0} \to \mathrm{J}/\psi\,\gamma$. When the $|\cos\Theta|$ distribution is no longer uniform (that is, the $\cos\Theta$ distribution is not uniform or linear) in the HX or CS frame of O, a non-uniform dilepton decay distribution will be observed in the CC frame, HX or CS, of V.

The resulting anisotropy parameters as observable in inclusive measurements (ignoring the $O \to V$ step) at the LHC are shown in Fig. 6.14 ($\mathrm{B} \to \mathrm{J}/\psi\,\mathrm{K}$, $\mathrm{B} \to \psi(2\mathrm{S})\,\mathrm{K}$) and in the left panels of Fig. 6.15 ($\chi_{c0} \to \mathrm{J}/\psi\,\gamma$): a practically isotropic dilepton distribution is observed only when the mass difference is as small as for the J/ψ from χ_{c0} decays.

It is important to notice that, as seen in those figures, the results depend on the experimental selections. For example, also the minimum-p_{T} requirements on the decay leptons sculpt the $\cos\Theta$ distributions (Figs. 6.12 and 6.13). Since the $\cos\Theta$ distribution is not observed and, therefore, not corrected for the lepton acceptance, this effect leads to an increase of the observed anisotropies. The selection criteria must become an integral part of the measurement definition.

In most measurements, additional criteria are applied to isolate events corresponding to the specific decay channel $O \to V + X$. Even if only the dilepton decay distribution of V is analysed, such selections, effectively requiring the presence of X with a laboratory momentum in a given acceptance domain, strongly sculpt the $\cos\Theta$ distribution (Fig. 6.10). In such "exclusive" measurements, stronger kinematic modulations are expected for the dilepton decay parameters of V, as shown by the comparison between the right and left panels in Figs. 6.8 and 6.15. Processes like $\mathrm{H} \to \mathrm{J}/\psi\,\gamma$ and $\mathrm{H} \to \mathrm{Z}\,\gamma$, which must be isolated with suitable selections on the photon, show particularly strong deviations from the isotropic limit (Fig. 6.17), because the mass difference is large with respect to the typical values of the observed V momentum spectrum.

The same smearing mechanism occurring in the decay $\chi_{c0} \to \mathrm{J}/\psi\,\gamma$ provides a key for the interpretation of the surprising observation, made at the LHC, that *di-*

rectly produced J/ψ mesons show polarization parameters compatible with being zero and with no significant dependence on p_{T} (Fig. 6.18). An exact cancellation of oppositely polarized mechanisms, leading to a p_{T}-independent result, is improbable, and a more natural explanation is provided by the colour-octet mechanism (a basic feature of NRQCD), where the observable vector meson results from the transformation of an unobserved ("pre-resonance") coloured $Q\overline{Q}$ pair, having a mass only slightly different from the final one and possibly different quantum numbers. The binding transition, happening via emission of soft gluons, leads to a seemingly unpolarized J/ψ if the pre-resonance $Q\overline{Q}$ has $J = 0$. Measurements in hadron collider experiments do indeed support the hypothesis of a dominance of partonic processes creating coloured $Q\overline{Q}$ pairs with respect to those producing already colour neutral states (Fig. 6.19). Moreover, recent global analyses of LHC data indicate that the ${}^1S_0^{[8]}$ colour-octet channel (of $J = 0$) is the prevalent one. It is, therefore, the peculiar nature of the J/ψ, a composite particle made of two heavy quarks, and the marked process hierarchy characterizing the high-energy domain explored at the LHC, that allow for the exceptional observation of unpolarized production.

Colour-octet dominance and unpolarized J/ψ production are not necessarily foreseen, nor observed, in low-p_{T} fixed-target production, in electromagnetic processes and, as exemplified by the several cases analysed in this chapter, in indirect production. In particular, the indirect J/ψ production from decays of B mesons, which can be studied inclusively by selecting "non-prompt" events, should show a significant longitudinal polarization if the sample is dominated by two-body decays of the kind $\mathrm{B} \to \mathrm{J}/\psi\,\mathrm{K}$. Multi-body decays, including processes producing a colour-octet $Q\overline{Q}$ state and more complex chains starting with $\mathrm{B} \to \chi_c$ or $\mathrm{B} \to \psi(2\mathrm{S})$ decays, may, however, dilute the overall polarization (Figs. 6.23 and 6.24).

The generalization of the previous considerations to the cases of a $J = 1$ or $J = 2$ mother particle ($\chi_{c1,2} \to \mathrm{J}/\psi\,\gamma$, $\mathrm{Z} \to \mathrm{J}/\psi\,\gamma$) shows the "smearing" effect turning into another phenomenon, where the shape of the mother's decay distribution is "cloned" into the one of the daughter's as observed in the CC frame (Fig. 6.26), reflecting the invariance of the four-dimensional angular distribution by exchange of the O and V decay angles (Eq. 6.28 and Fig. 6.25). Therefore, while the polarization (J_z composition) changes from mother to daughter, the one of the mother is still univocally reflected by the dilepton decay distribution of V, even when the O decay angles are integrated out. Also the $J = 0$ case, where both mother and daughter have isotopic decays distributions, is actually a case of cloning.

The cloning is verified in the CC frame, meaning that, at sufficiently high laboratory momentum, it is possible to measure the χ_{c1} and χ_{c2} polarizations in the "ordinary" HX or CS frames, by only determining the dilepton distribution of the daughter J/ψ and without performing a four-dimensional analysis including the χ_c decay angles. Just as the full spherical smearing in the $J = 0$ case, also the exact cloning is partially disrupted by experimental selections affecting the momentum of the accompanying particle X. The effect is small for J/ψ from χ_c decays (Figs. 6.27 and 6.28), but significant for large mother-daughter mass differences, as in the case of the decay $\mathrm{Z} \to \mathrm{J}/\psi\,\gamma$, where strong kinematic modulations appear for the dilepton

anisotropy parameters; the Z polarization is, however, still unequivocally reflected in the observable patterns.

Both the cHX ($x'y'z'$) and CC ($x''y''z''$) frames of Figs. 6.1 and 6.3, alternative choices for the measurement of the V decay distribution, require, in principle, the knowledge of the O (or X) momentum, besides the V one: for example, z' (cHX) and z'' (CC HX) represent the direction of O, respectively, in the V rest frame and in the laboratory. Correspondingly, the measurement of the correlated four-dimensional distribution of the cascade process provides the same amount of physics information with both frame choices.

However, for V momenta larger than the $O - V$ mass difference, the CC HX frame is simply determined as the V HX frame, using only the V momentum in the laboratory. Measurements of the dilepton distribution using the CC (HX or CS) frame and integrating over the O decay angles, as those considered in all examples of this chapter, require, therefore, significantly less experimental information than those choosing the cHX frame, which always rely on the knowledge of the O momentum. Apart from being more "economical" from the experimental point of view, the choice of the CC frame is also the only one of the two allowing the experiment to determine the polarization of O simply using the dilepton degrees of freedom, as was illustrated by the χ_{c1} and χ_{c2} examples. In fact, after integration over $\cos\Theta$ and Φ, the dilepton distribution in the cHX frame is blind to the O polarization (Eqs. 6.29 and 6.30, Fig. 6.33).

Interestingly, the dilepton measurement in the CC frame continues to provide the same full sensitivity to the O polarization even in the seemingly evasive example of the $\chi_{c1,2} \to J/\psi\,\gamma^*$ decays (Fig. 6.35), where the $\cos\Theta, \Phi$ distribution itself is always measured as isotropic independently of the χ_c polarization, an observation not to be mistaken as an indication that the χ_c is produced unpolarized.

References

[1] CMS Collaboration, "Measurement of J/ψ and ψ(2S) prompt double-differential cross sections in pp collisions at $\sqrt{s} = 7$ TeV", *Phys. Rev. Lett.* **114** (2015) 191802, doi:10.1103/PhysRevLett.114.191802, arXiv:1502.04155.

[2] CMS Collaboration, "Measurements of the Υ(1S), Υ(2S), and Υ(3S) differential cross sections in pp collisions at $\sqrt{s} = 7$ TeV", *Phys. Lett. B* **749** (2015) 14, doi:10.1016/j.physletb.2015.07.037, arXiv:1501.07750.

[3] CMS Collaboration, "Measurement of quarkonium production cross sections in pp collisions at $\sqrt{s}$ = 13 TeV", *Phys. Lett. B* **780** (2018) 251, doi:10.1016/j.physletb.2018.02.033, arXiv:1710.11002.

[4] ATLAS Collaboration, "Measurement of the differential cross-sections of prompt and non-prompt production of J/ψ and ψ(2S) in pp collisions at $\sqrt{s}$ = 7 and 8 TeV with the ATLAS detector", *Eur. Phys. J. C* **76** (2016) 283, doi:10.1140/epjc/s10052-016-4050-8, arXiv:1512.03657.

[5] ATLAS Collaboration, "Measurement of Υ production in 7 TeV pp collisions at ATLAS", *Phys. Rev. D* **87** (2013) 052004, doi:10.1103/PhysRevD.87.052004, arXiv:1211.7255.

[6] LHCb Collaboration, "Measurement of J/ψ production in pp collisions at $\sqrt{s}$ = 7 TeV", *Eur. Phys. J. C* **71** (2011) 1645, doi:10.1140/epjc/s10052-011-1645-y, arXiv:1103.0423.

[7] LHCb Collaboration, "Measurement of Υ production in pp collisions at $\sqrt{s}$ = 7 TeV", *Eur. Phys. J. C* **72** (2012) 2025, doi:10.1140/epjc/s10052-012-2025-y, arXiv:1202.6579.

[8] LHCb Collaboration, "Forward production of Υ mesons in pp collisions at $\sqrt{s}$ = 7 and 8 TeV", *JHEP* **11** (2015) 103, doi:10.1007/JHEP11(2015)103, arXiv:1509.02372.

[9] LHCb Collaboration, "Production of J/ψ and Υ mesons in pp collisions at $\sqrt{s}$ = 8 TeV", *JHEP* **06** (2013) 064, doi:10.1007/JHEP06(2013)064, arXiv:1304.6977.

[10] LHCb Collaboration, "Measurement of forward J/ψ production cross-sections in pp collisions at $\sqrt{s}$ = 13 TeV", *JHEP* **10** (2015) 172, doi:10.1007/JHEP10(2015)172, arXiv:1509.00771. [Erratum: *JHEP* **05** (2017) 063].

[11] LHCb Collaboration, "Measurement of Υ production in pp collisions at $\sqrt{s}$ = 13 TeV", *JHEP* **07** (2018) 134, doi:10.1007/JHEP07(2018)134, arXiv:1804.09214. [Erratum: *JHEP* **05** (2019) 076].

[12] ATLAS Collaboration, "Measurement of χ_{c1} and χ_{c2} production with $\sqrt{s}$ = 7 TeV pp collisions at ATLAS", *JHEP* **07** (2014) 154, doi:10.1007/JHEP07(2014)154, arXiv:1404.7035.

[13] CMS Collaboration, "Measurement of the relative prompt production rate of χ_{c2} and χ_{c1} in pp collisions at $\sqrt{s}$ = 7 TeV", *Eur. Phys. J. C* **72** (2012) 2251, doi:10.1140/epjc/s10052-012-2251-3, arXiv:1210.0875.

[14] CMS Collaboration, "Measurement of the production cross section ratio $\sigma(\chi_{b2}(1P))$ / $\sigma(\chi_{b1}(1P))$ in pp collisions at $\sqrt{s}$ = 8 TeV", *Phys. Lett. B* **743** (2015) 383, doi:10.1016/j.physletb.2015.02.048, arXiv:1409.5761.

[15] LHCb Collaboration, "Measurement of the cross-section ratio $\sigma(\chi_{c2})$ / $\sigma(\chi_{c1})$ for prompt χ_c production at $\sqrt{s}$ = 7 TeV", *Phys. Lett. B* **714** (2012) 215, doi:10.1016/j.physletb.2012.06.077, arXiv:1202.1080.

[16] LHCb Collaboration, "Measurement of the relative rate of prompt χ_{c0}, χ_{c1} and χ_{c2} production at $\sqrt{s} = 7$ TeV", *JHEP* **10** (2013) 115, doi:10.1007/JHEP10(2013)115, arXiv:1307.4285.

[17] LHCb Collaboration, "Measurement of the ratio of prompt χ_c to J/ψ production in pp collisions at $\sqrt{s} = 7$ TeV", *Phys. Lett. B* **718** (2012) 431, doi:10.1016/j.physletb.2012.10.068, arXiv:1204.1462.

[18] LHCb Collaboration, "Study of χ_b meson production in pp collisions at $\sqrt{s} = 7$ and 8 TeV and observation of the decay $\chi_b(3P) \to \Upsilon(3S)\gamma$", *Eur. Phys. J. C* **74** (2014) 3092, doi:10.1140/epjc/s10052-014-3092-z, arXiv:1407.7734.

[19] CMS Collaboration, "Constraints on the χ_{c1} versus χ_{c2} polarizations in proton-proton collisions at $\sqrt{s} = 8$ TeV", *Phys. Rev. Lett.* **124** (2020) 162002, doi:10.1103/PhysRevLett.124.162002, arXiv:1912.07706.

[20] ATLAS Collaboration, "Measurement of the production cross-section of $\psi(2S) \to J/\psi(\to \mu^+\mu^-)\pi^+\pi^-$ in pp collisions at $\sqrt{s} = 7$ TeV at ATLAS", *JHEP* **09** (2014) 079, doi:10.1007/JHEP09(2014)079, arXiv:1407.5532.

[21] P. Faccioli et al., "Quarkonium production at the LHC: a data-driven analysis of remarkably simple experimental patterns", *Phys. Lett. B* **773** (2017) 476, doi:10.1016/j.physletb.2017.09.006, arXiv:1702.04208.

[22] CDF Collaboration, "Measurement of the B^+ total cross section and B^+ differential cross section $d\sigma/dp_T$ in $p\bar{p}$ collisions at $\sqrt{s} = 1.8$ TeV", *Phys. Rev. D* **65** (2002) 052005, doi:10.1103/PhysRevD.65.052005, arXiv:hep-ph/0111359.

[23] ATLAS Collaboration, "Measurement of the differential cross-section of B^+ meson production in pp collisions at $\sqrt{s} = 7$ TeV at ATLAS", *JHEP* **10** (2013) 042, doi:10.1007/JHEP10(2013)042, arXiv:1307.0126.

[24] ATLAS Collaboration, "Combined measurement of differential and total cross sections in the $H \to \gamma\gamma$ and the $H \to ZZ^* \to 4\ell$ decay channels at $\sqrt{s} = 13$ TeV with the ATLAS detector", *Phys. Lett. B* **786** (2018) 114, doi:10.1016/j.physletb.2018.09.019, arXiv:1805.10197.

[25] CMS Collaboration, "Measurement of the B^+ production cross section in pp collisions at $\sqrt{s} = 7$ TeV", *Phys. Rev. Lett.* **106** (2011) 112001, doi:10.1103/PhysRevLett.106.112001, arXiv:1101.0131.

[26] CMS Collaboration, "Measurement and interpretation of differential cross sections for Higgs boson production at $\sqrt{s} = 13$ TeV", *Phys. Lett. B* **792** (2019) 369, doi:10.1016/j.physletb.2019.03.059, arXiv:1812.06504.

[27] P. Faccioli, C. Lourenço, M. Araújo, and J. Seixas, "Universal kinematic scaling as a probe of factorized long-distance effects in high-energy quarkonium production", *Eur. Phys. J. C* **78** (2018) 118, doi:10.1140/epjc/s10052-018-5610-x, arXiv:1802.01102.

[28] CMS Collaboration, "Measurement of the prompt J/ψ and $\psi(2S)$ polarizations in pp collisions at $\sqrt{s} = 7$ TeV", *Phys. Lett. B* **727** (2013) 381, doi:10.1016/j.physletb.2013.10.055, arXiv:1307.6070.

[29] LHCb Collaboration, "Measurement of J/ψ polarization in pp collisions at $\sqrt{s}$ = 7 TeV", *Eur. Phys. J. C* **73** (2013) 2631, doi:10.1140/epjc/s10052-013-2631-3, arXiv:1307.6379.

[30] LHCb Collaboration, "Measurement of ψ(2S) polarisation in pp collisions at $\sqrt{s}$ = 7 TeV", *Eur. Phys. J. C* **74** (2014) 2872, doi:10.1140/epjc/s10052-014-2872-9, arXiv:1403.1339.

[31] ALICE Collaboration, "J/ψ polarization in pp collisions at $\sqrt{s}$ = 7 TeV", *Phys. Rev. Lett.* **108** (2012) 082001, doi:10.1103/PhysRevLett.108.082001, arXiv:1111.1630.

[32] P. Faccioli, C. Lourenço, and T. Madlener, "From prompt to direct J/ψ production: new insights on the χ_{c1} and χ_{c2} polarizations and feed-down contributions from a global-fit analysis of mid-rapidity LHC data", *Eur. Phys. J. C* **80** (2020) 623, doi:10.1140/epjc/s10052-020-8201-6, arXiv:2006.15446.

[33] Y.-Q. Ma, K. Wang, and K.-T. Chao, "J/ψ (ψ') production at the Tevatron and LHC at $O(\alpha_s^4 v^4)$ in nonrelativistic QCD", *Phys. Rev. Lett.* **106** (2011) 042002, doi:10.1103/PhysRevLett.106.042002, arXiv:1009.3655.

[34] M. Butenschön and B. A. Kniehl, "Next-to-leading-order tests of NRQCD factorization with J/ψ yield and polarization", *Mod. Phys. Lett. A* **28** (2013) 1350027, doi:10.1142/S0217732313500272, arXiv:1212.2037.

[35] R. Baier and R. Rückl, "Hadronic collisions: a quarkonium factory", *Z. Phys. C* **19** (1983) 251, doi:10.1007/BF01572254.

[36] CDF Collaboration, "Quarkonia production at CDF", *Nucl. Phys. A* **610** (1996) 373c, doi:10.1016/S0375-9474(96)00371-5.

[37] CDF Collaboration, "J/ψ and ψ(2S) production in p$\bar{\text{p}}$ collisions at $\sqrt{s}$ = 1.8 TeV", *Phys. Rev. Lett.* **79** (1997) 572, doi:10.1103/PhysRevLett.79.572.

[38] G. T. Bodwin, E. Braaten, and P. Lepage, "Rigorous QCD analysis of inclusive annihilation and production of heavy quarkonium", *Phys. Rev. D* **51** (1995) 1125, doi:10.1103/PhysRevD.51.1125, arXiv:hep-ph/9407339. [Erratum: *Phys. Rev. D* **55** (1997) 5853].

[39] J.-P. Lansberg, "J/ψ production at $\sqrt{s}$ = 1.96 and 7 TeV: Color-Singlet Model, NNLO* and polarisation", *J. Phys. G* **38** (2011) 124110, doi:10.1088/0954-3899/38/12/124110, arXiv:1107.0292.

[40] Y.-Q. Ma, K. Wang, and K.-T. Chao, "A complete NLO calculation of the J/ψ and ψ(2S) production at hadron colliders", *Phys. Rev. D* **84** (2011) 114001, doi:10.1103/PhysRevD.84.114001, arXiv:1012.1030.

[41] M. Butenschön and B. A. Kniehl, "Reconciling J/ψ production at HERA, RHIC, Tevatron, and LHC with NRQCD factorization at next-to-leading order", *Phys. Rev. Lett.* **106** (2011) 022003, doi:10.1103/PhysRevLett.106.022003, arXiv:1009.5662.

[42] K.-T. Chao et al., "J/ψ polarization at hadron colliders in nonrelativistic QCD", *Phys. Rev. Lett.* **108** (2012) 242004, doi:10.1103/PhysRevLett.108.242004, arXiv:1201.2675.

[43] M. Butenschön and B. A. Kniehl, "J/ψ polarization at Tevatron and LHC: nonrelativistic-QCD factorization at the crossroads", *Phys. Rev. Lett.* **108** (2012) 172002, doi:10.1103/PhysRevLett.108.172002, arXiv:1201.1872.

[44] B. Gong, L.-P. Wan, J.-X. Wang, and H.-F. Zhang, "Polarization for prompt J/ψ and ψ(2S) production at the Tevatron and LHC", *Phys. Rev. Lett.* **110** (2013) 042002, doi:10.1103/PhysRevLett.110.042002, arXiv:1205.6682.

[45] M. Butenschön and B. A. Kniehl, "World data of J/ψ production consolidate NRQCD factorization at NLO", *Phys. Rev. D* **84** (2011) 051501, doi:10.1103/PhysRevD.84.051501, arXiv:1105.0820.

[46] G. T. Bodwin, H. S. Chung, U.-R. Kim, and J. Lee, "Fragmentation contributions to J/ψ production at the Tevatron and the LHC", *Phys. Rev. Lett.* **113** (2014) 022001, doi:10.1103/PhysRevLett.113.022001, arXiv:1403.3612.

[47] P. Faccioli, C. Lourenço, J. Seixas, and H. K. Wöhri, "Towards the experimental clarification of quarkonium polarization", *Eur. Phys. J. C* **69** (2010) 657, doi:10.1140/epjc/s10052-010-1420-5, arXiv:1006.2738.

[48] P. Faccioli et al., "Quarkonium production in the LHC era: a polarized perspective", *Phys. Lett. B* **736** (2014) 98, doi:10.1016/j.physletb.2014.07.006, arXiv:1403.3970.

[49] G. T. Bodwin et al., "Fragmentation contributions to hadroproduction of prompt J/ψ, χ_{cJ}, and ψ(2S) states", *Phys. Rev. D* **93** (2016) 034041, doi:10.1103/PhysRevD.93.034041, arXiv:1509.07904.

[50] P. Faccioli et al., "From identical S- and P-wave p_{T} spectra to maximally distinct polarizations: probing NRQCD with χ states", *Eur. Phys. J. C* **78** (2018) 268, doi:10.1140/epjc/s10052-018-5755-7, arXiv:1802.01106.

[51] BES Collaboration, "ψ(2S) $\to \pi^+\pi^-$J/ψ decay distributions", *Phys. Rev. D* **62** (2000) 032002, doi:10.1103/PhysRevD.62.032002, arXiv:hep-ex/9909038.

[52] M. Beneke, F. Maltoni, and I. Z. Rothstein, "QCD analysis of inclusive B decay into charmonium", *Phys. Rev. D* **59** (1999) 054003, doi:10.1103/PhysRevD.59.054003, arXiv:hep-ph/9808360.

[53] M. Beneke, G. A. Schuler, and S. Wolf, "Quarkonium momentum distributions in photoproduction and B decay", *Phys. Rev. D* **62** (2000) 034004, doi:10.1103/PhysRevD.62.034004, arXiv:hep-ph/0001062.

[54] CLEO Collaboration, "Inclusive decays of B mesons to charmonium", *Phys. Rev. D* **52** (1995) 2661, doi:10.1103/PhysRevD.52.2661.

[55] BaBar Collaboration, "Study of inclusive production of charmonium mesons in B decay", *Phys. Rev. D* **67** (2003) 032002, doi:10.1103/PhysRevD.67.032002, arXiv:hep-ex/0207097.

[56] CDF Collaboration, "Measurement of J/ψ and ψ(2S) polarization in p$\bar{\mathrm{p}}$ collisions at $\sqrt{s} = 1.8$ TeV", *Phys. Rev. Lett.* **85** (2000) 2886, doi:10.1103/PhysRevLett.85.2886, arXiv:hep-ex/0004027.

[57] S. Fleming, O. F. Hernandez, I. Maksymyk, and H. Nadeau, "NRQCD matrix elements in polarization of J/ψ produced from b decay", *Phys. Rev. D* **55** (1997) 4098, doi:10.1103/PhysRevD.55.4098, arXiv:hep-ph/9608413.

[58] V. Krey and K. R. S. Balaji, "Polarized J/ψ production from B mesons at the Tevatron", *Phys. Rev. D* **67** (2003) 054011, doi:10.1103/PhysRevD.67.054011, arXiv:hep-ph/0209135.

[59] P. Faccioli, C. Lourenço, J. Seixas, and H. K. Wöhri, "Determination of χ_c and χ_b polarizations from dilepton angular distributions in radiative decays", *Phys. Rev. D* **83** (2011) 096001, doi:10.1103/PhysRevD.83.096001, arXiv:1103.4882.

[60] ATLAS Collaboration, "Measurement of the Z/γ^* boson transverse momentum distribution in pp collisions at $\sqrt{s} = 7$ TeV with the ATLAS detector", *JHEP* **09** (2014) 145, doi:10.1007/JHEP09(2014)145, arXiv:1406.3660.

[61] CMS Collaboration, "Measurement of the transverse momentum spectra of weak vector bosons produced in proton-proton collisions at $\sqrt{s} = 8$ TeV", *JHEP* **02** (2017) 096, doi:10.1007/JHEP02(2017)096, arXiv:1606.05864.

[62] CMS Collaboration, "Measurement of the Z boson differential cross section in transverse momentum and rapidity in proton-proton collisions at 8 TeV", *Phys. Lett. B* **749** (2015) 187, doi:10.1016/j.physletb.2015.07.065, arXiv:1504.03511.

[63] B. Guberina, J. H. Kühn, R. D. Peccei, and R. Rückl, "Rare decays of the Z^0", *Nucl. Phys. B* **174** (1980) 317, doi:10.1016/0550-3213(80)90287-4.

[64] T.-C. Huang and F. Petriello, "Rare exclusive decays of the Z-boson revisited", *Phys. Rev. D* **92** (2015) 014007, doi:10.1103/PhysRevD.92.014007, arXiv:1411.5924.

[65] G. T. Bodwin, H. S. Chung, J.-H. Ee, and J. Lee, "Z-boson decays to a vector quarkonium plus a photon", *Phys. Rev. D* **97** (2018) 016009, doi:10.1103/PhysRevD.97.016009, arXiv:1709.09320.